THE UNIVERSITY *of* EDINBURGH

Calixarene Supported Transition Metal Clusters

Stephanie Merac Taylor

A Thesis Submitted for the Degree of Doctor of Philosophy

School of Chemistry

College of Science and Engineering

The University of Edinburgh

Edinburgh - September 2012

Abstract

This thesis describes a series of calix[*n*]arene polynuclear transition metal and lanthanide complexes. Calix[4]arenes possess lower-rim polyphenolic pockets that are ideal for the complexation of various transition metal and lanthanide centres. Surprisingly however, with only a few exceptions, the coordination chemistry of *p*-^{t}Bu-calix[4]arene (TBC[4]), *p*-^{t}Bu-calix[8]arene (TBC[8]) and *p*-^{t}Bu-homotrioxacalix[3]arene (TBOC[3]) with paramagnetic transition metal ions for the purpose of making and studying magnetically interesting molecules is unknown.

Chapter two describes the reaction of TBC[4] with manganese salts in the presence of an appropriate base (and in some cases co-ligand) resulting in the formation of a family of calixarene-supported $[Mn^{III}_2Mn^{II}_2]$ clusters (**1**-**7**) that behave as Single-Molecule Magnets (SMMs). These are: $[Mn^{III}_2Mn^{II}_2(OH)_2(TBC[4])_2(DMF)_6]\cdot 2MeOH$ (**1**), $[Mn^{III}_2Mn^{II}_2(OH)_2(TBC[4])_2(DMF)_4(H_2O)_2]\cdot 4MeOH\cdot 2DMF$ (**2**), $[Mn^{III}_2Mn^{II}_2(OH)_2(TBC[4])_2(DMF)_6]\cdot 2.8MeOH$ (**3**), $[Mn^{III}_2Mn^{II}_2(OH)_2(TBC[4])_2(DMF)_4(EtOH)(H_2O)]$ (**4**), $[Mn^{III}_2Mn^{II}_2(OH)_2(TBC[4])_2(DMSO)_6]\cdot 2MeOH\cdot 2DMSO$ (**5**), $[Mn^{III}_2Mn^{II}_2(OH)_2(TBC[4])_2(DMSO)_6]$ (**6**) and $[Mn^{III}_2Mn^{II}_2(OH)_2(C[4])_2(MeOH)_6]\cdot 4MeOH$ (**7**). Variation in the alkyl groups present at the upper-rim of the cone allows for the expression of a degree of control over the self-assembly of these SMM building blocks, whilst retaining the general magnetic properties. The presence of various different ligands around the periphery of the magnetic core has some effect over the extended self-assembly of these SMMs.

Chapter three describes how the combination of complementary cluster ligands; sodium phenylphosphinate and the N,O-chelate 2-(hydroxy-methyl)pyridine (hmpH) with TBC[4] results in the formation of two new calixarene-supported clusters. This being an unusual $[Mn^{III}Mn^{II}]_2$ dimer of dimers $[Mn^{III}Mn^{II}(O_2P(H)Ph)(DMF)_2(MeOH)_2]_2$ **(8)** and a ferromagnetic $[Mn_5]$ cage that displays the characteristic bonding modes of each support $[Mn^{III}_3Mn^{II}_2(OH)_2(TBC[4])_2(hmp)_2(DMF)_6](TBC[4]\text{-}H)\cdot xDMF\cdot xH_2O$ (**9**).

Chapter four details how using oxacalix[3]arenes can tune the nature of the metal binding site, by introduction of ≥ 1 ethereal bridge. This results in Mn(II) rather than Mn(III) bonding in the phenolic pocket, and that these components self-assemble with additional Mn(II) and Mn(III) ions to form a $[Mn_{10}]$ supertetrahedron with an unusual

oxidation state distribution, $[Mn^{II}_6Mn^{III}_4O_4(TBOC[3])_4(Cl)_4(DMF)_3]\cdot 3.3H_2O \cdot 1.5DMF$ **(10)**.

Chapter five introduces a family of lanthanide complexes formed using TBC[8]. Variation in the experimental conditions employed in the reaction of TBC[8] with lanthanide salts (LnX_3) provides access to Ln_1, Ln_2, Ln_4, Ln_5, Ln_6, Ln_7 and Ln_8 complexes, $[Gd(TBC[8]\text{-}2H)Cl(DMSO)_4]\cdot MeCN\cdot H_2O\cdot (DMSO)_2\cdot hex$ (**11**), $[Ce^{IV}_4(TBC[8]\text{-}6H)_2(\mu_3\text{-}O)_2(DMF)_4]\cdot (DMF)_5\cdot hex\cdot MeCN$ (**12**), $[Tb^{III}_5(TBC[8]\text{-}5H)(\mu_4\text{-}O)(\mu_3\text{-}OH)_4Cl(DMSO)_8(H_2O)_3]Cl_3\cdot (DMSO)_2(hex)_2$ (**13**), $[Ce^{IV}_6(TBC[8]\text{-}6H)_2(\mu_4\text{-}O)_2(\mu_2\text{-}OMe)_4(\mu_2\text{-}O)_2(DMF)_4]\cdot (DMF)_6\cdot hex$ (**14**), $[Dy_7(TBC[8]\text{-}7H)(TBC[8]\text{-}6H)(\mu_4\text{-}O)_2(\mu_3\text{-}OH)_2(\mu_2\text{-}OH)_2(DMF)_9]\cdot (DMF)_3$ (**15**) and $[Gd_8(TBC[8]\text{-}7H)_2(\mu_4\text{-}CO_3)_2(\mu_5\text{-}CO_3)_2(\mu_2\text{-}HCO_2)_2(DMF)_8]$ (**16**), with all polymetallic clusters containing the common bi-nuclear lanthanide fragment. Closer inspection of the structures of the polymetallic clusters reveals that all but one (Ln_8) are in fact based on metal octahedra or the building blocks of octahedra.

Acknowledgements

Obviously my first thanks has to be to my supervisor Professor Euan Brechin (The Boss) for giving me the opportunity to do a PhD in his group. His support and encouragement through the last three years has been tremendous and I cannot thank him enough. He has been great to work and I have thoroughly enjoyed my time in the group, especially the Michelin star Christmas lunch last year!

Next I must thank the members of the Brechin group who have been great to work with over the last three years: Ross Inglis- for being a wealth of knowledge on magnetism and being a fellow Biffy fan (although that's probably the only music we have in common). Kevin Mason- for making me suffer months with the Cheryl poster above my desk (until I masterfully hid it) and for almost killing me and Ross in China taking us to dodgy back alley bars, Alex Prescimone- always happy to help with crystallography and answer my daft questions, Tom Hooper- for being a fellow tea jenny at juice time. Also thanks to the newer members of the Brechin group. I also have to thank all you guys for teaching me how to handle my drink and I can now say that I can comfortably drink a whole bottle of wine now!

Some of the friends I have met at university; Miriam, there from the beginning, one of my best friends. I will miss our catch ups in the office which would end up being a half hour gossip, thanks for being a brilliant friend and a huge support. Andrew and Iain, again friends from the beginning and I bet you can't believe *I* managed to do a PhD after all my moaning of how much I hated chemistry!

I would also like to thank Dr's Scott Dalgarno and Ruaraidh McIntosh from Heriot Watt University, whom my PhD was in collaboration with. Thanks for making practically all my ligands for me and for all the crystallography. I must also thank Dr Stephen Moggach for taking the time to tutor me in crystallography and make it all seem so easy, even though its most definitely not!!

Thanks also to Dr Stergios Piligkos for fitting some mag data and to Dr Simon Teat for solving some of my crystal structures.

Finally I have to thank my family; Mum, Dad, Sean and Lisa for all their endless support and encouragement throughout my life, I could not have done it without you.

Finally, finally I must thank Kevin; my person, my everything. I need say no more.

Declaration

I hereby declare that except where specific reference is made to other sources, the work contained in this thesis is the original work of the author. It has been composed by the candidate and has not been submitted, in whole or in part, for any other degree, diploma, or other qualification.

Stephanie Merac Taylor

September 2012

Format of the Thesis

Each chapter of this thesis with the exception of Chapter 1 is composed of published or to be published papers. To fulfil the requirements of The University of Edinburgh regarding the preparation and submission of a thesis for the degree of Doctor of Philosophy, they have been reformatted accordingly.

Chapter 2

- S. M. Taylor, G. Karotsis, R. D. McIntosh, S. Kennedy, S. J. Teat, C. M. Beavers, W. Wernsdorfer, S. Piligkos, S. J. Dalgarno and E. K. Brechin, *Chem. Eur. J.*, 2011, **17**, 7521-7530.

Chapter 3

- S. M. Taylor, R. D. McIntosh, C. M. Beavers, S. J. Teat, S. Piligkos, S. J. Dalgarno and E. K. Brechin, *Chem. Commun.*, 2011, **47**, 1440-1442.
- S. M. Taylor, R. D. McIntosh, S. Piligkos, S. J. Dalgarno and E. K. Brechin, *Chem. Commun.*, 2012, **48**, 11190.

Chapter 4

- S. M. Taylor, R. D. McIntosh, J. Reze, S. J. Dalgarno and E. K. Brechin, *Chem. Commun.*, 2012, **48**, 9263-9265.

Chapter 5

- S. M. Taylor, S. Sanz, R. D. McIntosh, C. M. Beavers, S. J. Teat, E. K. Brechin and S. J. Dalgarno, *Chem. Eur. J.*, 2012, **18**, 16014-16022.

Work carried out by other people:

- Complex **1** synthesised by Georgios Karotsis.
- TBC[4] and TBOC[3] synthesised by Dr Ruaraidh McIntosh
- X-ray crystallography carried out by Drs Scott Dalgarno, Ruaraidh McIntosh and Simon Teat.
- Fitting of magnetic data for complexes **1, 8** and **9** carried out by Dr Stergios Piligkos.
- Hysteresis loop measurements by Dr Wolfgang Wernsdorfer.

Publications

1. J. Tian, L. V. Saraf, B. Schwenzer, S. M. Taylor, E. K. Brechin, J. Liu, S. J. Dalgarno and P. K. Thallapally, *J. Am. Chem. Soc.*, 2012, **134**, 9581-9584.
2. S. M. Taylor, S. Sanz, R. D. McIntosh, C. M. Beavers, S. J. Teat, E. K. Brechin and S. J. Dalgarno, *Chem. Eur. J.*, 2012., accepted for publication.
3. S. M. Taylor, R. D. McIntosh, J. Reze, S. J. Dalgarno and E. K. Brechin, *Chem. Commun.*, 2012, accepted for publication.
4. S. M. Taylor, R. D. McIntosh, S. Piligkos, S. J. Dalgarno and E. K. Brechin, *Chem. Commun.*, 2012, accepted for publication.
5. S. T. Meally, C. McDonald, P. Kealy, S. M. Taylor, E. K. Brechin and L. F. Jones, *Dalton Trans.*, 2012, **41**, 5610-5616.
6. E. Houton, S. M. Taylor, C. C. Beedle, J. Cano, S. Piligkos, S. Hill, A. G. Ryder, E. K. Brechin and L. F. Jones, *Dalton Trans.*, 2012, **41**, 8340-8347.
7. R. E. Fairbairn, R. McLellan, R. D. McIntosh, S. M. Taylor, E. K. Brechin and S. J. Dalgarno, *Chem. Commun.*, 2012, **48**, 8493-8495.
8. N. Berg, S. M. Taylor, A. Prescimone, E. K. Brechin and L. F. Jones, *CrystEngComm*, 2012, **14**, 2732-2738.
9. N. Berg, T. Rajeshkumar, S. M. Taylor, E. K. Brechin, G. Rajaraman and L. F. Jones, *Chem. Eur. J.*, 2012, **18**, 5906-5918.
10. S. M. Taylor, R. D. McIntosh, C. M. Beavers, S. J. Teat, S. Piligkos, S. J. Dalgarno and E. K. Brechin, *Chem. Commun.*, 2011, **47**, 1440-1442.
11. S. M. Taylor, G. Karotsis, R. D. McIntosh, S. Kennedy, S. J. Teat, C. M. Beavers, W. Wernsdorfer, S. Piligkos, S. J. Dalgarno and E. K. Brechin, *Chem. Eur. J.*, 2011, **17**, 7521-7530.
12. R. D. McIntosh, S. M. Taylor, S. Sanz, C. M. Beavers, S. J. Teat, E. K. Brechin and S. J. Dalgarno, *Dalton Trans.*, 2011, **40**, 12265-12270.
13. R. Inglis, S. M. Taylor, L. F. Jones, G. S. Papaefstathiou, S. P. Perlepes, S. Datta, S. Hill, W. Wernsdorfer and E. K. Brechin, *Dalton Trans.*, 2009, 9157-9168.

Conferences attended

2010

- Scottish Dalton Meeting; University of Glasgow (UK)
- ICMM 2010: The 12th International Conference on Molecule-based Magnets; Beijing (China), *poster presented*.

2011

- 94th Canadian Chemistry Conference and Exhibition; Montreal (Canada), *poster presented.*

2012

- Scottish Dalton Meeting; University of Strathclyde (UK)
- National High Magnetic Field Laboratory/EMR Workshop "Magnetostructural Correlations"; Tallahassee (Florida), *30 minute talk given*.

Contents

Abbreviations

ac	alternating current
C[4]	Calix[4]arene
D	Zero-field splitting parameter
dc	direct current
DMF	Dimethylformamide
DMSO	Dimethyl sulfoxide
hex	hexane
Ln	lanthanide
MeCN	acetonitrile
NEt_3	triethylamine
MCE	Magnetocaloric Effect
SMM	Single Molecule Magnet
TBC[4]	*p-tert*-butyl-calix[4]arene
TBC[8]	*p-tert*-butyl-calix[8]arene
TBOC[3]	*p- tert*-butyl-homotrioxacalix[3]arene
THF	Tetrahydrofuran
TM	Transition Metal

Chapter 1

Introduction

1.1 Calixarenes

1.1.1 History of Calix[n]arenes

Calix[n]arenes are cyclic polyphenols formed from the condensation reaction of *p*-substituted phenols with formaldehyde and were first studied by von-Bayer in 1872.[1-3] He discovered that formaldehyde behaves like other aldehydes in that it produces resins when reacted with phenol, in the presence of acid. Unfortunately no materials pure enough to analyse were obtained from this, so this chemistry was largely forgotten. Then, in the 1900's Leo Baekeland, a Belgian chemist began studying phenol formaldehyde chemistry. This led to the revolutionary discovery of Bakelite, the first synthetic plastic.[4] It was however not until the 1940's that Zinke and co-workers decided to investigate the reaction of *p*-substituted phenols with formaldehyde in the hope of reducing the formation of cross-linked polymers and producing linear polymers.[5,6] In 1944 Zinke suggested that cyclic condensation products could be formed from these phenols and formaldehyde with sodium hydroxide and assigned cyclic tetrameric structures to the products obtained from this reaction (Figure 1).[6,7] This was based on work done by Niederl and Vogel in 1940, who had assigned cyclic tetrameric structures to acid catalysed reactions of aldehydes and phenols.[8] Following on from this, Zinke and co-workers synthesised a collection of cyclic tetramers from a variety of *p*-substituted phenols.[9,10]

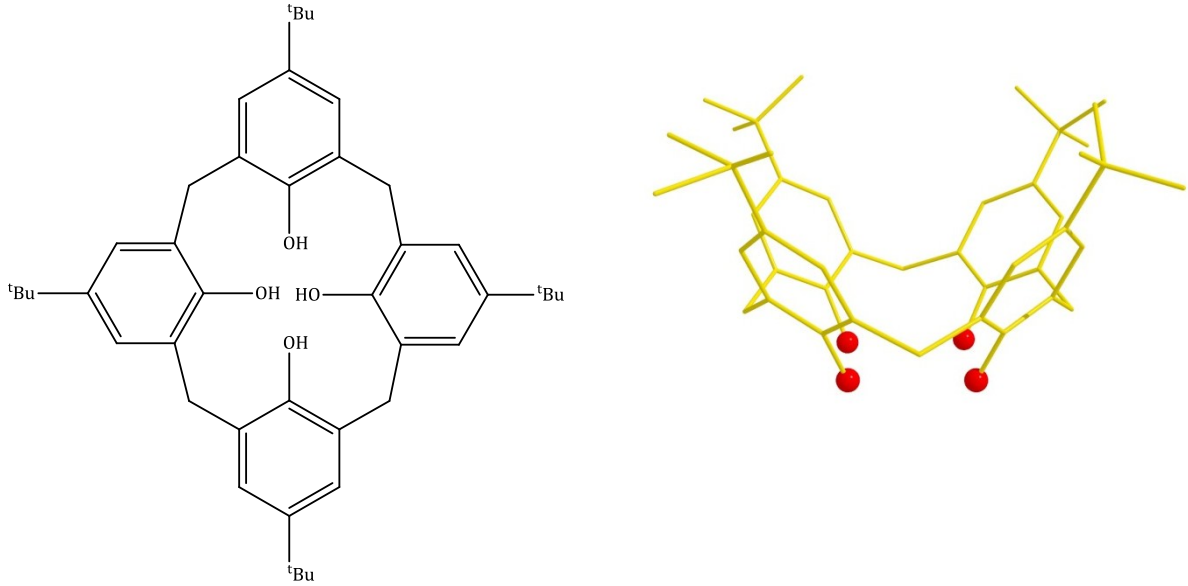

Figure 1. Structure of a cyclic tetramer based on *p*-tert-butylphenol, *p*-^{t}Bu-calix[4]arene (TBC[4]) (left). Molecular structure of TBC[4] (right), colour code; C = gold, O = red. H-atoms omitted for clarity.

In 1955 John Cornforth, an Australian chemist was interested in compounds which could inhibit the growth of the tubercle bacterium. Some of the compounds Cornforth was interested in included Zinke's cyclic tetramers.[11] His work demonstrated that Zinke's synthetic method was not clean, producing a mixture of cyclic products.[11,12] Around this time the Petrolite Company began patenting procedures for producing Zinke's cyclic tetramers for use as demulsifiers.[13,14] In the 1970's Gutsche, a chemist at Washington University, became interested Zinke's cyclic tetramers in the hope they could have applications in the field of bioorganic chemistry and in particular as candidates for enzyme mimics.[3] The latter idea was to produce a receptor for a particular substrate molecule that could be functionalised with the appropriate groups required for reacting with the substrate molecule. In comparison to other candidates, such as crown ethers, the cyclic tetramers were more appealing because of their basket-like, rather than loop-like structures. Cyclodextrins, the natural "analogues" of calix[n]arenes, were also thoroughly examined in this respect.[15-20] The Gutsche group confirmed Cornforth's, suggestion that the Zinke procedures for synthesising cyclic tetramers produced a mixture of products,[21] indeed they reported that the reactions produce both the cyclic hexamer, octamer, along with some tetramer.[21] Isolating the different products was achieved through subtle changes in reaction conditions.[21-24]

The nomenclature chemists have employed to describe these cyclic tetramers has varied considerably over the years; for example Zinke and Ziegler called them "cyclischen mehrkernmethylenephenolverbindungen",[6] and Chemical Abstracts designated them as "pentacyclo[19.3.1.1^{3,7}1^{9,13}1^{15,19}]octacosa-1(25),3,5,7(28),9,11,13(27), 15, 17,19(26)21,23-dodecaene-25,26,27.28-tetrol".[21] However in 1975 Gutsche adopted the name "*calixarene*" as the cyclic tetramer resembled the shape of a Greek vase called a calyx krater due to the bowl or cone conformation that they commonly adopt (Figure 2).[21] The name is derived from the Greek *calyx* meaning chalice and *arene* which indicates the presence of the aromatic rings. Andreetti and co-workers crystallographically confirmed this conformation in 1979.[25] The commonly accepted abbreviation is thus *p*-R-calix[*n*]arene where R is the group *para* to the OH group of the phenol and *n* is the number of phenolic residues present.[7]

Figure 2. An example of a calyx krater (left) and a space fill representation of TBC[4] (right), depicting the reasoning behind the name calixarenes. Colour code: C = grey, O = red, H = white.

The procedure first published by Gutsche for the synthesis of TBC[4] follows on from the original synthetic method by Zinke but aims to prevent obtaining a mixture of products.[22,26] The Gutsche procedure is as follows: a mix of *p*-^{t}Bu-phenol, 37 % formaldehyde and sodium hydroxide is heated at 120 °C for 2h, using a Dean-Stark apparatus to remove the water that is produced.[22,26] The presence of base is crucial in order to induce cyclisation and the quantity and temperature play a role in determining the nature of the product.[24] It is trivial to mistakenly synthesise a mix of different products (tetramers, hexamers, octamers and sometimes linear oligomers) in the same reaction unless care is taken. This initial step produces a solid precursor, and to this diphenyl ether is added and the mixture heated to reflux for 4h.[22,26] The reaction mixture is then left to cool and ethylacetate is added and the product separated via suction filtration to yield white crystals.[22,26] The overall reaction pathway is summarised in Scheme 1.[3] The pathway proceeds by means of an electrophilic aromatic substitution, followed by elimination of water and then a second aromatic substitution. The reaction is initiated by formation of phenoxide (which acts as carbon nucleophile), which induces nucleophilic addition to the reactive C=O on formaldehyde.[3,27]

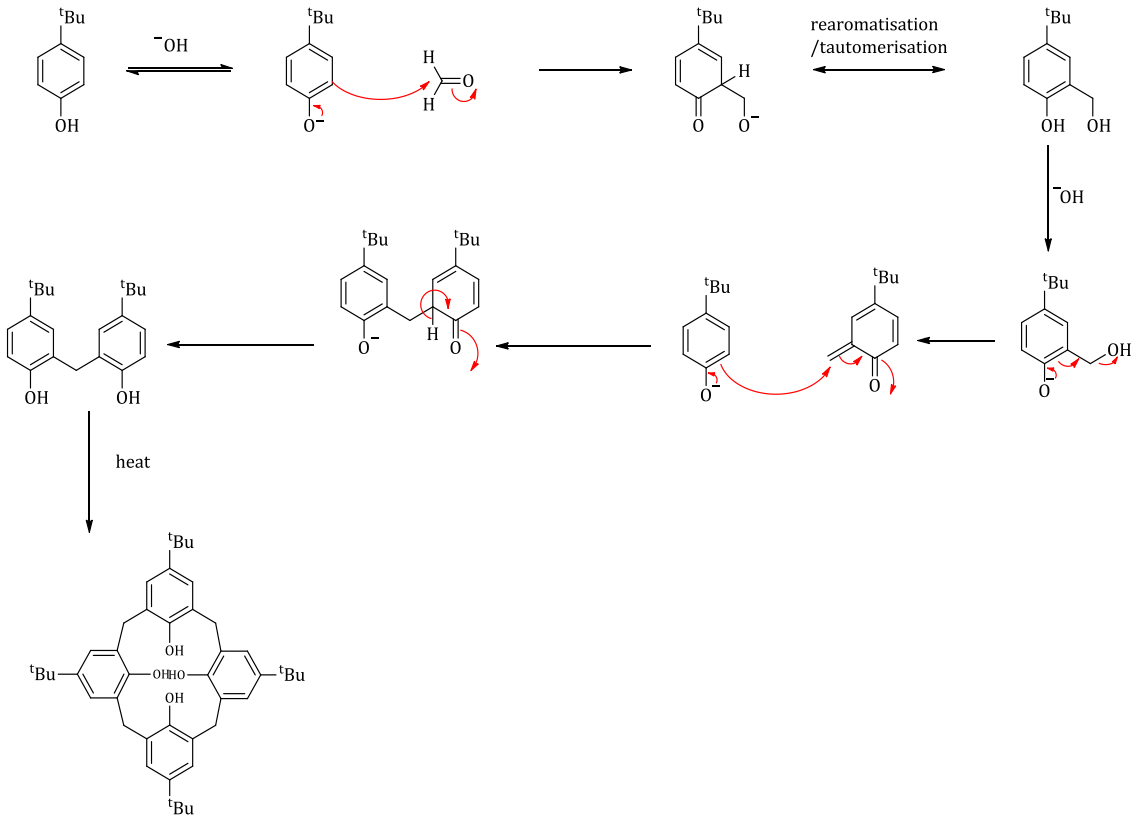

Scheme 1. Pathway for the synthesis of *p*-^{t}Bu-calix[4]arene.[3]

Calixarenes can also be synthesised in an acid-catalysed reaction but this is less commonly employed as the yields of small calixarenes (n = 4-8) are < 1 % (unpublished observations by Gutsche).[28] Greater amounts of larger calixarenes are present in the acid catalysed reaction of *p*-^{t}Bu-phenol and formaldehyde, where calix[n]arenes as large as n = 20 are present.[28]

Calixarenes are versatile organic compounds as they can exist in several conformations.[11] In particular, calix[4]arenes can exist in four different conformations; cone, partial cone, 1,3 alternate and 1,2 alternate (Figure 3).[29] The cone conformation is described by all *p*-groups pointing "up"; partial cone, when one *p*-group is rotated "downward"; 1,3-alternate as two "up" and two "down", and 1,2-alternate as two "up" and two "down".[29] They exist favourably in the cone conformation but are conformationally mobile at room temperature.[30] The intermolecular hydrogen bonding that occurs between the OH groups and non-bonding steric hindrance also play a part in the degree of conformational flexibility.[29] When a conformational transformation occurs an aromatic group is rotated round the C2/C6 axis that brings the OH groups

through the centre of the macrocyclic ring.[29] The OH groups only experience a moderate degree of interference, whereas larger groups would be expected to experience a greater constraint. The derivation of the calixarenes can hold the molecule in a particular conformation, for example most calix[4]arenes functionalised at the lower-rim with ester or ether groups are held in a partial cone conformation and are conformationally rigid at room temperature.[29] The energy difference between the cone and the partial cone, 1,3-alternate and 1,2-alternate is 16.2, 19.8 and 30.2 kcal mol^{-1} respectively.[31]

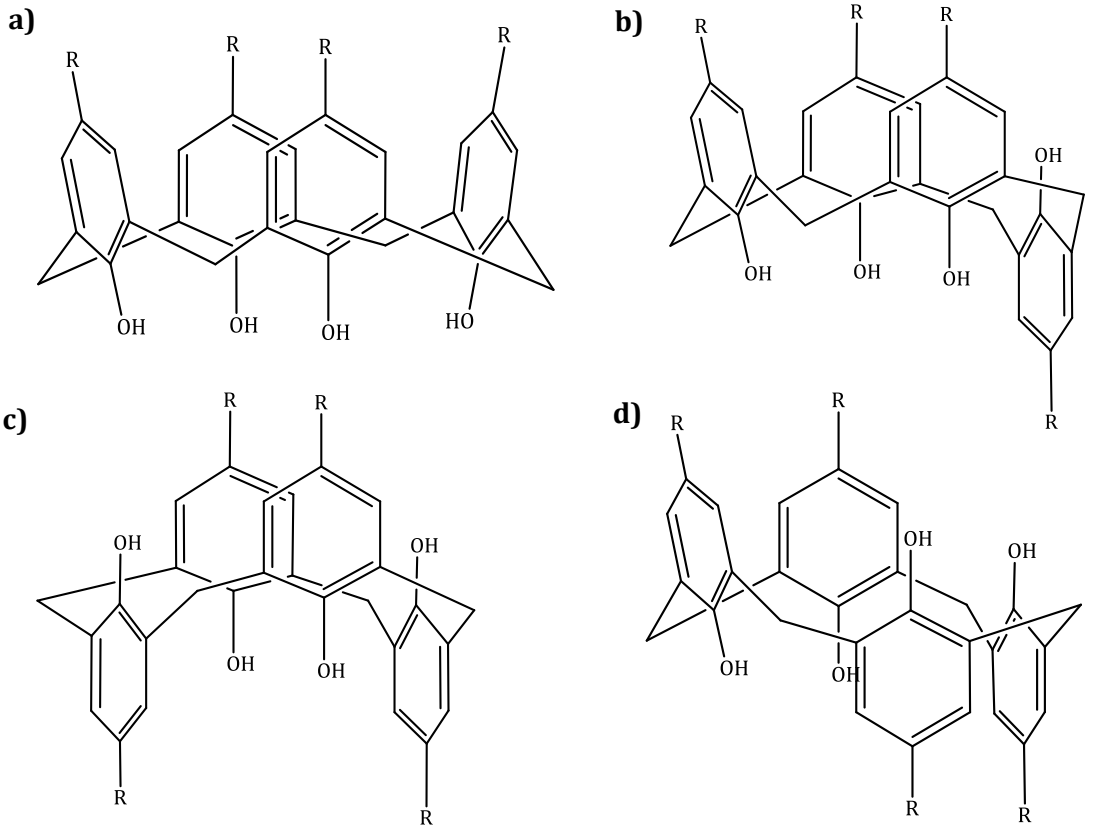

Figure 3. The four conformations of calix[4]arenes, a) cone conformation b) partial cone, c) 1,3-alternate and d) 1,2-alternate.

As the number of phenolic residues increases in the calixarene, the number of possible conformations increases. For example calix[4]arenes have four conformers, calix[6]arenes have eight conformers, calix[8]arenes have sixteen and so on.[32]

Calixarenes are versatile ligands as they can be functionalised at various parts of the structure. For example the number of phenolic residues can be changed, n = 4, 5, 6, 7, 8…etc, the *p*-substituent at the upper rim can be functionalised as can the groups bridging the phenolic moieties and the groups bonded to the phenolic oxygens at the

lower-rim (Figure 3). They can act as hosts for cations, anions and neutral molecules depending on their functionalisation.[33,34]

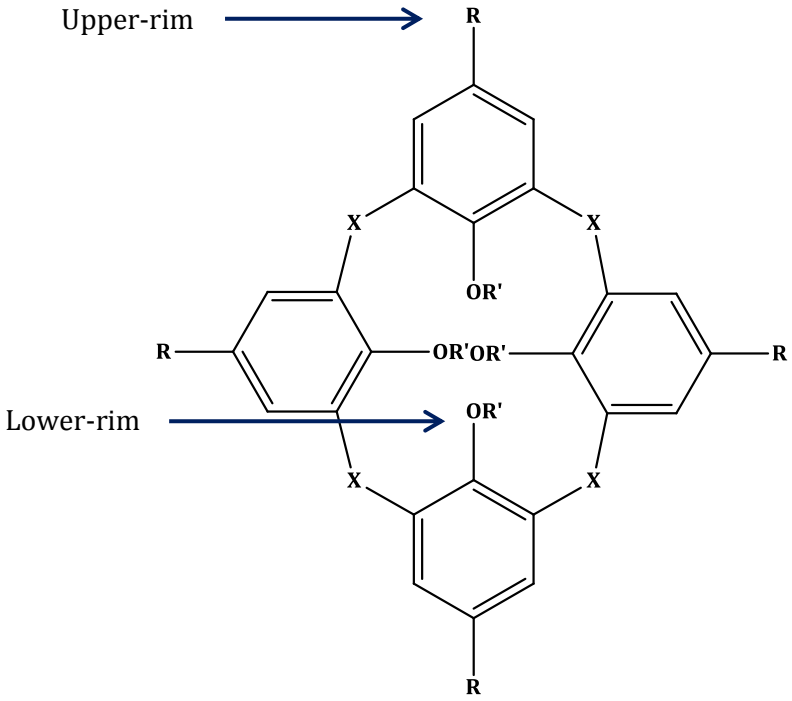

Figure 3. Schematic diagram of calix[n]arene framework, where R = *p*- substituent at the upper-rim, X = bridging moiety, R' = substituent at the lower-rim.

Much work has been done by Atwood, Barbour and Ripmeester on the self-assembly of TBC[4] and its inclusion complexes, in order to understand the structural motifs and properties required for molecular recognition.[35-37] TBC[4] has been shown to form different polymorphs depending on the conditions of crystallisation.[38] The majority of the inclusion complexes of calix[4]arenes crystallise in tetragonal space groups.[39-42] Inclusion complexes of TBC[4] more often than not crystallise with the host molecules, (TBC[4]) packing in bilayers (Figure 4).[38] This bilayer packing can be separated into two groups: A, where the space group is tetragonal $P4/n$, with a host : guest ratio of 1:1 and each guest molecule (e.g. toluene) partially inserted into the calixarene cavity;[25] B, with the tetragonal space group of $P4/nnc$, host : guest ratio 2:1 with two TBC[4] molecules facing each other to form a dimeric capsule which completely encapsulates the guest molecule (e.g. anisole).[42] In the packing of A the calixarenes facing one another are arranged in an offset fashion. In B the bilayers are translated across the layer with respect to the bilayers in A and this is what allows the facing calixarenes to

form dimeric capsules. The surfaces of the bilayer consist of the ^{t}Bu groups, interdigitated with the cavities of the calixarene.[38]

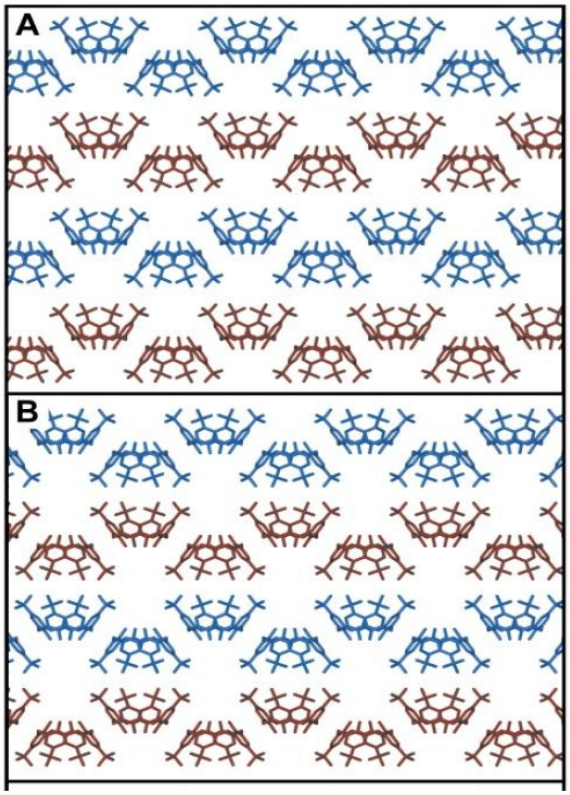

Figure 4. Packing diagram of the two most common bilayer packing arrangements of TBC[4] (host = toluene). A, the space group is tetragonal *P*4/*n*, host : guest ratio of 1:1 and B, with tetragonal space group of *P*4/*nnc*, host : guest ratio 2:1. Adjacent bilayers are depicted by alternating red and blue, guest molecules are omitted for clarity.[38]

Other guest molecules, such as long chain alkanes, can be housed in the TBC[4] cavity. For example, heating TBC[4] with tetradecane for three days at 70 °C, gives guest free structures, where the molecules pack in a bilayer type array (Figure 5).[43] Here the TBC[4] cavities are occupied by ^{t}butyl groups of molecules in the adjacent bilayer, giving a self-included structure. However, on heating at the same temperature for eight days, the tetradecane molecule is now included as a guest (Figure 5).[43] This structure shows a host : guest ratio of 1:1 and the guest molecule can exist in two different motifs. One motif consists of the guest in the host cavity and on leaving the cavity the molecule bends allowing the other terminal end of the molecule to be encapsulated in a host molecule of the adjacent bilayer (Figure 5, motif 1). The other motif involves the guest existing in two positions; one where the guest has both termini housed in host cavities of adjacent bilayers and the other guest located in the space between the

encapsulated guest molecules (motif 2).[43] The bilayer packing arrangement is favourable regardless of the guest molecule in these inclusion complexes, clearly demonstrating that the calixarene is directing the packing arrangement of the molecules in these structures.[35-37,43]

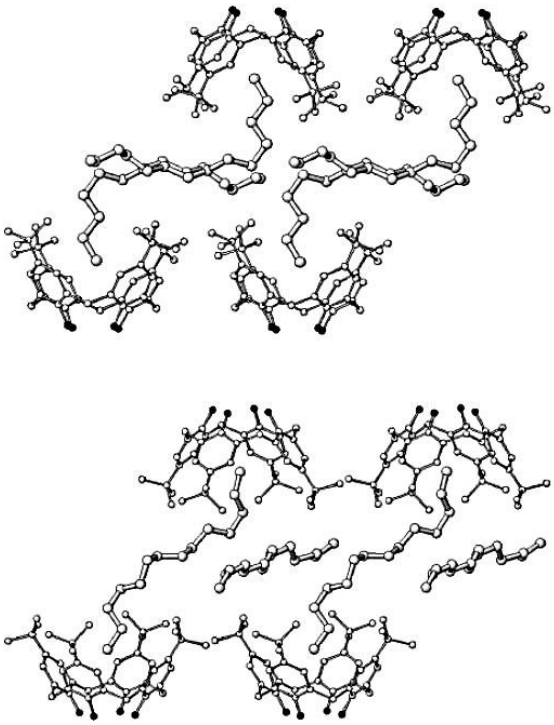

Figure 5. Packing diagram of the TBC[4]- tetradecane inclusion complex, showing the guest molecule in motif 1 (top) and motif 2 (bottom).[43]

1.1.2 Calix[4]arene- Supported 1st Row Transition Metal Clusters

The first transition metal complexes made with calixarenes as ligands were reported in 1985 by Power and co-workers who employed TBC[4] in combination with the amido complexes $[Ti^{IV}(NMe_2)_4]$, $[Fe^{III}\{N(SiMe_3)_2\}_3]$ and $[(Co^{II}\{N(SiMe_3)_2\}_2)_2]$ to synthesise the complexes $[Ti^{IV}(TBC[4])_2]\cdot 6PhMe$, $[\{Fe^{III}(NH_3)(TBC[4])OSiMe_3\}_2]\cdot 3n\text{-}C_6H_{14}$ and $[Co^{II}_3\{(TBC[4])OSiMe_3\}_2]\cdot 5PhMe$, respectively.[44] The Cambridge Structural Database (CSD) now lists a total of 149 first row transition metal cluster compounds containing calix[4]arene ligands, the majority of which involve functionalised calix[4]arenes, either at the upper or lower rims[45-61] and others which utilise calix[n]arenes with other coordinating groups in the bridge (e.g. the thiacalix[*n*]arenes with a -S- bridge)[62-68] or

thiacalix[*n*]arenes which are functionalised at the upper or lower rim.[69,70] Many of the original calix[n]arene complexes incorporated Ti [44] and there have been several others synthesised since,[71,72] including $[Na_4(THF)_8][Ti^{IV}_2(O)_2(C[4])_2]$ (Figure 6)[71] and $[Ti^{IV}_4(O)_4(TBC[4])(\eta^5\text{-}C_5H_5)_4]$ (Figure 7)[72] which was the first characterised titanium complex with an underivatised calix[4]arene, the first transition metal cluster compound containing four metal ions and an unusual example of a cluster in which the metal ions are all bonded to the same calix[n]arene.[72]

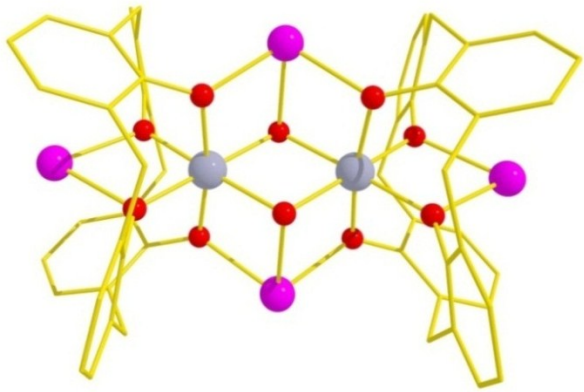

Figure 6. The molecular structure of the dinuclear Ti complex $[Na_4(THF)_8][Ti^{IV}_2(O)_2(C[4])_2]$. Colour code: Ti^{IV} = grey, Na = pink, O = red, C = gold, H-atoms omitted for clarity.[71]

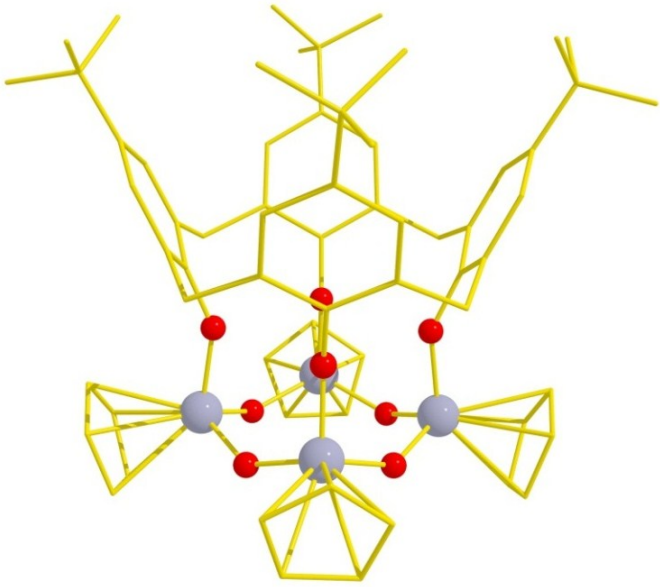

Figure 7. Molecular structure of $[Ti^{IV}_4(\mu\text{-}O)_4(TBC[4])(\eta^5\text{-}C_5H_5)_4]$, showing four Ti atoms bound to the same TBC[4] molecule with the coordination of each Ti atom completed by a $\eta^5\text{-}C_5H_5$ ligand. Colour code: Ti = grey, O = red, C = gold, H-atoms omitted for clarity.[72]

Other examples of first row transition metal TBC[4]/C[4] complexes include those containing vanadium[59,73-75], chromium,[76,77] manganese,[78-80], iron[81,82], copper[83] and zinc.[84,85] The vanadium complexes have been primarily synthesised in order to probe their potential catalytic behaviour. For example, the complex $(NBu_4)[V^{V}O(TBC[4])]$ shown in Figure 8a has been studied as a potential catalyst for the aerobic oxidation of 1-phenyl-1propargyl alcohol[75] and $[\{V^{IV}(TBC[4])(NCMe)\}_2]\cdot 6MeCN$ (Figure 8b) synthesised by Redshaw and co-workers has shown good activity as a pro-catalyst for the polymerisation of ethylene.[59] Calixarenes are used here for catalytic purposes as they act as a support for the vanadium oxide catalytic centre.

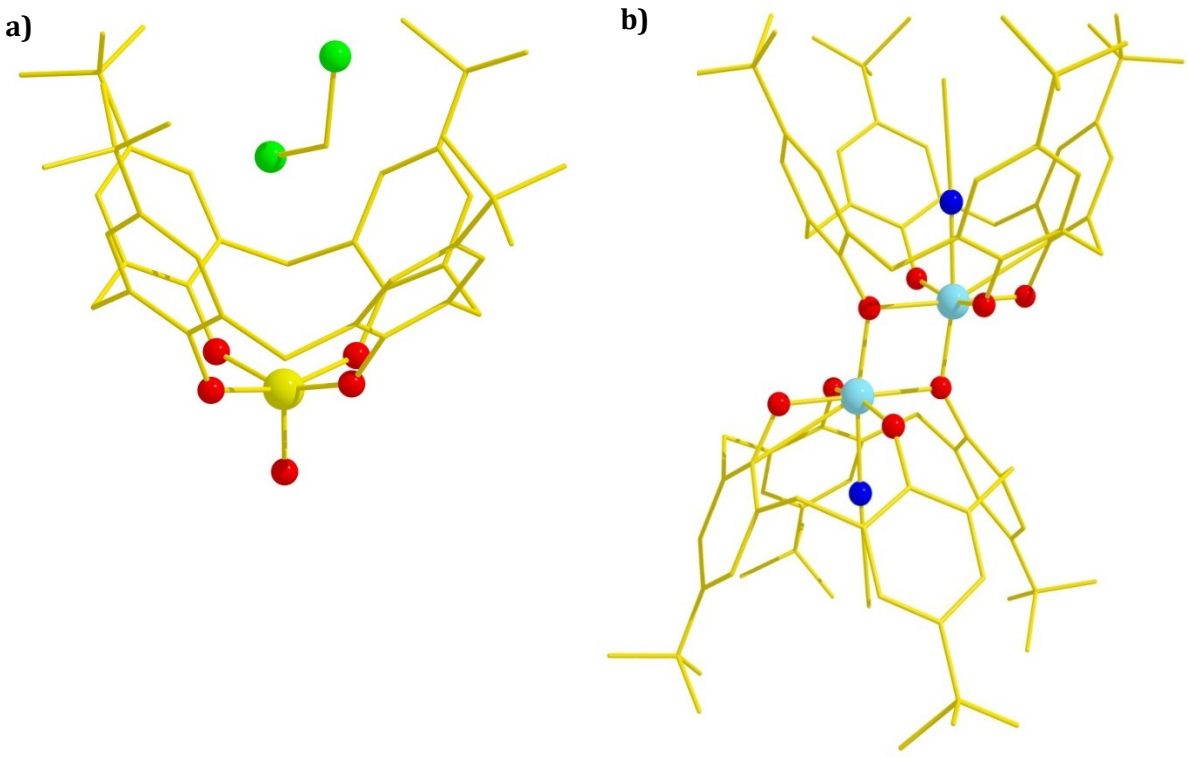

Figure 8. a)$(NBu_4)[V^{V}O(TBC[4])]$, showing host-guest interaction of TBC[4] with a solvent molecule (DCM) where the vanadium ion is in the 5+ oxidation state.[75] b) Vanadium dimer $[\{V^{IV}(TBC[4])(NCMe)\}_2]\cdot 6MeCN$, each vanadium is in the 4+ oxidation state. Colour code: V^{V} = yellow, V^{IV} = light blue, O = red, N = blue, Cl = green, C = gold, H-atoms omitted for clarity.[59]

Another example of a vanadium calix[n]arene complex is the compound $[V^{III}V^{IV}_5O_6(OCH_3)_8(TBC[4])(CH_3OH)]^-$ (Figure 9a)[73], which was synthesised solvothermally and describes an octahedron of six V ions surrounding a central μ_6-O^{2-} ion. The sole TBC[4] ligand uses its phenolic O-atoms to bridge the four equatorial V ions to one apical V ion across four edges of the octahedron. Perhaps of more interest and relevance to the work presented herein, is the observation that the cluster displays

ferromagnetic exchange interactions between the five (s = 1/2) V^{IV} ions and one (s = 1) V^{III} ion and thus a spin ground state of S = 7/2.[73] An example of an iron- TBC[4] complex is shown in Figure 9b. This iron(III) dimer was screened as a potential catalyst for the ring opening polymerization of ε-caprolactone.[81] Polycaprolactone is an important polyester as it has potential applications in drug delivery and other biomedical applications

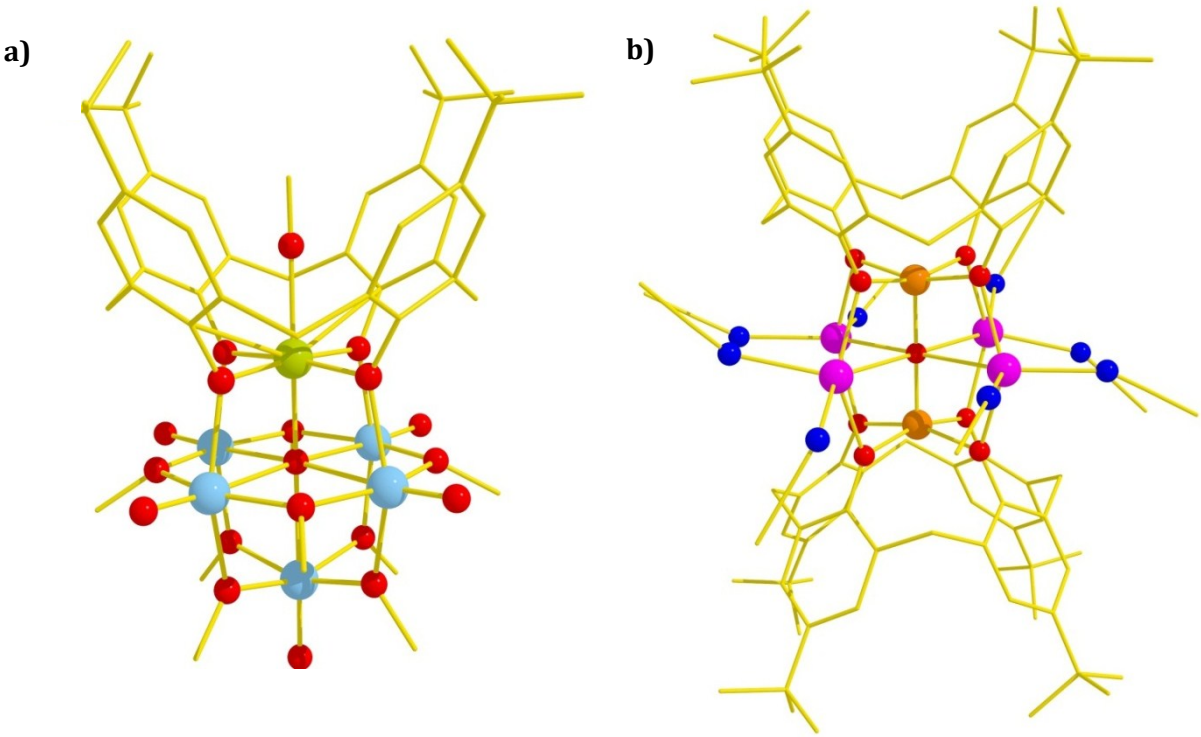

Figure 9. a) Structure of the mixed valent, ferromagnetic polyoxovanadate(III,IV) cluster $[V^{III}V^{IV}_5O_6(OCH_3)_8(TBC[4])(CH_3OH)]^-$ containing a calixarene (TBC[4]) "cap". Colour code: V^{III} = green, V^{IV} = light blue, O = red, C = gold, H-atoms omitted for clarity.[73] b) TBC[4] supported iron(III) cluster, $\{Fe^{III}[Na(NCMe)_2]TBC[4]\}_2(\mu_6\text{-}O)$. Colour code: Fe = orange, Na = pink, N = blue, O = red, C = gold, H-atoms omitted for clarity.[81]

1.1.3 Calix[4]arene- Supported 2nd and 3rd Row Transition Metal Complexes

There are over 200 calix[4]arene complexes with second and third row transition metals, reported in the CSD. However, as with the 3d metals, these are mainly with derivatised calixarenes rather than TBC[4]/C[4]. These include complexes of yttrium[86], molybdenum[87-89], rhodium[90], zirconium,[46,91,92], niobium[93], palladium[94], silver [95-98], tantalum[93,99-101], tungsten[88,102-104], rhenium[94,105] and platinum[106]. Of the complexes using TBC[4]/C[4] there are >100 involving molybdenum[107-120] and tungsten[103,109,111-113,118,119,121-135]. Some of these Mo and W complexes exhibit metal-metal multiple bonds,

including M-M triple bonds.[112,113,118,126,134] Figure 10 shows an example where a Mo^{III} ion is encapsulated within the lower-rim bowl of the calixarene, coordinated by the two phenolic oxygen atoms from each TBC[4].[112] There are also a series of dimolybdenum TBC[4] and C[4] complexes containing quadruple Mo-Mo bonds[107,108,115] and one complex containing a W-W quadruple bond.[126]

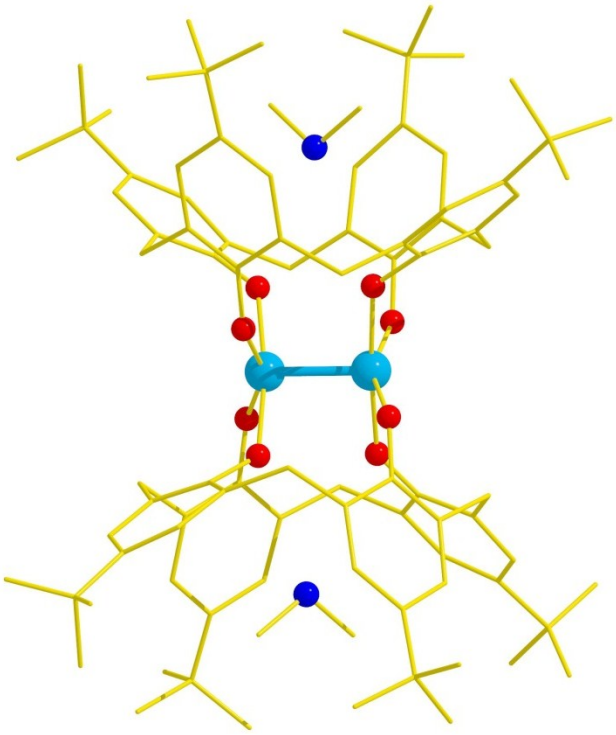

Figure 10. Structure of $(H_2NMe_2)_2[Mo^{III}(TBC[4])]_2$, a Mo TBC[4] dimer, showing a Mo-Mo triple bond of 2.193 Å (light blue), displaying host-guest interactions with acetonitrile housed inside the TBC[4] cavity. Colour code: Mo^{III} = light blue, O = red, N = blue, C = gold, H-atoms omitted for clarity.[112]

Calixarenes have also been used in combination with rhenium in order to produce novel anti-cancer agents.[105] Redshaw and co-workers synthesised a series of Re^{V} complexes using TBC[4] and the monomethoxycalix[4]arene as ligands because ^{186}Re and ^{188}Re act as β-emitters and the calix[4]arene is a strong carrier molecule which is also non-toxic to cells. This group also produced the first example of Re-Re metal-metal bonded dimers with supporting calixarenes (in this case TBC[4]), shown in Figure 11.[105] Complexes of TBC[4] have also been reported with niobium and tantalum and their inclusion complexes with toluene, acetonitrile and water, where these solvent molecules are held in the cavity of the calixarene. [93]

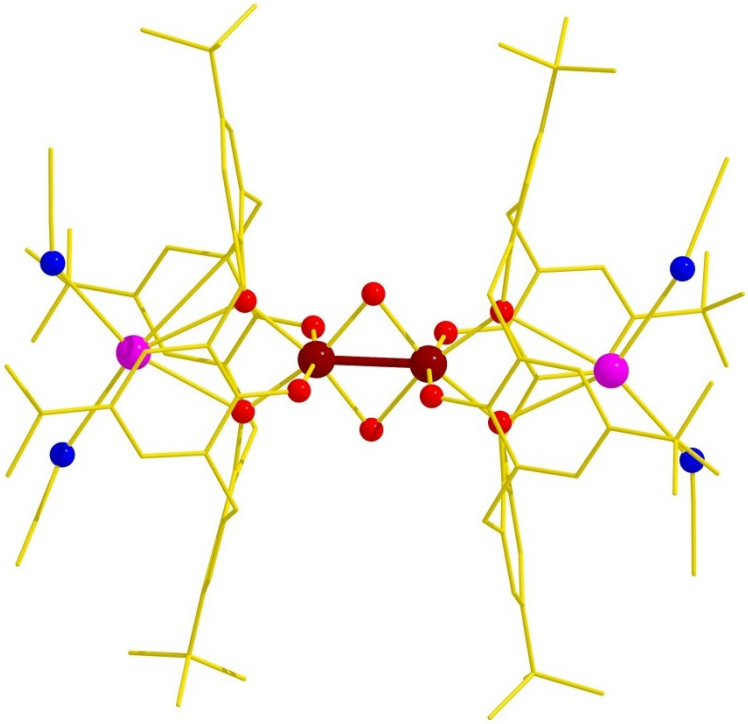

Figure 11. An example of a Re^{V} dimer $[Re^{V}(TBC[4])K(NCMe)_2(\mu\text{-}O)]_2$, which is being used in the development of new anti-cancer agents. It is the first example of Re-Re bonding supported by calixarenes.[105] Colour code: Re = dark red, K = pink, O = red, N = blue, C = gold, H-atoms omitted for clarity.

1.1.4 Current Work

The breadth of calix[4]arene chemistry is utterly vast – as reflected in the plethora of reviews and books written on the subject - and it is thus very surprising to learn that, with only a few exceptions, the coordination chemistry of TBC[4]/C[4] with paramagnetic transition metal ions for the purpose of making and studying magnetically interesting molecules is unknown.[73,78,83,136,137] The work currently being undertaken in the Brechin group tries to address this situation.

From a coordination chemistry perspective calix[4]arenes are potentially excellent ligands for metal complexation; ligands containing one or more alkoxide "arms" have been tremendously successful in cluster synthesis.[138-146] Indeed our own group has employed triols (e.g. 1,1,1tris(hydroxymethyl)methane and its derivatives) for many years and other groups have used diols to equally good effect.[147-152] The use of calixarenes can therefore been seen as a simple extension of the above strategy but one which allows for much greater variety, since the organic framework is so easily derivatised. Phenol itself is an excellent ligand for 1st row transition metals and thus the

tetraphenolic pocket present at the lower-rim of calix[4]arenes is an attractive feature for cluster synthesis. Initial work in the Brechin group by Karotsis lead to the synthesis of $[Mn^{III}_2Mn^{II}_2(OH)_2(TBC[4])_2(dmf)_6]$, the first calixarene-based Single-Molecule Magnet (SMM), and the first manganese cluster to be built with any methylene bridged calixarene (Figure 12).[78] It was made via the reaction of $MnCl_2$ with TBC[4] or C[4] in the presence of NEt_3 and in a solvent combination of MeOH and DMF. The structure describes a butterfly or diamond-like $Mn^{III}_2Mn^{II}_2$ metallic core housed between two TBC[4] or C[4] molecules, in which the wing-tip Mn ions are in the 3+ oxidation state and the body Mn ions are in the 2+ oxidation state.[78]

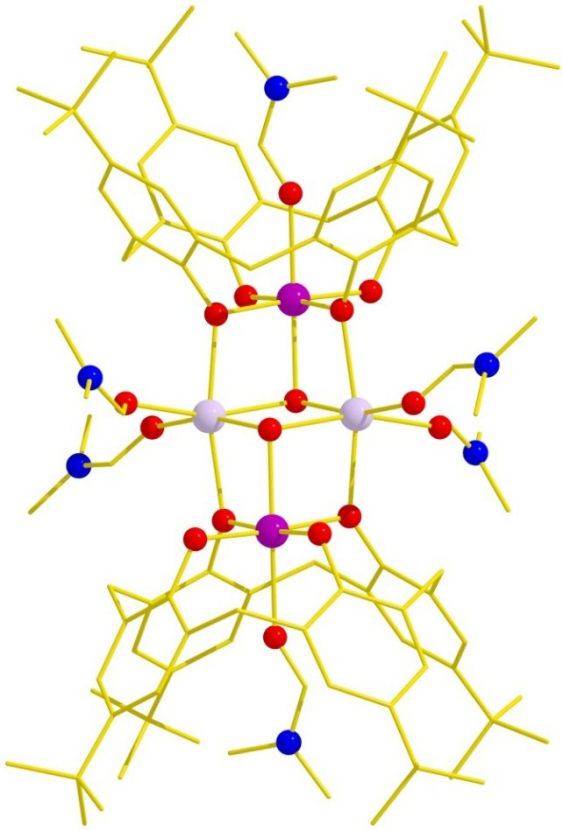

Figure 12. Molecular structure of the first calixarene-based SMM, of $[Mn^{III}_2Mn^{II}_2(OH)_2(TBC[4])_2(dmf)_6]$. Colour code: Mn^{III} = purple, Mn^{II} = pale purple O = red, N = blue, C = gold, H-atoms omitted for clarity.[78]

Karotsis also synthesised the first C[4]/TBC[4]-stabilised mixed 3d/4f metal cluster $[Mn^{III}_4Ln^{III}_4(OH)_4(C[4])_4(NO_3)_2(dmf)_6(H_2O)_6](OH)_2$ (Figure 13).[136] The complex is best described as a square of Ln^{3+} ions inside a square of Mn^{3+} ions. The complex displays ferromagnetic exchange between the metal centres resulting in an S = 22 spin ground

state with practically zero anisotropy, when Ln = Gd. This combination of properties, combined with the weak exchange inherent to 4f ions, allows the complex to display an enhanced Magneto-Caloric Effect (MCE) which describes changes in magnetic entropy with applied field, making it a candidate for low temperature refrigeration.[136,137] When the Ln ion is either Tb^{3+} or Dy^{3+} the molecule behaves as an SMM.

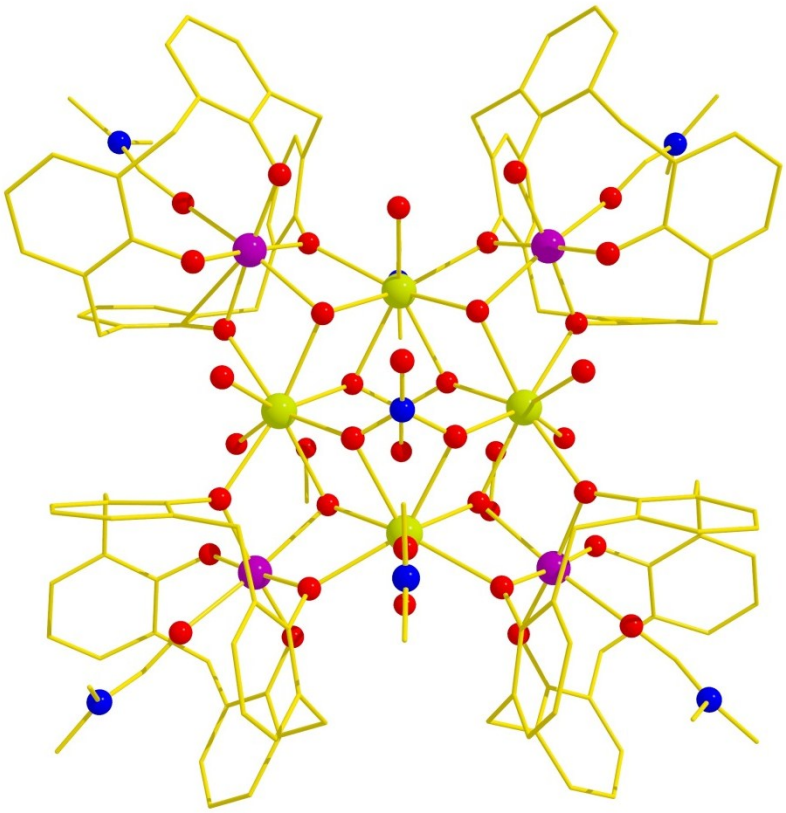

Figure 13. Molecular structure of the first 3d/4f TBC[4]/C[4] complex, $[Mn^{III}_4Ln^{III}_4(OH)_4(C[4])_4(NO_3)_2(dmf)_6(H_2O)_6](OH)_2$. Colour code: Mn = purple, Ln = green, O = red, N = blue, C = gold, H-atoms omitted for clarity.[136,137]

1.2 Other Calixarenes

1.2.1 Calix[8]arene

Calix[8]arenes are produced from an almost identical reaction to that of calix[4]arenes.[23,153] *p*-tert-butylcalix[8]arene (TBC[8]), shown in Figure 14, is synthesised as follows; a mix of *p*-tert-butylphenol, paraformaldehyde and sodium hydroxide (0.03 equivalents w.r.t. phenol) in xylene is heated to reflux for 4h, using a

Dean-Stark apparatus to remove the water that is produced. The mixture is allowed to cool to room temperature and the product collected by filtration. The product is recrystallised from chloroform, however on standing the crystals turn to a white amorphous powder which is attributed to loss of solvent of crystallisation.[153,154]

The larger annulus of the calix[8]arenes, which provides 16 different "up" "down" conformations (as in TBC[4]) would appear to allow for greater conformational flexibility. The solid state form of TBC[8] is that of a flat molecule with the eight hydroxyl groups arranged in an almost planar fashion and intramolecularly hydrogen bonded, described as a pleated-loop.[154] Space filling models indicate that this conformation is ideal in enabling "circular" hydrogen bonding. However, in solution the dynamic ^{1}H NMR behaviour of TBC[8] is analogous to that of TBC[4] in non-polar solvents.[30] It was postulated that this could be due to TBC[8] adopting a "pinched" conformation in solution (pyridine), which maximises intramolecular hydrogen bonding to yield a structure which is essentially two pairs of circular hydrogen bonded arrays with four hydroxide groups in each pair.[23,30] It was later suggested that this "pinched" conformation was actually due to the TBC[8] molecule (crystallised from pyridine) sitting on an inversion centre in the crystal lattice and therefore forms a conformation resembling that of a "chair", which could also be interpreted as two calix[4]arene molecules in partial cone conformations, also known as a "double cone" conformation.[155,156]

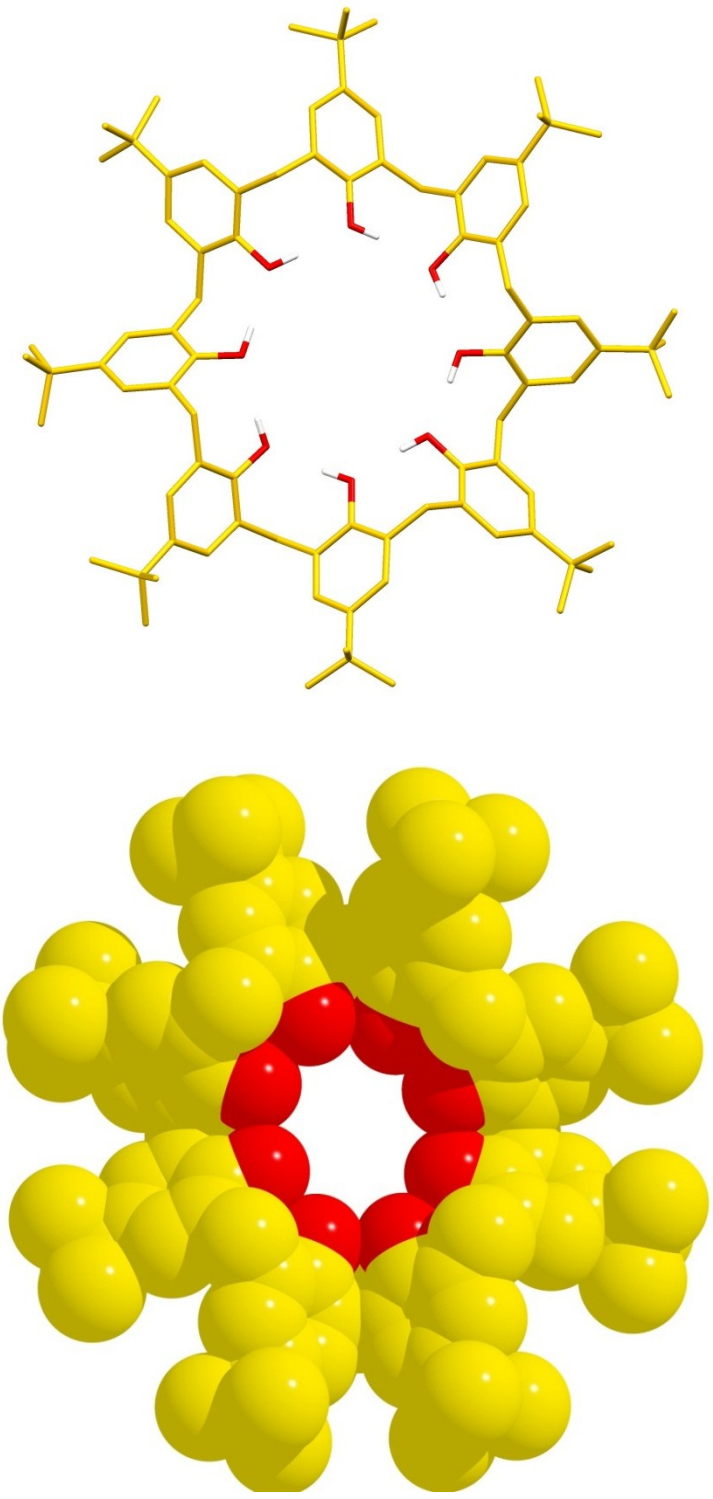

Figure 14. Structure of *p*-tert-butylcalix[8]arene (TBC[8]) (top). Space-fill representation of TBC[8] (bottom) in the pleated-loop conformation, highlighting the circular shape of the OH groups of the lower rim, responsible for the circular H-bonding. Colour code; C = gold, O = red, H = white.

TBC[8] also forms other inclusion complexes with guest molecules, such as acetonitrile,[157] in which the TBC[8] molecule is in the pleated-loop conformation, with the OH groups lying above and below the average plane of the molecule in order to maximise hydrogen bonding.[157] The guest solvent molecules sit in the V-shaped cleft formed by the pleated loop conformation of the host (Figure 15).[157]

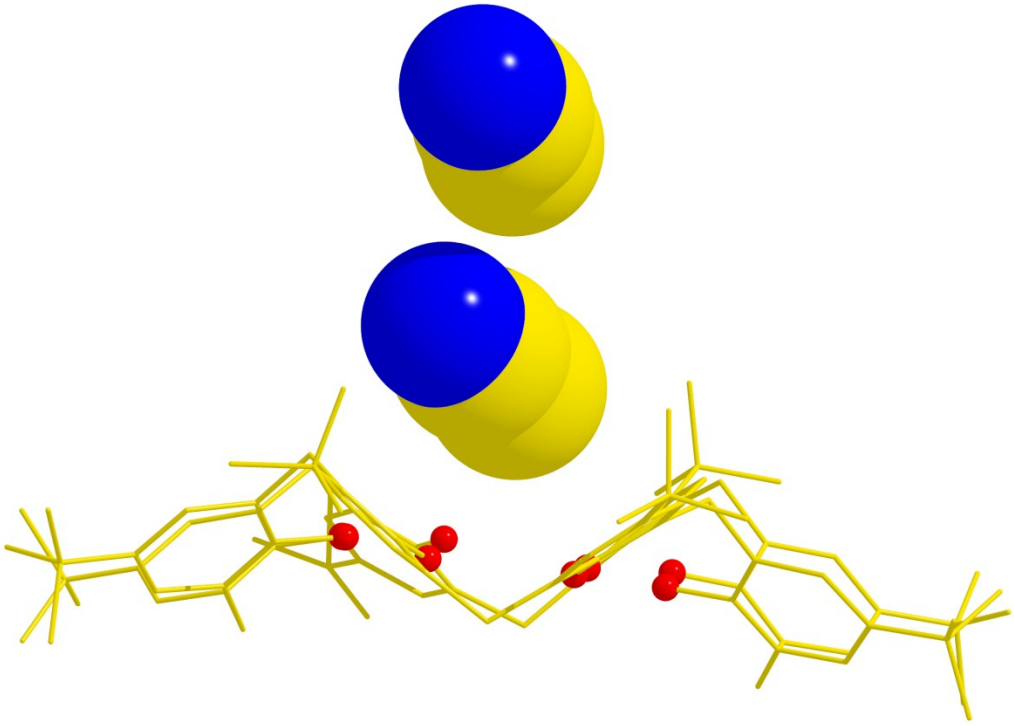

Figure 15. Space-fill representation of MeCN guest molecules in the V-shaped cleft formed by TBC[8] in the pleated loop conformation. Colour code: C = gold, O = red, N = blue, H-atoms omitted for clarity.

1.2.2 Calix[8]arene - Supported Metal Clusters

When complexed with metal ions, TBC[8] is known to form the pleated loop[158-167], double cone[158,166,168-172] and another conformation where the TBC[8] molecule "twists" to encapsulate a small cluster molecule, like the shell of a tennis ball.[75,135,173-177] There are 20 first row transition metal complexes with TBC[8]/C[8] in the literature.[75,167,173-175,178-180] Of these complexes, 13 contain titanium[173,174], 3 contain vanadium[75,174,175], there is 1 complex of manganese[180], 3 of iron[81,178,179] and 1 of cobalt.[167] Figure 16 shows the structures of two vanadium complexes containing TBC[8],[75,175] Figure 16a shows the TBC[8] molecule in the "tennis ball" conformation, encapsulating the V_2O_2 unit.[75] The molecule in Figure 16b is an example of a vanadium dimer which has been shown

to polymerise ethylene at room temperature.[175]

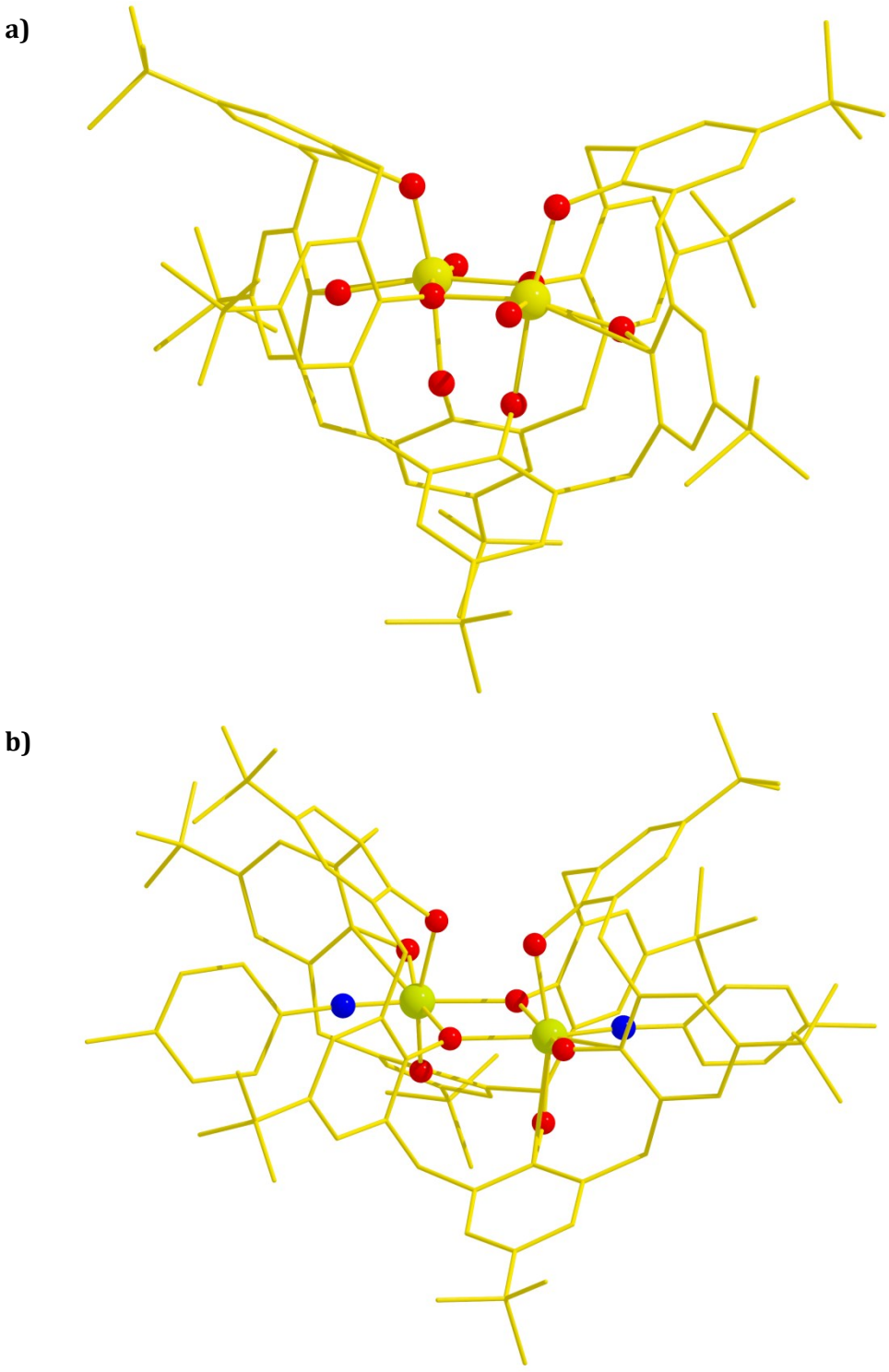

Figure 16. a) Molecular structure of the cation $[O_2V^V_2(HTBC[8])]^+$ with the TBC[8] molecule in the "tennis ball" conformation. b) Molecular structure of $[V^{III}_2(N\text{tolyl-}p)_2(H_2TBC[8])]$, which can be used in the polymerisation of ethylene at room temperature. Colour code: V^V = yellow, V^{III} = green, C = gold, O = red, N = blue, H-atoms and solvent molecules of crystallisation omitted for clarity.

Of relevance to the work presented herein is the Co^{II} dimer $(Et_3NH)_2[Co^{II}_2(H_5TBC[8])_2]$, shown in Figure 17.[167] This dimer consists of two cobalt ions coordinated to two TBC[8] ligands, which are in the pleated loop conformation with the triethylammonium cations sitting in the V-shaped cleft created by the pleated loop (Figure 18). The tetrahedral cobalt ions are bound to four phenolic O-atoms from both TBC[8] molecules (two from each) and are in a tetrahedral geometry. Magnetic studies of this complex revealed antiferromagnetic coupling between the Co^{II} centres as a result of hydrogen bonding.[167]

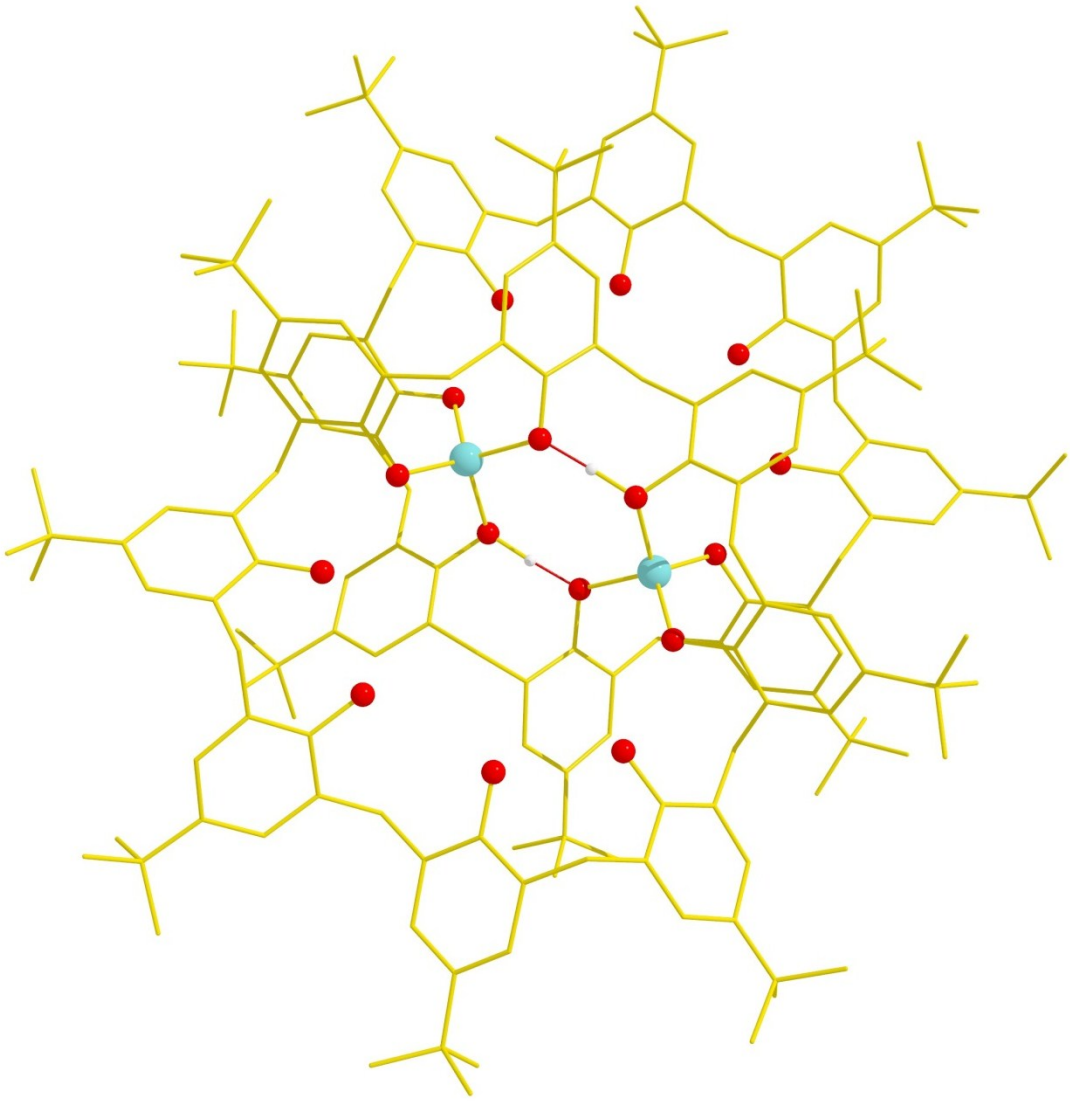

Figure 17. Molecular structure of $[Co^{II}_2(H_5TBC[8])_2]^{2+}$.Colour code: Co^{II} = light blue, C = gold, O = red, hydrogen bonding shown in red.

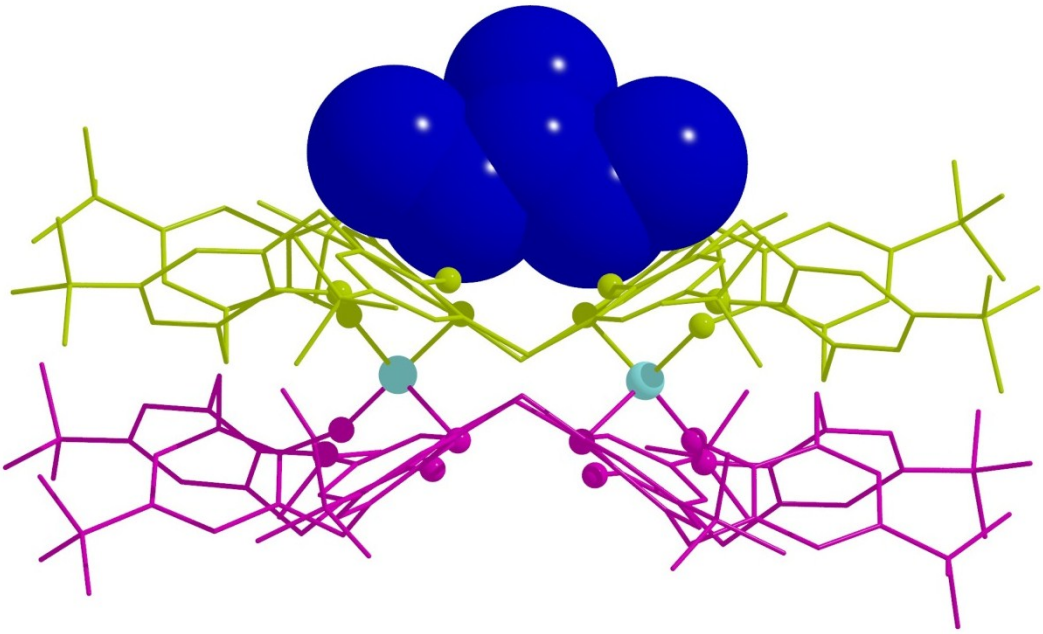

Figure 18. Space fill representation of one of the triethylammonium $(Et_3NH)^+$ cations of $(Et_3NH)_2[Co^{II}_2(TBC[8])_2]$ in the v-shaped cleft created by the TBC[8] molecules in the pleated conformation. Colour code: Co = light blue, individual TBC[8] ligands = green and purple, Et_3NH = blue, H-atoms have been omitted for clarity.

There are also complexes of TBC[8]/C[8] with second and third row transition metals[135,177,181,182] and with lanthanides and actinides.[158-160,165,166,168,169,172,183,184] The TBC[8]/C[8] molecule has been shown to support M-M multiple bonding, the first example of a M-M triple bond supported by a large calixarene ligand is shown in Figure 19.[177] The complex $\{[W^{III}_2(TBC[8])]Na_2(MeCN)_5\}\cdot 5MeCN$ consists of two 5-coordinate tungsten(III) ions which are in a square based pyramidal geometry.[177] The TBC[8] ligand is in the "tennis ball" conformation.

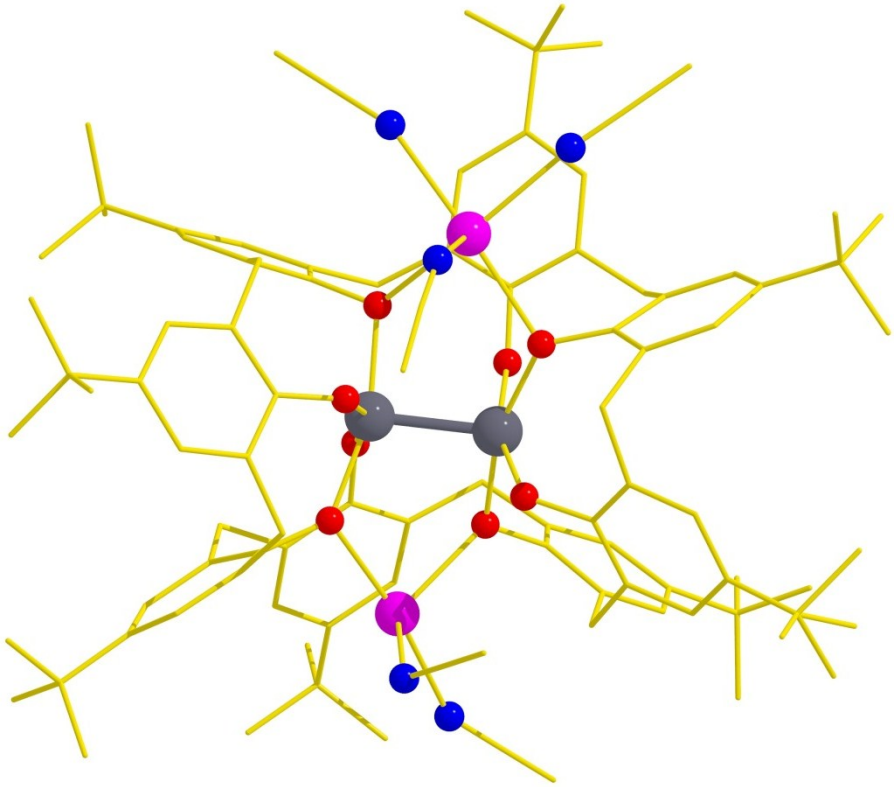

Figure 19. Molecular structure of {[W_2(TBC[8])]Na_2(MeCN)$_5$}·5MeCN, highlighting the W-W triple bond in dark grey. Colour code: W = dark grey, Na = pink, C = gold, O = red, N = blue, H-atoms omitted for clarity.

1.2.3 Oxacalix[3]arene - Supported Transition Metal Clusters

As previously discussed, the Gutsche group published that different procedures for synthesising cyclic tetramers produced a mixture of products, notably the cyclic tetramer, hexamer and octamer.[21] However, other calix[4]arene and a calix[3]arene molecules were also present in the mix. Analytical studies determined that one molecule contained four ^{t}Bu-phenol groups in a cyclic array with three connecting methylene bridging groups and one bridging ether group (CH_2OCH_2).[185] The molecule was called *p*-^{t}Bu-dihomooxacalix[4]arene (Figure 20a)[23] and the other cyclic product was *p*-^{t}Bu-homotrioxacalix[3]arene (TBOC[3]) (Figure 20b).[23,185]

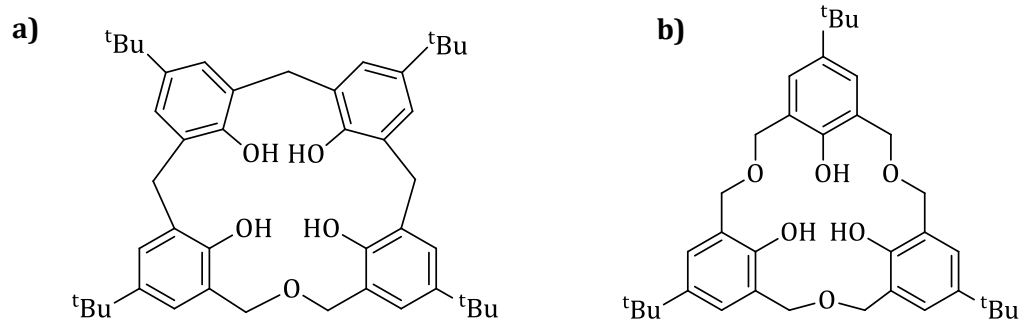

Figure 20. a) Structure of *p*-ᵗBu-dihomooxacalix[4]arene (TBOC[4]) and b) *p*-ᵗBu-homotrioxacalix[3]arene (TBOC[3]).

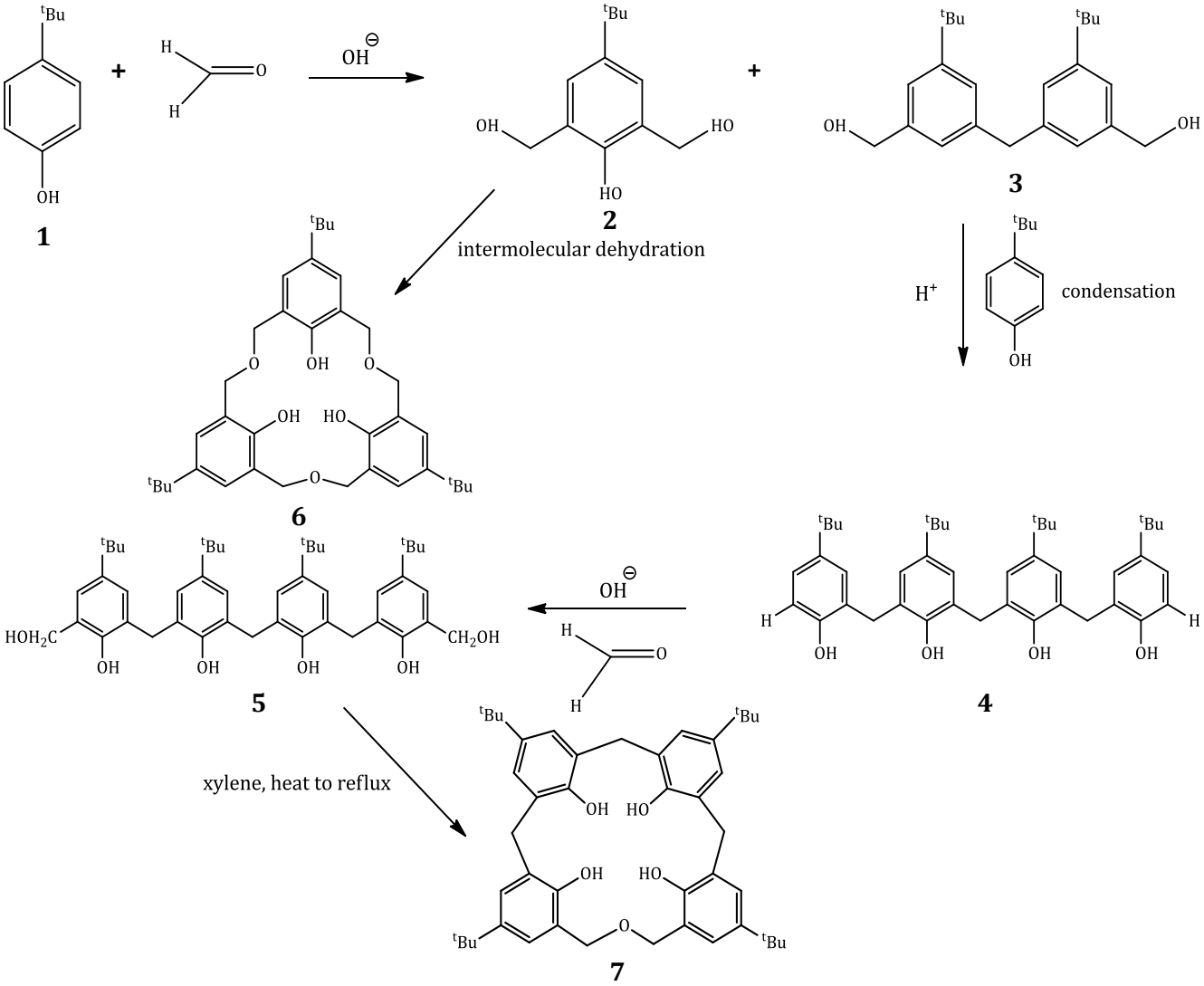

Scheme 2. Reaction pathway from the mixture formed in the reaction of tBu-phenol and formaldehyde, showing the proposed synthetic route to the oxacalixarenes TBOC[3] (6) and TBOC[4] (7).[185]

However, isolating these products in good yields and in pure form from the mix proved difficult.[185] The postulated scheme for the formation of oxacalixarenes is summarised in Scheme 2.[185] The reaction of aqueous formaldehyde with ^{t}Bu-phenol and base, under mild conditions produces the bis(hydroxymethyl) monomer (2) shown in Scheme 2.[9,185] If the conditions are harsher the bis(hydroxymethyl) dimer (3) is formed.[9,185] Condensation of (3) with ^{t}Bu-phenol in the presence of *p*-toluenesulfonic acid produces the linear tetramer (4). Reaction of (4) with aqueous formaldehyde and base yields another linear tetramer (5); when this is dissolved in xylene and heated to reflux, it converts to give the oxacalixarene *p*-^{t}Bu-dihomooxacalix[4]arene (TBOC[4]) (7).[185] However, this reaction scheme produces a mix of cyclotrimers and hexamers. In 1991 Vicens and co-workers isolated TBOC[3] and TBOC[4] through dehydration of 2,6-bis(hydroxymethyl)- *p*-^{t}Bu-phenol[186] and in 1992 reported the crystal structure of TBOC[3] showing that it exists in a bowl-shaped cone conformation (Figure 22).[187]

In 1993 Daitch and co-workers devised an improved synthetic method for producing TBOC[3].[188] Utilising the fact that bis(hydroxymethyl)- *p*-^{t}Bu-phenol can lead to TBOC[3] , they took this and under acidic conditions condensed it under high dilution to yield a mix of oxacalixarenes, one of which was TBOC[3].[188] Calixarenes were not formed under these conditions and only low yields of oxacalixarene were observed. The mono-sodium or potassium salts of TBOC[3] can be synthesised and protonation of these gives TBOC[3] in pure form and in yields of ~20-30 %.[188] Like calix[4]arenes TBOC[3] is conformationally mobile and can exist as a cone or partial cone conformer.[189]

A search of the CCDC data base shows that most metal complexes with TBOC[3] involve 4f/5f metals[190-194], with only 9 examples in the literature containing 3d metals (Sc, Ti, Fe, V, Y, Nb and Ta).[59,81,190,195-197] The examples with vanadium, tantalum(V) and niobium(V) have shown catalytic activity for the polymerization of ethylene (Figure 21).[59,197] The two vanadium(V) complexes (Figure 22) have shown the highest catalytic activity for non-metallocene systems.[59]

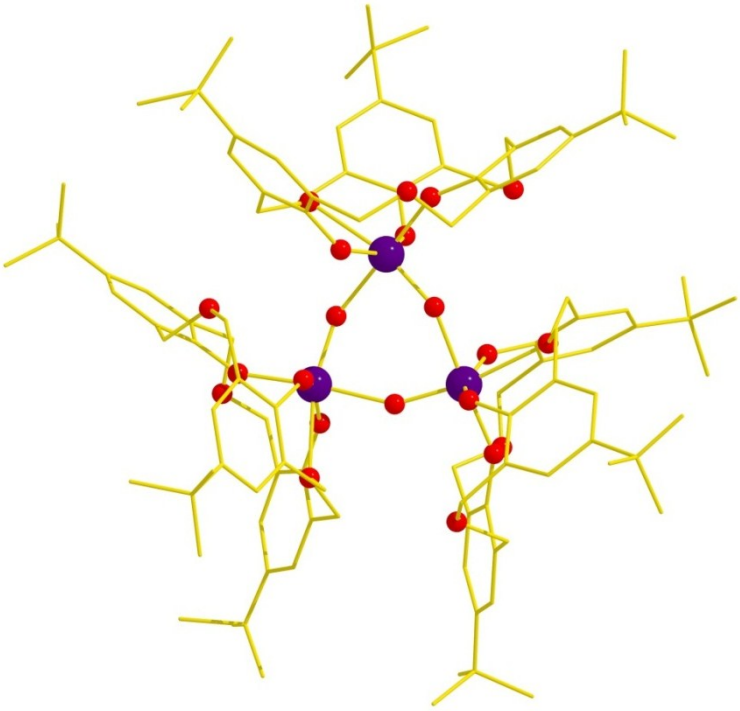

Figure 21. Molecular structure of [{M(TBOC[3])(O)}$_3$], where M = Nb^V or Ta^V. Both complexes show catalytic activity for polymerization of ethylene. Colour code: M = dark purple, C = gold, O = red, H-atoms omitted for clarity.

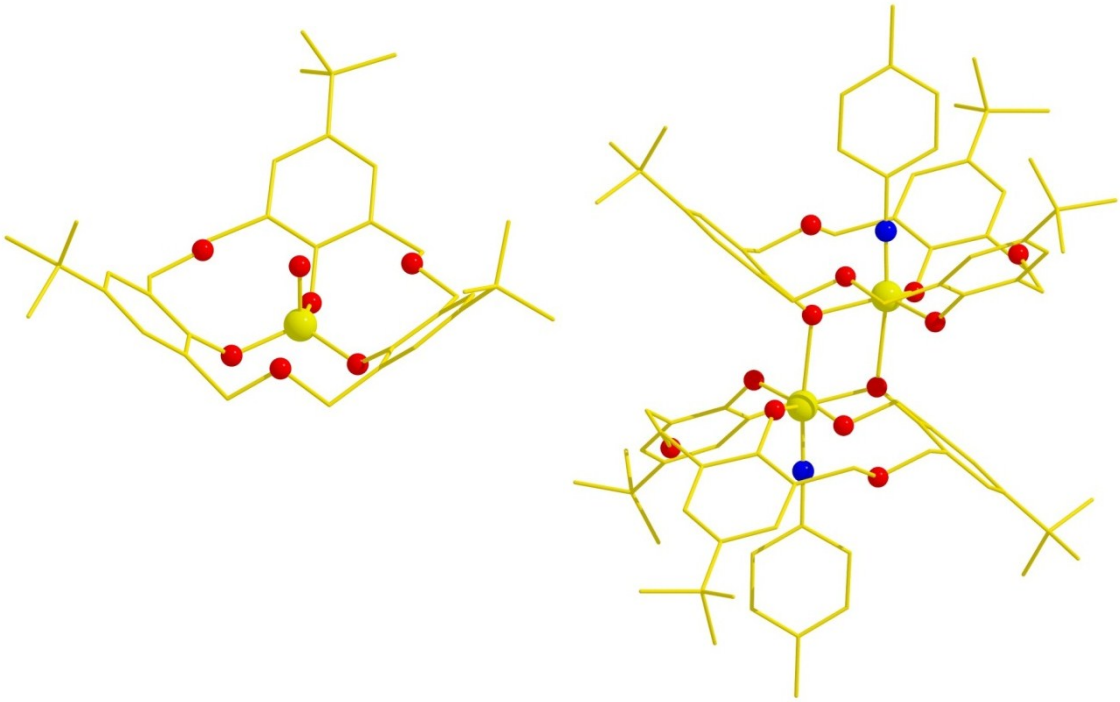

Figure 22. a) Molecular structure of two vanadium TBOC[3] complexes, [{V^V(O)(TBOC[3])}] and b)[{V^V(N-*p*-tolyl)(TBOC[3])}$_2$] (bottom), which show the highest catalytic activity for polymerization of ethylene for non-metallocene complexes. Colour code: V^V = yellow, C = gold, O = red, N = blue, H- atoms omitted for clarity.

Only two of the TBOC[3] transition metal complexes are polynuclear[59,197] and to date there have been no complexes synthesised for the study of their magnetic properties.

1.3 References

1. A. Baeyer, *Berichte der deutschen chemischen Gesellschaft*, 1872, **5**, 280-282.
2. A. Baeyer, *Berichte der deutschen chemischen Gesellschaft*, 1872, **5**, 1094-1100.
3. C. D. Gutsche, *Calixarenes*, RSC, 1992.
4. L. H. Baekeland, *US Patent* 1907, **942**, 699.
5. N. J. L. Megson, *Phenolic Resin Chemistry*, Academic Press, New York; Butterworths, London, 1958.
6. A. Zinke and E. Ziegler, *Chem. Ber.*, 1944, **77**, 264-272.
7. J. Vicens and V. Böhmer, *Calixarenes: A Versatile Class of Macrocyclic Compounds*, Springer, 1990.
8. J. B. Niederl and H. J. Vogel, *J. Am. Chem. Soc.*, 1940, **62**, 2512-2514.
9. A. Zinke, R. Kretz, E. Leggewie, K. Hössinger, G. Hoffmann, P. Weber v. Ostwalden, E. Wiesenberger and M. Sobotka, *Monatsh. Chem.*, 1952, **83**, 1213-1227.
10. A. Zinke, G. Zigeuner, K. Hössinger and G. Hoffmann, *Monatsh. Chem.*, 1948, **79**, 438-439.
11. J. W. Cornforth, P. D. Hart, G. A. Nicholls, R. J. W. Rees and J. A. Stock, *Br. J. Pharmacol.*, 1955, **10**, 73-86.
12. J. W. Cornforth, E. D. Morgan, K. T. Potts and R. J. W. Rees, *Tetrahedron*, 1973, **29**, 1659-1667.
13. R. S. Buriks, A. R. Fauke and J. H. Munch, *US Patent*, 1977, 4032514.
14. R. S. Buriks, A. R. Fauke and F. E. Mange, *US Patent*, 1978, 4098717.
15. F. Cramer and W. Kampe, *J. Am. Chem. Soc.*, 1965, **87**, 1115-1120.
16. R. L. VanEtten, J. F. Sebastian, G. A. Clowes and M. L. Bender, *J. Am. Chem. Soc.*, 1967, **89**, 3242-3253.
17. R. Breslow and S. D. Dong, *Chem. Rev.*, 1998, **98**, 1997-2012.
18. R. Breslow, A. W. Czarnik, M. Lauer, R. Leppkes, J. Winkler and S. Zimmerman, *J. Am. Chem. Soc.*, 1986, **108**, 1969-1979.
19. F. Cramer, *Angew. Chem.*, 1961, **73**, 49-56.
20. N. Hennrich and F. Cramer, *J. Am. Chem. Soc.*, 1965, **87**, 1121-1126.
21. C. D. Gutsche and R. Muthukrishnan, *J. Org. Chem.*, 1978, **43**, 4905-4906.
22. C. D. Gutsche, M. Iqbal and D. Stewart, *J. Org. Chem.*, 1986, **51**, 742-745.
23. C. D. Gutsche, B. Dhawan, K. No, H. and R. Muthukrishnan, *J. Am. Chem. Soc.*, 1981, **103**, 3782-3792.
24. B. Dhawan, S. I. Chen and C. D. Gutsche, *Die Makromolekulare Chemie*, 1987, **188**, 921-950.
25. G. D. Andreetti, R. Ungaro and A. Pochini, *J. Chem. Soc., Chem. Commun.*, 1979, 1005-1007.
26. C. D. Gutsche and M. Iqbal, *Org. Synth.*, 1990, **68**, 234.
27. C. D. Gutsche, in *Calixarenes: An Introduction*, RSC, 2008, pp. 27-60.
28. C. D. Gutsche, *Calixarenes Revisited*, RSC, 1998.
29. C. D. Gutsche, B. Dhawan, J. A. Levine, K. Hyun No and L. J. Bauer, *Tetrahedron*, 1983, **39**, 409-426.
30. C. D. Gutsche and L. J. Bauer, *Tetrahedron Lett.*, 1981, **22**, 4763-4766.
31. A. Amiri, F. Babaeie and M. Monajjemi, *Phys. Chem. Liq.*, 2008, **46**, 379-389.

32. C. D. Gutsche, in *Calixarenes: An Introduction*, The Royal Society of Chemistry, 2008, pp. 77-115.
33. J. L. Atwood, L. J. Barbour, P. K. Thallapally and T. B. Wirsig, *Chem. Commun.*, 2005, 51-53.
34. S. G. Bott, A. W. Coleman and J. L. Atwood, *J. Am. Chem. Soc.*, 1986, **108**, 1709-1710.
35. C. A. Schalley, R. K. Castellano, M. S. Brody, D. M. Rudkevich, G. Siuzdak and J. Rebek, *J. Am. Chem. Soc.*, 1999, **121**, 4568-4579.
36. E. B. Brouwer, K. A. Udachin, G. D. Enright, C. I. Ratcliffe and J. A. Ripmeester, *Chem. Commun.*, 1998, 587-588.
37. F. Gasparrini, D. Misiti, F. Della Negra, M. Maggini, G. Scorrano and C. Villani, *Tetrahedron*, 2001, **57**, 6997-7002.
38. J. L. Atwood, L. J. Barbour and A. Jerga, *Chem. Commun.*, 2002, 2952-2953.
39. E. B. Brouwer, R. D. M. Gougeon, J. Hirschinger, K. A. Udachin, R. K. Harris and J. A. Ripmeester, *Phys. Chem. Chem. Phys.*, 1999, **1**, 4043-4050.
40. E. B. Brouwer, G. D. Enright, C. I. Ratcliffe, G. A. Facey and J. A. Ripmeester, *J. Phys. Chem. B*, 1999, **103**, 10604-10616.
41. E. B. Brouwer, G. D. Enright and J. A. Ripmeester, *J. Am. Chem. Soc.*, 1997, **119**, 5404-5412.
42. R. Ungaro, A. Pochini, G. D. Andreetti and P. Domiano, *J. Chem. Soc., Perkin Trans. 2*, 1985, 197-201.
43. E. B. Brouwer, K. A. Udachin, G. D. Enright, J. A. Ripmeester, K. J. Ooms and P. A. Halchuk, *Chem. Commun.*, 2001, 565-566.
44. M. M. Olmstead, G. Sigel, H. Hope, X. Xu and P. P. Power, *J. Am. Chem. Soc.*, 1985, **107**, 8087-8091.
45. E. Bukhaltsev, I. Goldberg and A. Vigalok, *Organometallics*, 2004, **23**, 4540-4543.
46. S. R. Dubberley, A. Friedrich, D. A. Willman, P. Mountford and U. Radius, *Chem. Eur. J.*, 2003, **9**, 3634-3654.
47. N. Kotzen, I. Goldberg and A. Vigalok, *Organometallics*, 2009, **28**, 929-932.
48. J. Hesschenbrouck, E. Solari, C. Floriani, N. Re, C. Rizzoli and A. Chiesi-Villa, *J. Chem. Soc., Dalton. Trans.*, 2000, 191-198.
49. M. I. Ogden, B. W. Skelton and A. H. White, *J. Chem. Soc., Dalton. Trans.*, 2001, 3073-3077.
50. J. Zeller, S. Koenig and U. Radius, *Inorg. Chim. Acta*, 2004, **357**, 1813-1821.
51. A. Friedrich and U. Radius, *Eur. J. Inorg. Chem.*, 2004, **2004**, 4300-4316.
52. J. V. Kingston, V. Sarveswaran, S. Parkin and F. T. Ladipo, *Organometallics*, 2002, **22**, 136-144.
53. U. Radius and A. Friedrich, *Z. Anorg. Allg. Chem.*, 1999, **625**, 2154-2159.
54. E. Bukhaltsev, I. Goldberg and A. Vigalok, *Organometallics*, 2005, **24**, 5732-5736.
55. A. J. Clulow, J. D. Selby, M. G. Cushion, A. D. Schwarz and P. Mountford, *Inorg. Chem.*, 2008, **47**, 12049-12062.
56. M. Giusti, E. Solari, L. Giannini, C. Floriani, A. Chiesi-Villa and C. Rizzoli, *Organometallics*, 1997, **16**, 5610-5612.
57. V. Esposito, E. Solari, C. Floriani, N. Re, C. Rizzoli and A. Chiesi-Villa, *Inorg. Chem.*, 2000, **39**, 2604-2613.
58. A. Zanotti-Gerosa, E. Solari, L. Giannini, C. Floriani, N. Re, A. Chiesi-Villa and C. Rizzoli, *Inorg. Chim. Acta*, 1998, **270**, 298-311.
59. C. Redshaw, M. A. Rowan, L. Warford, D. M. Homden, A. Arbaoui, M. R. J. Elsegood, S. H. Dale, T. Yamato, C. P. Casas, S. Matsui and S. Matsuura, *Chem. Eur. J.*, 2007, **13**, 1090-1107.
60. E. Hoppe, C. Limberg, B. Ziemer and C. Mugge, *J. Mol. Catal. A: Chem.*, 2006, **251**, 34-40.

61. P. D. Beer, M. G. B. Drew, P. B. Leeson and M. I. Ogden, *J. Chem. Soc., Dalton. Trans.*, 1995, 1273-1283.
62. Y. Bi, Y. Li, W. Liao, H. Zhang and D. Li, *Inorg. Chem.*, 2008, **47**, 9733-9735.
63. Y. Bi, W. Liao, G. Xu, R. Deng, M. Wang, Z. Wu, S. Gao and H. Zhang, *Inorg. Chem.*, 2010, **49**, 7735-7740.
64. Y. Bi, X.-T. Wang, W. Liao, X. Wang, R. Deng, H. Zhang and S. Gao, *Inorg. Chem.*, 2009, **48**, 11743-11747.
65. Y. Bi, X.-T. Wang, W. Liao, X. Wang, X. Wang, H. Zhang and S. Gao, *J. Am. Chem. Soc.*, 2009, **131**, 11650-11651.
66. A. Bilyk, J. W. Dunlop, R. O. Fuller, A. K. Hall, J. M. Harrowfield, M. W. Hosseini, G. A. Koutsantonis, I. W. Murray, B. W. Skelton, R. L. Stamps and A. H. White, *Eur. J. Inorg. Chem.*, 2010, **2010**, 2106-2126.
67. C. Desroches, G. Pilet, S. A. Borshch, S. Parola and D. Luneau, *Inorg. Chem.*, 2005, **44**, 9112-9120.
68. C. Desroches, G. Pilet, P. Á. Szilágyi, G. Molnár, S. A. Borshch, A. Bousseksou, S. Parola and D. Luneau, *Eur. J. Inorg. Chem.*, 2006, 357-365.
69. A. Ali, S. Salunke-Gawali, C. P. Rao and J. Linares, *Inorg. Chem. Commun.*, 2004, **7**, 1298-1301.
70. A. D. Martin and C. L. Raston, *Chem. Commun.*, 2011, **47**, 9764-9772.
71. A. F. Cotton, E. V. Dikarev, C. A. Murillo and M. A. Petrukhina, *Inorg. Chim. Acta*, 2002, **332**, 41-46.
72. A. J. Petrella, N. K. Roberts, C. L. Raston, M. Thornton-Pett and R. N. Lamb, *Chem. Commun.*, 2003, 1238-1239.
73. C. Aronica, G. Chastanet, E. Zueva, S. A. Borshch, J. M. Clemente-Juan and D. Luneau, *J. Am. Chem. Soc.*, 2008, **130**, 2365-2371.
74. B. Castellano, E. Solari, C. Floriani, R. Scopelliti and N. Re, *Inorg. Chem.*, 1999, **38**, 3406-3413.
75. E. Hoppe, C. Limberg and B. Ziemer, *Inorg. Chem.*, 2006, **45**, 8308-8317.
76. C. Redshaw, D. Homden, D. L. Hughes, J. A. Wright and M. R. J. Elsegood, *Dalton Trans.*, 2009, 1231-1242.
77. V. C. Gibson, C. Redshaw, W. Clegg and M. R. J. Elsegood, *Chem. Commun.*, 1997, 1605-1606.
78. G. Karotsis, S. J. Teat, W. Wernsdorfer, S. Piligkos, S. J. Dalgarno and E. K. Brechin, *Angew. Chem. Int. Ed*, 2009, **48**, 8285-8288.
79. S. M. Taylor, G. Karotsis, R. D. McIntosh, S. Kennedy, S. J. Teat, C. M. Beavers, W. Wernsdorfer, S. Piligkos, S. J. Dalgarno and E. K. Brechin, *Chem. Eur. J.*, 2011, **17**, 7521-7530.
80. S. M. Taylor, R. D. McIntosh, C. M. Beavers, S. J. Teat, S. Piligkos, S. J. Dalgarno and E. K. Brechin, *Chem. Commun.*, 2011, **47**, 1440-1442.
81. A. Arbaoui, C. Redshaw, M. R. J. Elsegood, V. E. Wright, A. Yoshizawa and T. Yamato, *Chem.Asian J.*, 2010, **5**, 621-633.
82. H. Deligöz, Ö. Özen and G. K. Çilgi, *J. Coord. Chem.*, 2007, **60**, 73-83.
83. G. Karotsis, S. Kennedy, S. J. Dalgarno and E. K. Brechin, *Chem. Commun.*, 2010, **46**, 3884-3886.
84. J. L. Atwood, P. C. Junk, S. M. Lawrence and C. L. Raston, *Supramol. Chem.*, 1996, **7**, 15.
85. M. G. Gardiner, S. M. Lawrence, C. L. Raston, Brian W. Skelton and Allan H. White, *Chem. Commun.*, 1996, 2491-2492.
86. R. Anwander, J. Eppinger, I. Nagl, W. Scherer, M. Tafipolsky and P. Sirsch, *Inorg. Chem.*, 2000, **39**, 4713-4720.
87. L. Liu, L. N. Zakharov, J. A. Golen, A. L. Rheingold, W. H. Watson and T. A. Hanna, *Inorg. Chem.*, 2006, **45**, 4247-4260.

88. A. J. Millar, J. M. White, C. J. Doonan and C. G. Young, *Inorg. Chem.*, 2000, **39**, 5151-5155.
89. J. Zeller, S. Büschel, B. K. H. Reiser, F. Begum and U. Radius, *Eur. J. Inorg. Chem.*, 2005, **2005**, 2037-2043.
90. Y. Ishii, K.-i. Onaka, H. Hirakawa and K. Shiramizu, *Chem. Commun.*, 2002, 1150-1151.
91. A. Caselli, L. Giannini, E. Solari, C. Floriani, N. Re, A. Chiesi-Villa and C. Rizzoli, *Organometallics*, 1997, **16**, 5457-5469.
92. L. Giannini, A. Caselli, E. Solari, C. Floriani, A. Chiesi-Villa, C. Rizzoli, N. Re and A. Sgamellotti, *J. Am. Chem. Soc.*, 1997, **119**, 9198-9210.
93. J. A. Acho, L. H. Doerrer and S. J. Lippard, *Inorg. Chem.*, 1995, **34**, 2542-2556.
94. K. Iwasa, T. Kochi and Y. Ishii, *Angew. Chem. Int. Ed*, 2003, **42**, 3658-3660.
95. J. Budka, P. Lhoták, I. Stibor, J. Sýkora and I. Císařová, *Supramol. Chem.*, 2003, **15**, 353-357.
96. A. F. Danil de Namor, O. E. Piro, L. E. Pulcha Salazar, A. F. Aguilar-Cornejo, N. Al-Rawi, E. E. Castellano and F. J. Sueros Velarde, *J. Chem. Soc., Faraday Trans.*, 1998, **94**, 3097-3104.
97. W. Xu, R. J. Puddephatt, K. W. Muir and A. A. Torabi, *Organometallics*, 1994, **13**, 3054-3062.
98. M. S. Wong, P. F. Xia, P. K. Lo, X. H. Sun, W. Y. Wong and S. Shuang, *J. Org. Chem.*, 2006, **71**, 940-946.
99. B. Castellano, E. Solari, C. Floriani, N. Re, A. Chiesi-Villa and C. Rizzoli, *Chem. Eur. J.*, 1999, **5**, 722-737.
100. J. Espinas, J. r. m. Pelletier, E. Jeanneau, U. Darbost, K. C. Szeto, C. Lucas, J. Thivolle-Cazat, C. Duchamp, N. Henriques, D. Bouchu, J.-M. Basset, H. Chermette, I. Bonnamour and M. Taoufik, *Organometallics*, 2011, **30**, 3512-3521.
101. A. Zanotti-Gerosa, E. Solari, L. Giannini, C. Floriani, A. Chiesi-Villa and C. Rizzoli, *Chem. Commun.*, 1997, 183-184.
102. P. Mongrain, J. Douville, J. Gagnon, M. Drouin, A. Decken, D. Fortin and P. D. Harvey, *Can. J. Chem.*, 2004, **82**, 1452-1461.
103. A. Vigalok, Z. Zhu and T. M. Swager, *J. Am. Chem. Soc.*, 2001, **123**, 7917-7918.
104. B. Xu, P. J. Carroll and T. M. Swager, *Angew. Chem., Int. Ed. Engl.*, 1996, **35**, 2094-2097.
105. C. Redshaw, X. Liu, S. Zhan, D. L. Hughes, H. Ballie-Johnson, M. R. J. Elsegood and S. H. Dale, *Eur. J. Inorg. Chem.*, 2008, 2698-2712.
106. N. Kotzen, I. Goldberg, S. Lipstman and A. Vigalok, *Inorg. Chem.*, 2006, **45**, 5266-5268.
107. J. A. Acho and S. J. Lippard, *Inorg. Chim. Acta*, 1995, **229**, 5-8.
108. J. A. Acho, T. Ren, J. W. Yun and S. J. Lippard, *Inorg. Chem.*, 1995, **34**, 5226-5233.
109. J. Attner and U. Radius, *Chem. Eur. J.*, 2001, **7**, 783-790.
110. J. Attner and U. Radius, *Z. Anorg. Allg. Chem.*, 2002, **628**, 2345-2352.
111. D. Buccella and G. Parkin, *J. Am. Chem. Soc.*, 2006, **128**, 16358-16364.
112. M. H. Chisholm, K. Folting, W. E. Streib and D.-D. Wu, *Inorg. Chem.*, 1999, **38**, 5219-5229.
113. M. H. Chisholm, K. Folting and D.-D. Wu, *Chem. Commun.*, 1998, 379-380.
114. F. Corazza, C. Floriani, A. Chiesi-Villa and C. Guastini, *J. Chem. Soc., Chem. Commun.*, 1990, 640-641.
115. F. A. Cotton, L. M. Daniels, C. Lin and C. A. Murillo, *Inorg. Chim. Acta*, 2003, **347**, 1-8.
116. V. C. Gibson, C. Redshaw, W. Clegg and M. R. J. Elsegood, *Chem. Commun.*, 1998, 1969-1970.

117. G. Guillemot, E. Solari, R. Scopelliti and C. Floriani, *Organometallics*, 2001, **20**, 2446-2448.
118. U. Radius and J. Attner, *Eur. J. Inorg. Chem.*, 1998, **1998**, 299-303.
119. U. Radius and J. Attner, *Eur. J. Inorg. Chem.*, 1999, 2221-2231.
120. U. Radius and J. Attner, *Inorg. Chem.*, 2004, **43**, 8587-8599.
121. G. Guillemot, E. Solari, C. Floriani and C. Rizzoli, *Organometallics*, 2001, **20**, 607-615.
122. L. Giannini, E. Solari, S. Dovesi, C. Floriani, N. Re, A. Chiesi-Villa and C. Rizzoli, *J. Am. Chem. Soc.*, 1999, **121**, 2784-2796.
123. L. Giannini, G. Guillemot, E. Solari, C. Floriani, N. Re, A. Chiesi-Villa and C. Rizzoli, *J. Am. Chem. Soc.*, 1999, **121**, 2797-2807.
124. L. Giannini, S. Dovesi, E. Solari, C. Floriani, A. Chiesi-Villa and C. Rizzoli, *Angew. Chem. Int. Ed*, 1999, **38**, 807-810.
125. S. Dovesi, E. Solari, R. Scopelliti and C. Floriani, *Angew. Chem. Int. Ed*, 1999, **38**, 2388-2391.
126. L. Giannini, E. Solari, C. Floriani, N. Re, A. Chiesi-Villa and C. Rizzoli, *Inorg. Chem.*, 1999, **38**, 1438-1445.
127. F. Corazza, C. Floriani, A. Chiesi-Villa and C. Rizzoli, *Inorg. Chem.*, 1991, **30**, 4465-4468.
128. A. Lehtonen and R. Sillanpää, *Polyhedron*, 1998, **17**, 3327-3330.
129. A. Arduini, C. Massera, A. Pochini, A. Secchi and F. Ugozzoli, *New J. Chem.*, 2006, **30**, 952-958.
130. M. Brown and C. Jablonski, *Can. J. Chem.*, 2001, **79**, 463.
131. L. Giannini, E. Solari, C. Floriani, A. Chiesi-Villa and C. Rizzoli, *J. Am. Chem. Soc.*, 1998, **120**, 823-824.
132. G. Guillemot, E. Solari and C. Floriani, *Organometallics*, 2000, **19**, 5218-5230.
133. L. Giannini, E. Solari, A. Zanotti-Gerosa, C. Floriani, A. Chiesi-Villa and C. Rizzoli, *Angew. Chem., Int. Ed. Engl.*, 1996, **35**, 2825-2827.
134. L. Giannini, E. Solari, A. Zanotti-Gerosa, C. Floriani, A. Chiesi-Villa and C. Rizzoli, *Angew. Chem., Int. Ed. Engl.*, 1997, **36**, 753-754.
135. C. Redshaw and M. R. J. Elsegood, *Inorg. Chem.*, 2000, **39**, 5164-5168.
136. G. Karotsis, M. Evangelisti, S. J. Dalgarno and E. K. Brechin, *Angew. Chem. Int. Ed*, 2009, **121**, 10112-10115.
137. G. Karotsis, S. Kennedy, S. J. Teat, C. M. Beavers, D. A. Fowler, J. J. Morales, M. Evangelisti, S. J. Dalgarno and E. K. Brechin, *J. Am. Chem. Soc.*, 2010, **132**, 12983-12990.
138. M. I. Khan, Q. Chen, H. Hope, S. Parkin, C. J. O'Connor and J. Zubieta, *Inorg. Chem.*, 1993, **32**, 2929-2937.
139. M. H. Chisholm, K. Folting, J. C. Huffman and E. M. Kober, *Inorg. Chem.*, 1985, **24**, 241-245.
140. A. L. Barra, A. Caneschi, A. Cornia, F. Fabrizi de Biani, D. Gatteschi, C. Sangregorio, R. Sessoli and L. Sorace, *J. Am. Chem. Soc.*, 1999, **121**, 5302-5310.
141. M. Murugesu, J. Raftery, W. Wernsdorfer, G. Christou and E. K. Brechin, *Inorg. Chem.*, 2004, **43**, 4203-4209.
142. T. C. Stamatatos, K. M. Poole, K. A. Abboud, W. Wernsdorfer, T. A. O'Brien and G. Christou, *Inorg. Chem.*, 2008, **47**, 5006-5021.
143. I. S. Tidmarsh, L. J. Batchelor, E. Scales, R. H. Laye, L. Sorace, A. Caneschi, J. Schnack and E. J. L. McInnes, *Dalton Trans.*, 2009, 9402-9409.
144. P. King, W. Wernsdorfer, K. A. Abboud and G. Christou, *Inorg. Chem.*, 2005, **44**, 8659-8669.
145. R. Bagai, K. A. Abboud and G. Christou, *Inorg. Chem.*, 2008, **47**, 621-631.
146. N. Lah, I. Leban and R. Clerac, *Eur. J. Inorg. Chem.*, 2006, 4888-4894.

147. R. T. W. Scott, S. Parsons, M. Murugesu, W. Wernsdorfer, G. Christou and E. K. Brechin, *Angew. Chem. Int. Ed*, 2005, **44**, 6540-6543.
148. A. Prescimone, J. Wolowska, G. Rajaraman, S. Parsons, W. Wernsdorfer, M. Murugesu, G. Christou, S. Piligkos, E. J. L. McInnes and E. K. Brechin, *Dalton Trans.*, 2007, 5282-5289.
149. M. Manoli, A. Collins, S. Parsons, A. Candini, M. Evangelisti and E. K. Brechin, *J. Am. Chem. Soc.*, 2008, **130**, 11129-11139.
150. J. Yoo, W. Wernsdorfer, E.-C. Yang, M. Nakano, A. L. Rheingold and D. N. Hendrickson, *Inorg. Chem.*, 2005, **44**, 3377-3379.
151. Y. Li, W. Wernsdorfer, R. Clérac, I. J. Hewitt, C. E. Anson and A. K. Powell, *Inorg. Chem.*, 2006, **45**, 2376-2378.
152. E. E. Moushi, T. C. Stamatatos, W. Wernsdorfer, V. Nastopoulos, G. Christou and A. J. Tasiopoulos, *Inorg. Chem.*, 2008, **48**, 5049-5051.
153. J. H. Munch and C. D. Gutsche, *Org. Synth.*, 1990, **68**, 243.
154. C. D. Gutsche, A. E. Gutsche and A. I. Karaulov, *J. Inclusion Phenom. Macrocyclic Chem.*, 1985, **3**, 447-451.
155. M. Czugler, S. Tisza and G. Speier, *J. Inclusion Phenom. Macrocyclic Chem.*, 1991, **11**, 323-331.
156. R.-B. Huang, N.-F. Zheng, S.-Y. Xie and L.-S. Zheng, *J. Inclusion Phenom. Macrocyclic Chem.*, 2001, **40**, 121-124.
157. S. H. Dale, M. R. J. Elsegood and C. Redshaw, *CrystEngComm*, 2003, **5**, 368-373.
158. J. Harrowfield, M. Ogden and A. White, *Aust. J. Chem.*, 1991, **44**, 1237-1247.
159. J. M. Harrowfield, M. I. Ogden, W. R. Richmond and A. H. White, *J. Chem. Soc., Dalton. Trans.*, 1991, 2153-2160.
160. P. Thuéry, N. Keller, M. Lance, J.-D. Vigner and M. Nierlich, *Acta Crys.*, 1995, **51**, 1570-1574.
161. N. P. Clague, J. D. Crane, D. J. Moreton, E. Sinn, S. J. Teat and N. A. Young, *J. Chem. Soc., Dalton. Trans.*, 1999, 3535-3536.
162. N. P. Clague, J. D. Crane, E. Sinn, N. A. Young, W. Clegg, S. J. Coles, S. J. Teat and D. J. Moreton, *Chem. Commun.*, 1999, 379-380.
163. R. D. Bergougnant, A. Y. Robin and K. M. Fromm, *Cryst. Growth Des.*, 2005, **5**, 1691-1694.
164. R. D. Bergougnant, A. Y. Robin and K. M. Fromm, *Tetrahedron*, 2007, **63**, 10751-10757.
165. J. M. Harrowfield, M. I. Ogden, B. W. Skelton and A. H. White, *Dalton Trans.*, 2010, **39**, 8313-8318.
166. J.-C. G. Bünzli and F. Besançon, *Phys. Chem. Chem. Phys.*, 2005, **7**, 2191-2198.
167. S. Petit, G. Pilet, D. Luneau, L. F. Chibotaru and L. Ungur, *Dalton Trans.*, 2007, 4582-4588.
168. B. M. Furphy, J. M. Harrowfield, D. L. Kepert, B. W. Skelton, A. H. White and F. R. Wilner, *Inorg. Chem.*, 1987, **26**, 4231-4236.
169. J. Harrowfield, M. Ogden and A. White, *Aust. J. Chem.*, 1991, **44**, 1249-1262.
170. L. Liu, L. N. Zakharov, J. A. Golen, A. L. Rheingold and T. A. Hanna, *Inorg. Chem.*, 2008, **47**, 11143-11153.
171. D. Mendoza-Espinosa, A. L. Rheingold and T. A. Hanna, *Dalton Trans.*, 2009, 5226-5238.
172. S. Fleming, C. D. Gutsche, J. M. Harrowfield, M. I. Ogden, B. W. Skelton, D. F. Stewart and A. H. White, *Dalton Trans.*, 2003, 3319-3327.
173. G. E. Hofmeister, F. E. Hahn and S. F. Pedersen, *J. Am. Chem. Soc.*, 1989, **111**, 2318-2319.
174. G. E. Hofmeister, E. Alvarado, J. A. Leary, D. I. Yoon and S. F. Pedersen, *J. Am. Chem. Soc.*, 1990, **112**, 8843-8851.

175. V. C. Gibson, C. Redshaw and M. R. J. Elsegood, *J. Chem. Soc., Dalton. Trans.*, 2001, 767-769.
176. V. C. Gibson, C. Redshaw and M. R. J. Elsegood, *New J. Chem.*, 2002, **26**, 16-19.
177. V. C. Gibson, C. Redshaw and M. R. J. Elsegood, *Chem. Commun.*, 2002, 1200-1201.
178. A. E. Wetherby, L. R. Goeller, A. G. DiPasquale, A. L. Rheingold and C. S. Weinert, *Inorg. Chem.*, 2007, **46**, 7579-7586.
179. R. A. Green, A. L. Rheingold and C. S. Weinert, *Inorg. Chim. Acta*, 2009, **362**, 3159-3164.
180. R. D. McIntosh, S. M. Taylor, S. Sanz, C. M. Beavers, S. J. Teat, E. K. Brechin and S. J. Dalgarno, *Dalton Trans.*, 2011, **40**, 12265-12270.
181. C. Redshaw and M. R. J. Elsegood, *Eur. J. Inorg. Chem.*, 2003, 2071-2074.
182. V. C. Gibson, C. Redshaw, W. Clegg and M. R. J. Elsegood, *J. Chem. Soc., Chem. Commun.*, 1995, 2371-2372.
183. J. C. G. Bünzli, P. Froidevaux and J. M. Harrowfield, *Inorg. Chem.*, 1993, **32**, 3306-3311.
184. P. Froidevaux and J. C. G. Buenzli, *J. Phys. Chem.*, 1994, **98**, 532-536.
185. B. Dhawan and C. D. Gutsche, *J. Org. Chem.*, 1983, **48**, 1536-1539.
186. P. Zerr, M. Mussrabi and J. Vicens, *Tetrahedron Lett.*, 1991, **32**, 1879-1880.
187. K. Suzuki, H. Minami, Y. Yamagata, S. Fujii, K. Tomita, Z. Asfari and J. Vicens, *Acta Crys.*, 1992, **48**, 350-352.
188. P. D. Hampton, Z. Bencze, W. Tong and C. E. Daitch, *J. Org. Chem.*, 1994, **59**, 4838-4843.
189. K. Cottet, P. M. Marcos and P. J. Cragg, *Beilstein J. Org. Chem.*, 2012, **8**, 201-226.
190. C. E. Daitch, P. D. Hampton, E. N. Duesler and T. M. Alam, *J. Am. Chem. Soc.*, 1996, **118**, 7769-7773.
191. P. Thuéry, M. Nierlich, B. Masci, Z. Asfari and J. Vicens, *J. Chem. Soc., Dalton. Trans.*, 1999, 3151-3152.
192. B. Masci, M. Nierlich and P. Thuery, *New J. Chem.*, 2002, **26**, 120-128.
193. B. Masci, M. Nierlich and P. Thuery, *New J. Chem.*, 2002, **26**, 766-774.
194. B. Masci and P. Thuery, *Acta. Crys.,*, 2005, **61**, m2278-m2280.
195. C. E. Daitch, P. D. Hampton and E. N. Duesler, *Inorg. Chem.*, 1995, **34**, 5641-5645.
196. P. D. Hampton, C. E. Daitch, T. M. Alam, Z. Bencze and M. Rosay, *Inorg. Chem.*, 1994, **33**, 4750-4758.
197. C. Redshaw, M. Rowan, D. M. Homden, M. R. J. Elsegood, T. Yamato and C. Pérez-Casas, *Chem. Eur. J.*, 2007, **13**, 10129-10139.

Chapter 2
A Family of Calix[4]arene-Supported [$Mn^{III}_2Mn^{II}_2$] Clusters

2.1 Introduction

Synthetic strategies for making polymetallic clusters of paramagnetic transition-metal ions range from serendipitous self-assembly through to "rational" design and can employ ligands ranging from very small, simple organic molecules that are commercially available to large and complicated organic molecules made by means of multistep procedures.[1-11] The goal of both approaches is the same—the synthesis and characterisation of molecules that chemists, physicists and theoreticians find magnetically interesting, whether that pertains to a greater understanding of the fundamental physical laws governing the behaviour or an advancement toward applicability.[12-15] One of our long-standing synthetic strategies for making high-spin molecules of the first-row of transition metals is the use of polyalkoxide ligands, such as the tripodal 1,1,1-tris(hydroxymethyl)ethane and its many analogues (Figure 1a).[16]

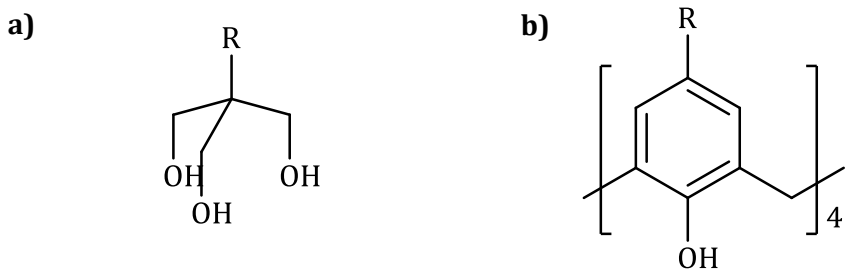

Figure 1.a) Structure of 1,1,1tris(hydroxymethyl)ethane (R=H). b) General structure of calix[4]arenes TBC[4] (R=^{t}Bu) and C[4] (R=H).

These are triangular face-capping ligands that have been shown to bridge up to a maximum of seven metal centres (a centred metallic hexagon) when fully deprotonated.[17] The basic [M_3] triangular building blocks formed in situ self-assemble to direct the formation of elaborate molecular structures depending on the reaction conditions employed.[18] The use of tetrapodal alkoxides, such as calix[4]arenes (Figure 1b), is a natural extension to this strategy but one that offers a great deal more flexibility and "control", since the organic skeleton of the ligand is, in theory, easy to derivatise pre- or post-cluster synthesis, allowing much scope for design.

These cyclic, typically bowl-shaped molecules have been used previously and extensively in the formation of supramolecular structures and across a vast breadth of organic and inorganic chemistry.[19-23] The calixarene *p*-*t*Bu-calix[4]arene (TBC[4]; Figure 1b, R = ^{t}Bu) is readily accessible from cheap starting materials on a large scale and is the general starting point for alteration to the general molecular framework.[24,25]

An example of such alteration is the facile de-*tert*butylation of TBC[4] to afford calix[4]arene (C[4]; Figure 1b, R=H).[25] Such transformations can also be carried out on a large scale, often at limited cost, and the range of possible functionalisation/alteration to the general framework is virtually unlimited, presenting the chemist with a virtually unbounded range of molecular building blocks.

From a coordination chemist's perspective, the calix[4]arene polyphenolic pocket at the lower-rim is a hugely attractive feature for metal complexation.[26,27] Phenol, biphenols and other bi-, tri- and polyols have proven to be tremendously successful ligands in cluster synthesis,[28-31] and in this regard thia- and sulfonyl-bridged calix[4]arenes[32-35] have been widely exploited for this purpose. This is predominantly due to the fact that the S, SO or SO_2 groups can heavily influence the resulting coordination chemistry. Generally, the presence of these donor atoms has the effect of "translating" the target metal ions away from the centre of the polyphenolic pocket (Figure 2a), and this results in the formation of various polynuclear metal-cluster motifs. The use of methylene-bridged calix[4]arenes for such purposes has been extremely limited,[36-41] perhaps due to the lack of such additional bridging donor atoms. From our perspective however, this may be viewed as an advantage, and offers an alternative type of control over the positioning of transition-metal centres and subsequent polynuclear metal-cluster formation (Figure 2b).

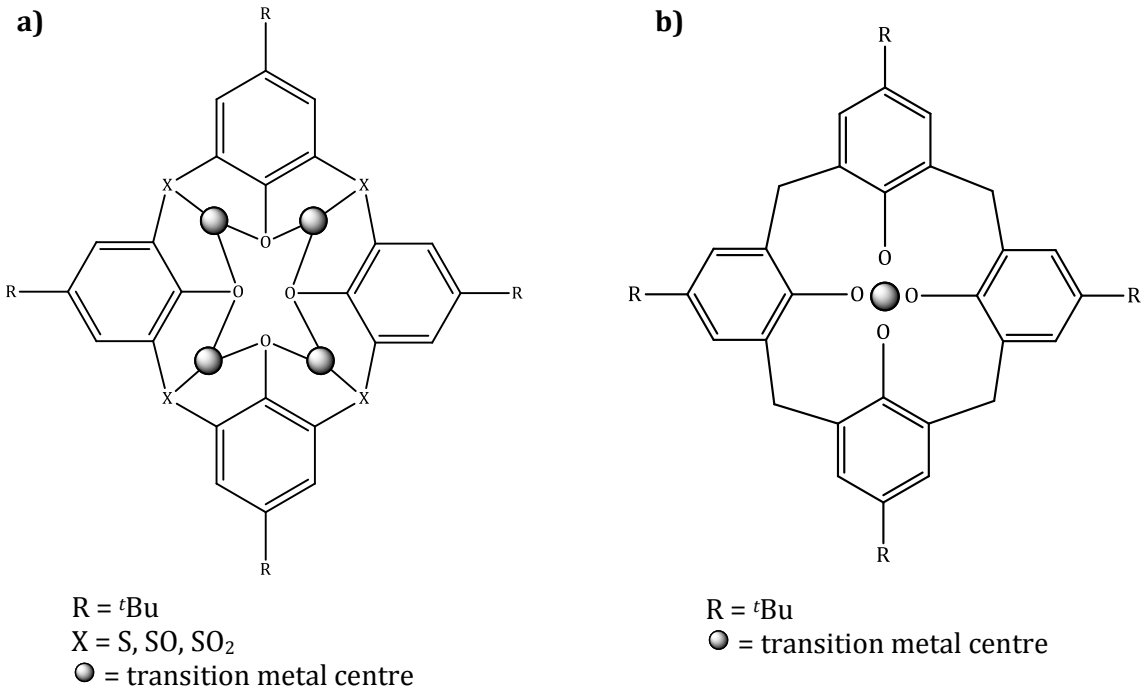

Figure 2. a) Schematic showing the "translation" of transition metal ions away from the polyphenolic pocket in thia- and sulfonyl-bridged calix[4]arenes due to the influence of additional donor atoms. b) Schematic showing positioning of transition metal ions within the polyphenolic pocket of methylene-bridged calix[4]arenes.

Our recent studies into cluster formation with methylene bridged calix[4]arenes have afforded, amongst others, a family of enneanuclear Cu^{II} tri-capped trigonal prismatic clusters that act as versatile - binding materials (Figure 3 a) and a family of [$Mn^{III}_4Ln^{III}_4$] clusters in which the replacement of one Ln^{III} ion for another invokes changes in the observed magnetic properties ranging from single-molecule magnet (SMM) behaviour to an enhanced magnetocaloric effect (MCE) in otherwise structurally analogous molecules (Figure 3b).[36-41] In addition to the above, we also communicated the formation and magnetic properties of the calixarene-supported cluster [$Mn^{III}_2Mn^{II}_2(OH)_2$(TBC[4])$_2(DMF)_6$]·2MeOH (**1**) that behaves as an SMM.[40,41]

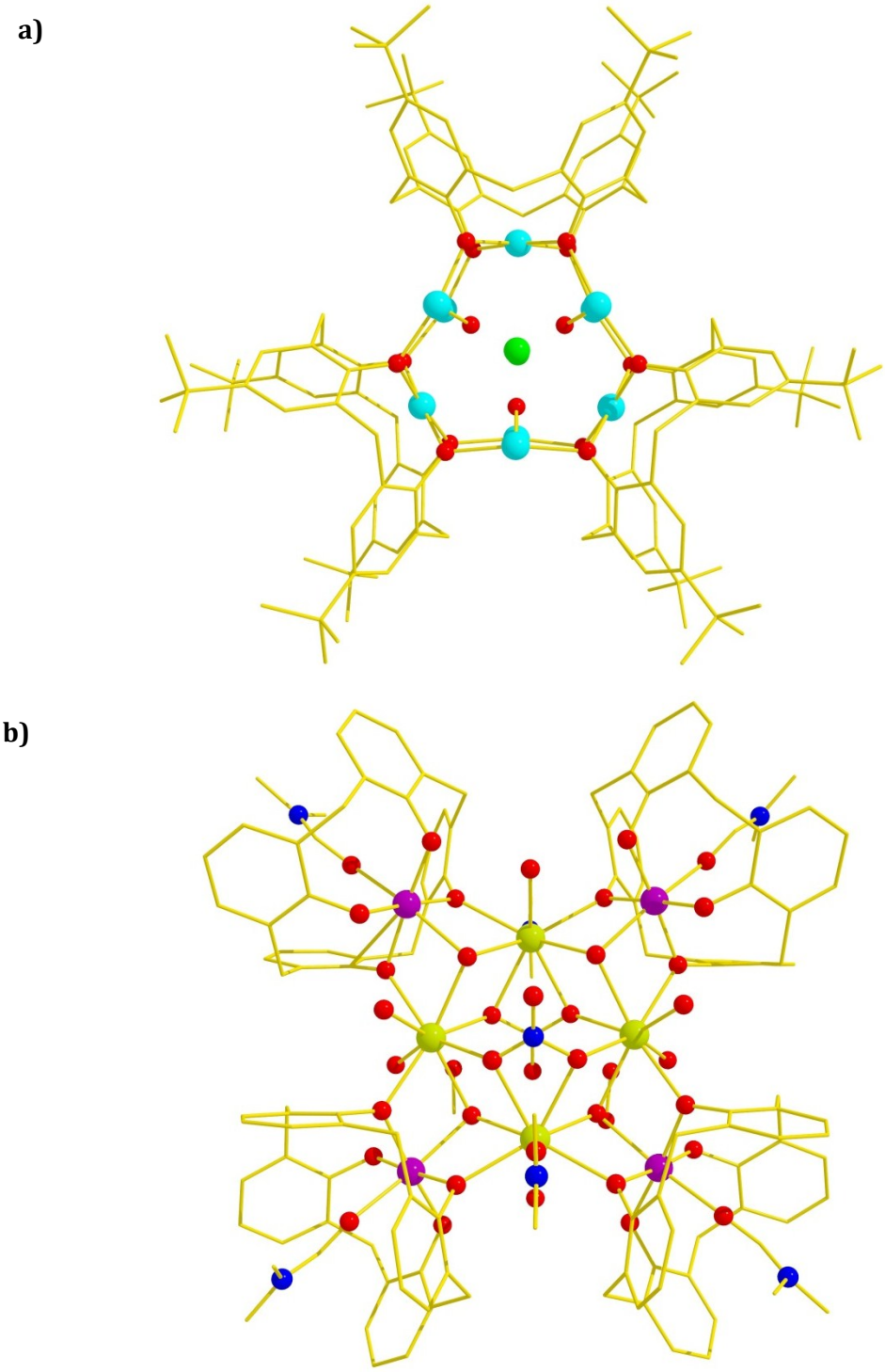

Figure 3. a) Molecular structure of TBC[4] supported [Cu^{II}_9] trigonal prismatic cluster viewed down the triangular faces of the prism. b) Molecular structure of a C[4] supported [$Mn^{III}_4Ln^{III}_4$] cluster describing a square of Ln ions housed within a square of Mn ions. Colour code: Mn^{III} = purple, Ln = green, Cu = light blue, O = red, N = blue, C = gold, H-atoms omitted for clarity.

Herein we report the extension of these studies describing the formation and self-assembly properties of a family of seven such calix[4]arene-stabilised [$Mn^{III}_2Mn^{II}_2$] clusters (**1**–**7**). The molecular formulae for these complexes are as follows:

$[Mn^{III}_2Mn^{II}_2(OH)_2(TBC[4])_2(DMF)_4(H_2O)_2]\cdot 4MeOH\cdot 2DMF$ (**2**)

$[Mn^{III}_2Mn^{II}_2(OH)_2(TBC[4])_2(DMF)_6]\cdot 2.8MeOH$ (**3**)

$[Mn^{III}_2Mn^{II}_2(OH)_2(TBC[4])_2(DMF)_4(EtOH)(H_2O)]$ (**4**)

$[Mn^{III}_2Mn^{II}_2(OH)_2(TBC[4])_2(DMSO)_6]\cdot 2MeOH\cdot 2DMSO$ (**5**)

$[Mn^{III}_2Mn^{II}_2(OH)_2(TBC[4])_2(DMSO)_6]$ (**6**)

$[Mn^{III}_2Mn^{II}_2(OH)_2(C[4])_2(MeOH)_6]\cdot 4MeOH$ (**7**)

The syntheses (see Experimental Section) of all seven members of the family are essentially the same; the most basic recipe involving the reaction of hydrated Mn^{II} chloride with TBC[4] or C[4] and base in a 50:50 solvent mixture of DMF or DMSO and alcohol. The majority of the syntheses reported here also involved addition of carboxylate co-ligands. In this regard we have screened many potential co-ligands, but in all cases we found that these were not included in the resulting assemblies. These different condition sets afford variant clusters possessing disparate ligated and co-crystallised solvent molecules relative to our reported motif, a feature that influences the extended self-assembly of these SMM building blocks. For the sake of brevity we will discuss the general structural and magnetic properties common to all complexes, and will then describe differences in the composition of peripheral/co-crystallised solvent molecules around the cluster cores and their resulting extended structures. Full crystallographic details for the structures reported here are listed in Table 1 and selected bond lengths are given in the appendix.

Table 1. Crystal structure information for **2**-**7**.

	2[a]	**3**[a]	**4**[a,b]	**5**[a]	**6**[b,c]	**7**[a]
Chemical formula	$C_{110}H_{168}Mn_4N_6O_{22}$	$C_{108.80}H_{159.20}Mn_4N_6O_{18.80}$	$C_{102}H_{142}Mn_4N_4O_{16}$	$C_{106}H_{138}Mn_4O_{20}S_8$	$C_{100}H_{142}Mn_4O_{16}S_6$	$C_{66}H_{80}Mn_4O_{20}$
M_r	2146.26	2071.78	1899.96	2208.40	2012.26	1413.06
Crystal system	Triclinic	Monoclinic	Triclinic	Triclinic	Monoclinic	Orthorhombic
Space group	*P*-1	$P2_1/n$	*P*-1	*P*-1	*C*2/*c*	*Pnma*
a (Å)	12.47(3)	21.2033(14)	12.483(2)	12.1723(17)	25.9355(15)	19.504(7)
b (Å)	12.76(3)	12.5350(8)	12.574(2)	12.4088(18)	24.3125(14)	20.999(6)
c (Å)	18.94(4)	22.3564(14)	19.522(4)	18.397(3)	21.6817(13)	15.510(8)
α (°)	94.72(6)	90	107.842(8)	87.094(5)	90	90
β (°)	105.80(5)	114.581(3)	99.363(7)	83.541(5)	118.169(1)	90
γ (°)	95.51(10)	90	92.051(7)	85.961(6)	90	90
V (Å^3)	2868(12)	5403.5(6)	2866.2(9)	2751.7(7)	12052.3(12)	6352(4)
Z	1	2	1	1	4	4
F(000)	1146	2209	1010	1162	4264	2944
Crystal size (mm)	0.35 × 0.30 × 0.28	0.50 × 0.45 × 0.40	0.30 × 0.30 × 0.25	0.35 × 0.30 × 0.30	0.14 × 0.12 × 0.03	0.45 × 0.35 × 0.30
No. of measured, independent and observed [$I > 2\sigma(I)$] reflections	22471, 5660, 3888	52047, 13376, 10412	17136, 4895, 3236	34247, 8996, 6346	70552, 13359, 10397	30484, 6174, 4512
R_{int}	0.084	0.038	0.067	0.055	0.067	0.056
$R_1[I > 2\sigma(I)]$	0.078	0.048	0.095	0.074	0.105	0.046
$wR_2(F^2)$	0.189	0.135	0.254	0.216	0.316	0.098
GOF on F^2	1.11	1.04	1.62	1.03	2.17	1.04

[a] Data collected on a Bruker Apex II diffractometer operating with $Mo_{K\alpha}$ radiation (λ = 0.71073 Å) at 100(2) K. [b] The routine SQUEEZE was applied in order to remove diffuse electron density associated with co-crystallised solvent molecules that could not be modelled appropriately. [c] Data collected on a Bruker Apex II diffractometer operating with synchrotron radiation (λ= 0.7749 Å) at 100(2) K.

2.2 Experimental

2.2.1 Syntheses

All manipulations were performed under aerobic conditions using materials as received (reagent grade). Elemental analyses (C, H, N) were performed by the EaStCHEM microanalysis service. Variable-temperature, solid-state direct current (dc) magnetic susceptibility data down to 5 K were collected on a Quantum Design MPMS-XL SQUID magnetometer equipped with a 7 T dc magnet. Diamagnetic corrections were applied to the observed paramagnetic susceptibilities using Pascal's constants. TBC[4] and C[4] were synthesised according to literature procedures,[24,25,42] and were checked for purity by ^{1}H NMR and mass spectrometry prior to use in cluster synthesis.

$[Mn^{III}_2Mn^{II}_2(OH)_2(TBC[4])_2(DMF)_6]\cdot 2MeOH$ (1)[40]

$MnCl_2\cdot 4H_2O$ (0.1 g, 0.5 mmol), TBC[4] (0.1 g, 0.15 mmol) and NEt_3 (0.1 g, 1.0 mmol) were dissolved in a mixture of DMF (10 mL) and MeOH (10 mL) and stirred for 1 h. X-ray quality crystals of **1** were obtained in good yield (~ 40 %) after slow evaporation of the mother liquor. Elemental analysis found (calc. %) for $C_{106}H_{146}Mn_4N_6O_{16}$: C 64.02 (64.30), H 7.54 (7.43) , N 4.21 (4.24).

$[Mn^{III}_2Mn^{II}_2(OH)_2(TBC[4])_2(DMF)_4(H_2O)_2]\cdot 4MeOH\cdot 2DMF$ (2)

$MnCl_2.4H_2O$ (0.1 g, 0.5 mmol), TBC[4] (0.1 g, 0.15 mmol), NaO_2CCCl_3 (0.150 g, 1.0 mmol) and NEt_3 (0.1 g, 1.0 mmol) were dissolved in a mixture of DMF (10 mL) and MeOH (15 mL) and stirred for 2.5 h. X-ray quality crystals were obtained in reasonable yield (~30 %) after filtration and slow evaporation the mother liquor. Elemental analysis found (calc. %) for: $C_{110}H_{168}Mn_4N_6O_{22}$: C 61.37 (61.55), H 7.77 (7.90), N 3.89 (3.94).

$[Mn^{III}_2Mn^{II}_2(OH)_2(TBC[4])_2(DMF)_6]\cdot 2.8MeOH$ (3)

$MnCl_2.4H_2O$ (0.1 g, 0.5mmol), TBC[4] (0.16 g, 0.25 mmol), $NaO_2C(C_5H_5N)$ (0.145 g, 1.0 mmol) and NEt_3 (0.05 g, 0.5 mmol) were dissolved in a mixture of DMF (10 mL) and MeOH (15 mL) and stirred for 2.5 h. X-ray quality crystals were obtained in reasonable yield (~35 %) after filtration and slow evaporation the mother liquor. Elemental analysis found (calc. %) for: $C_{108.8}H_{159.2}Mn_4N_6O_{18.8}$: C 63.41 (63.50), H 7.62 (7.79), N 4.11 (4.05).

$[Mn^{III}_2Mn^{II}_2(OH)_2(TBC[4])_2(DMF)_4(EtOH)(H_2O)]$ (4)

$MnCl_2.4H_2O$ (0.1 g, 0.5 mmol), TBC[4] (0.16 g, 0.25 mmol), sodium 2-thiophenecarboxylate ($NaO_2CC_4H_3S$) (0.150 g, 1.0 mmol) and NEt_3 (0.05 g, 0.5 mmol) were dissolved in a mixture of DMF (10 mL) and EtOH (15 mL) and stirred for 2.5 h. X-ray quality crystals were obtained in sufficient yield (~35 %) after filtration and slow evaporation the mother liquor. Elemental analysis found (calc. %) for: $C_{102}H_{142}Mn_4N_4O_{16}$: C 64.33 (64.48), H 7.46 (7.53), N 2.89 (2.95).

$[Mn^{III}_2Mn^{II}_2(OH)_2(TBC[4])_2(DMSO)_6]$·2MeOH·2DMSO (5)

$MnCl_2.4H_2O$ (0.1 g, 0.5 mmol), TBC[4] (0.1 g, 0.15 mmol), sodium 4-nitrobenzoate ($NaO_2CPh(NO_2)$) (0.189 g, 1.0 mmol), NH_4ClO_4 (0.117 g, 1 mmol) and NEt_4OH (0.1 g, 1.0 mmol) were dissolved in a mixture of DMSO (10 mL) and MeOH (15 mL) and stirred for 2.5 h. X-ray quality crystals were obtained in good yield (~40 %) after filtration and slow evaporation the mother liquor. Elemental analysis found (calc. %) for: $C_{106}H_{138}Mn_4O_{20}S_8$: C 57.61 (57.66), H 6.34 (6.28).

$[Mn^{III}_2Mn^{II}_2(OH)_2(TBC[4])_2(DMSO)_6]$ (6)

$MnCl_2.4H_2O$ (0.15 g, 0.75 mmol), TBC[4] (0.1 g, 0.15 mmol), sodium 3,5-dimethylbenzoate ($NaO_2CPh(3,5\text{-}Me)_2$) (0.172 g, 1.0 mmol) and NEt_4OH (0.1 g, 1.0 mmol) were dissolved in a mixture of DMSO (10 mL) and MeOH (15 mL) and stirred for 2.5 h. X-ray quality crystals were obtained in good yield (~ 40%) after filtration and slow evaporation the mother liquor. Elemental analysis found (calc. %) for: $C_{100}H_{142}Mn_4O_{16}S_6$: C 59.87 (59.68), H 7.21 (7.12).

$[Mn^{III}_2Mn^{II}_2(OH)_2(C[4])_2(MeOH)_6]$·4MeOH (7)

$MnCl_2.4H_2O$ (0.1 g, 0.5 mmol), C[4] (0.1 g, 0.2 mmol), sodium trichloroacetate (NaO_2CCCl_3) (0.150 g, 1.0 mmol) and NEt_3 (0.1 g, 1.0 mmol) were dissolved in MeOH (20 mL) and stirred for 2.5 h. X-ray quality crystals were obtained in sufficient yield (~30 %) after filtration and slow evaporation the mother liquor. Elemental analysis found (calc. %) for: $C_{66}H_{80}Mn_4O_{20}$: C 55.93 (56.12), H 5.55 (5.71).

2.3 Results and Discussion

2.3.1 General Cluster Core Structure

The molecular structure of **1** is shown in Figure 4. The metallic skeleton describes a planar diamond or butterfly-like topology in which the wing-tip manganese ions (Mn1 and symmetry equivalent, housed inside the calixarene cavity) are in the oxidation state +3, and the body manganese ions (Mn2 and symmetry equivalent) are in the oxidation state +2 (Figure 4). These ions are linked to each other through two μ_3-OH^- ions located in the centre of the diamond forming a $[Mn^{III}_2Mn^{II}_2(OH)_2]^{8+}$ core. Mn1 and its symmetry equivalent lie in distorted octahedral geometries in $\{MnO_6\}$ coordination spheres, with the Jahn–Teller axes being defined by the O(DMF)-Mn-O(OH) vector. The four remaining positions around the equatorial plane of Mn1 are occupied by the oxygen atoms of the TBC[4] ligand, two of which μ-bridge to the central Mn^{2+} ions (Mn2 and symmetry equivalent). The two remaining equatorial sites on Mn2 are occupied by two terminally bonded DMF ligands, completing the distorted $\{MnO_6\}$ octahedral geometry. The oxidation states of the metal and OH^- ions were confirmed by charge balance and bond length considerations, and bond valence sum calculations which compare the sum of the observed bond lengths around an atom against tabulated bond lengths.[43,44]

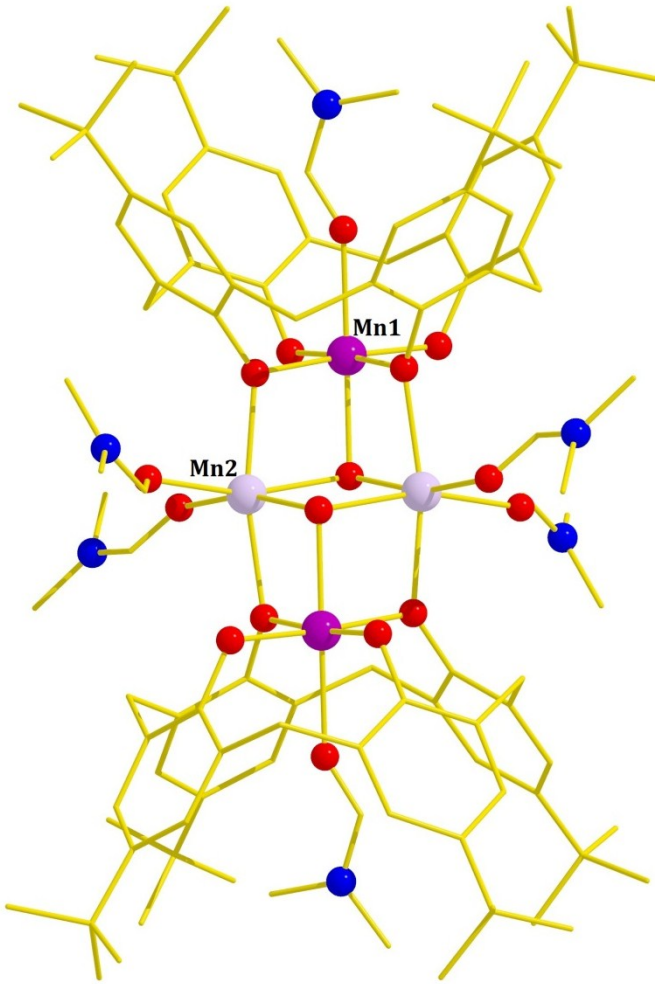

Figure 4. Molecular structure of **1** showing the butterfly-like topology of the metal ions and the ligated DMF molecules. Mn1 and symmetry equivalent are housed within the cavity of the TBC[4] ligands at the "top" and "bottom" of the molecule as depicted. Colour code: Mn^{III} = purple, Mn^{II} = pale purple, C = gold, O = red, N = blue, H-atoms omitted for clarity.

The butterfly or planar diamond moiety is a common structural type in manganese cluster chemistry, but it is far more commonly observed in the $[Mn^{III}_4O_2]^{8+}$ form, in which four Mn^{3+} ions are bridged by two μ_3-O^{2-} ions.[45] The first example of a mixed-valent $[Mn^{III}_2Mn^{II}_2(OR)_2]^{8+}$ central core in SMM chemistry was seen in the complex $[Mn_4(O_2CMe)_2$-$(pdmH)_4]$ ($pdmH_2$ = pyridine-2, 6-dimethanol)[46] and then later in the analogous $[Mn_4(hmp)_4Br_2(H_2O)_2]Br_2$ (and related) clusters (hmpH= 2-(hydroxymethyl)pyridine).[47] In these complexes the Mn^{3+} ions occupy the body positions of the butterfly, and the Mn^{2+} ions the wing-tip positions. In both cases dominant ferromagnetic exchange interactions between the metal centres is observed leading to S = 9 spin ground states. However, the oxidation state distribution in

complexes **1**–**7** is somewhat unusual, being "reversed" from the examples above with the body manganese ions being 2+ and the wing-tip ions 3+. Indeed, such a reversed core has been seen only once before, in the cluster $[Mn^{III}_2Mn^{II}_2(teaH)_2(acac)_4(MeOH)_2]^{2+}$ ($teaH_3$=triethanolamine, Hacac=acetylacetone) and its analogues.[48]

The examination of the extended structure of **1** shows that the $[Mn_4]$ building blocks assemble into a skewed bilayer array, somewhat resembling those found in solvates of TBC[4] (Figure 5).[49] In all but one of the structures reported here, the $[Mn_4]$ building blocks are also found to assemble as bilayer type arrays, despite the presence of different ligated and co-crystallised solvent molecules. For clarity we will describe notable features in the structures of **2**–**7** separately.

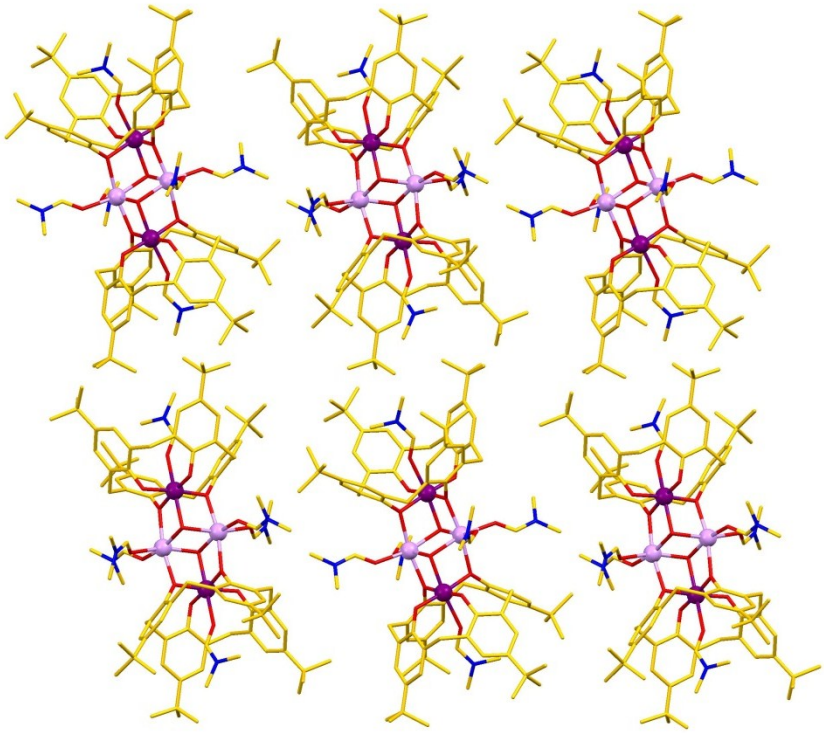

Figure 5. Extended structure of **1** (viewed along the crystallographic *b* axis) showing self-assembly into a skewed bi-layer array, reminiscent of calixarene packing in various solvates of TBC[4]. Colour code: Mn^{III} = purple, Mn^{II} = pale purple, C = gold, O = red, N = blue, H-atoms omitted for clarity.

[$Mn^{III}_2Mn^{II}_2(OH)_2(TBC[4])_2(DMF)_4(H_2O)_2$]·4MeOH·2DMF (2):

Structural analysis of crystals of **2** shows that the reaction conditions employed result in the formation of the same {$Mn^{III}_2Mn^{II}_2(OH)_2(TBC[4])_2$} cluster motif, but that the cluster periphery is composed of four DMF and two water ligands (Figure 6a). In addition to this there are four MeOH and two DMF molecules of crystallisation, all of which form an intricate hydrogen-bonding network around the cluster (Figure 6b). One crystallographically unique water ligand (O6) hydrogen bonds to a TBC[4] lower-rim oxygen atom (O2) with an O···O distance of 2.7659(91) Å, and an O atom (O11) of a methanol molecule with an O···O distance of 2.6842(124) Å. This O atom (O11) hydrogen bonds to an O atom (O9) of a DMF molecule with an O···O distance of 2.663(5) Å. Finally, an O atom (O10) from the second crystallographically unique co-crystallised MeOH molecule hydrogen bonds to a TBC4 lower-rim O atom (O3) with an O···O distance of 2.750(8) Å. Further symmetry expansion shows the extended structure to be a bilayer array (Figure 7) that differs to that found in **1** (Figure 5), as the upper-rims of the TBC[4] molecules are in an offset head-to-head planar arrangement.

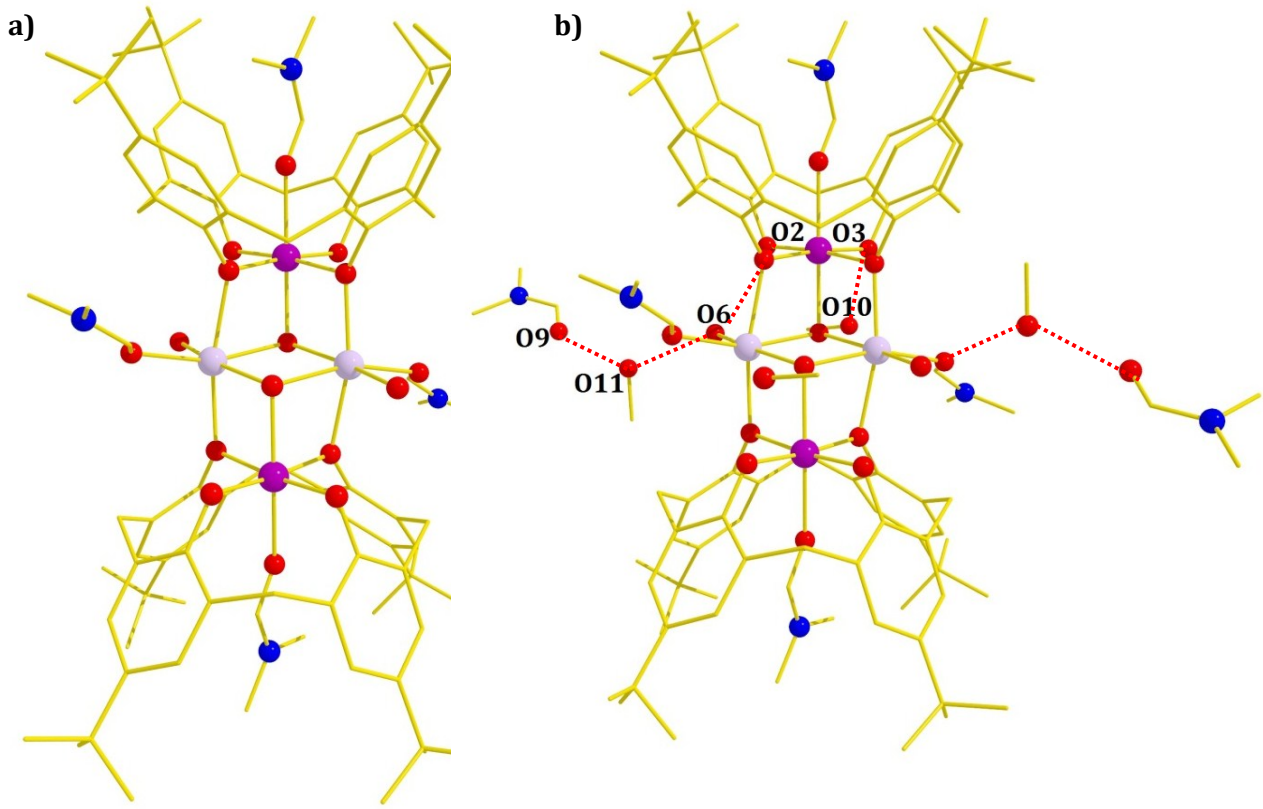

Figure 6. a) Molecular structure of **2**. b) Alternative view of **2** showing co-crystallised MeOH and DMF molecules and associated hydrogen bonding interactions (shown as dashed lines). Colour code as in Figure 5.

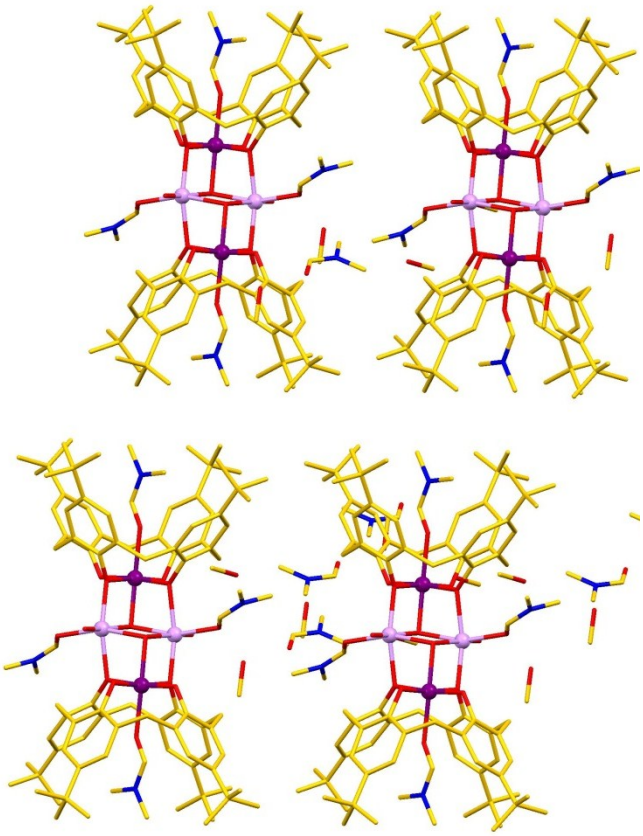

Figure 7. Extended structure of **2** (viewed along the crystallographic *a* axis) showing self-assembly into a planar bi-layer array and positioning of co-crystallised MeOH and DMF molecules. Colour code as in Figure 5.

[$Mn^{III}_2Mn^{II}_2(OH)_2$(TBC[4])$_2$$(DMF)_6$]·2.8MeOH (3)

Structural analysis of crystals of **3** shows that the reaction conditions employed result in the formation of the {$Mn^{III}_2Mn^{II}_2(OH)_2$(TBC[4])$_2$} cluster motif, but that the cluster periphery is composed of six DMF ligands (Figure 8a). In addition to this, there are disordered MeOH molecules of crystallisation that form hydrogen-bonding interactions with acceptor atoms of the cluster core (Figure 8b). Given this disorder, structure description will be limited to these molecules in only one position. An O atom (O9) of one MeOH of crystallisation hydrogen bonds to a TBC[4] lower-rim O atom (O1) with an O···O distance of 2.7918(38) Å. In addition to this, an O atom (O10) from a second disordered MeOH position hydrogen bonds to another TBC[4] lower-rim O atom (O4) with an O···O distance of 2.7464(64) Å. Further symmetry expansion shows the extended structure to be a skewed bilayer array that is markedly different to that found in **2** (Figure 9).

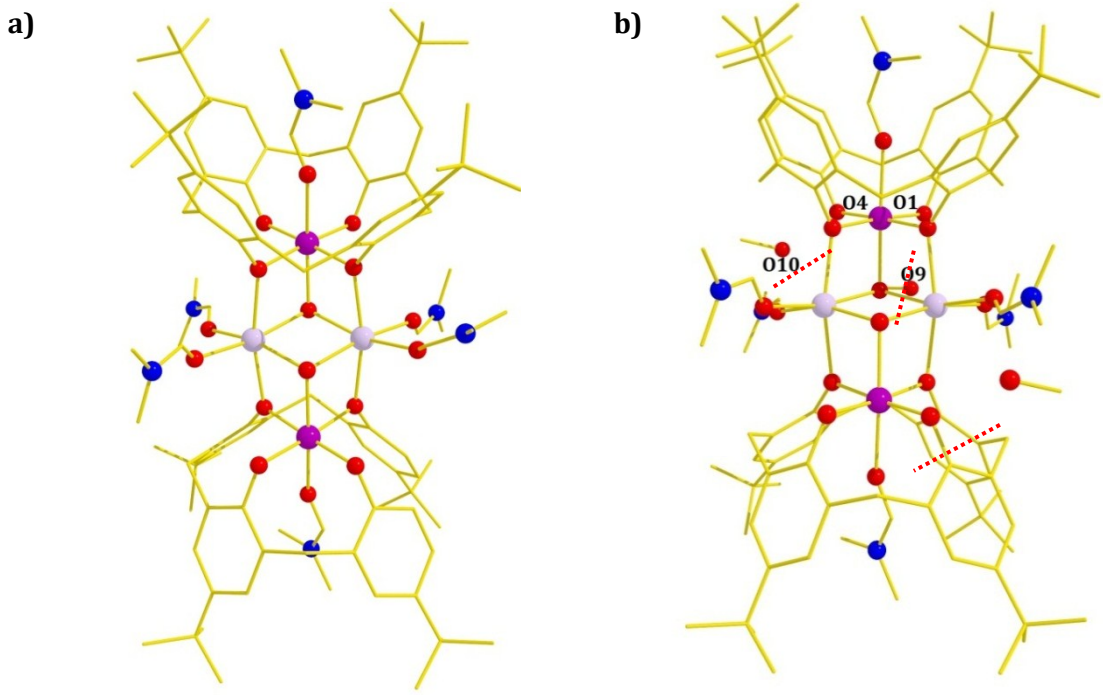

Figure 8. a) Molecular structure of **3**. b) Alternative view of **3** showing disordered co-crystallised MeOH molecules and associated hydrogen bonding interactions (shown as dashed lines). Colour code as in Figure 5.

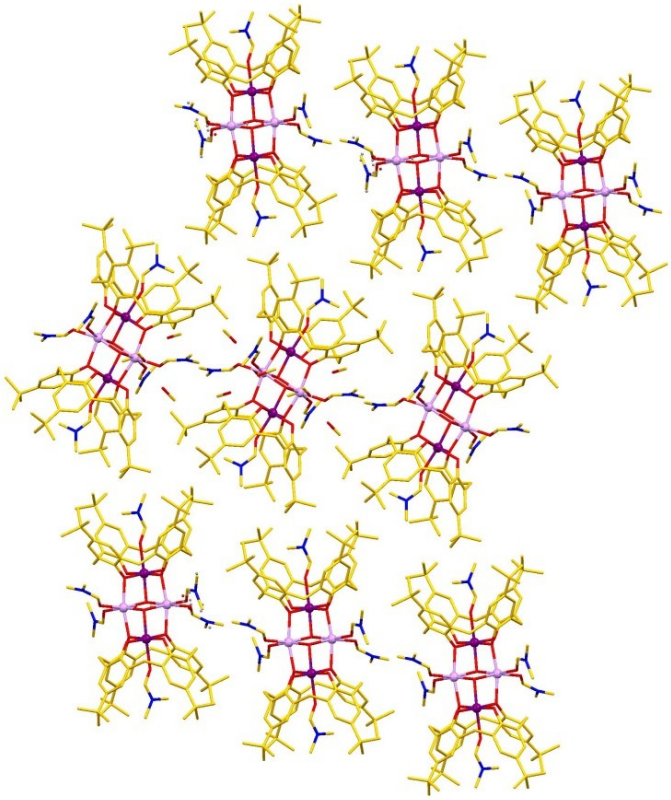

Figure 9. Extended structure of **3** (viewed along the crystallographic *a* axis) showing self-assembly into a skewed bi-layer and positioning of disordered co-crystallised MeOH molecules. Colour code as in Figure 5.

[$Mn^{III}_2Mn^{II}_2(OH)_2(TBC[4])_2(DMF)_4(EtOH)(H_2O)$] (4)

Structural analysis of crystals of **4** shows that the reaction conditions employed result in the formation of the {$Mn^{III}_2Mn^{II}_2(OH)_2(TBC[4])_2$} cluster motif, but that the cluster periphery is composed of four DMF ligands, as well as one EtOH and one H_2O molecule that are disordered over two symmetry equivalent positions (Figure 10a). The quality of the single crystal X-ray diffraction data collected for **4** was limited, and it was evident that there was badly disordered co-crystallised solvent present in the crystal lattice. It was not possible to model this disorder effectively and given this the routine SQUEEZE was applied.[50] This had the effect of dramatically improving the agreement indices, but precludes discussion of the intermolecular interactions between the clusters and co-crystallised solvent species. Although this is the case, symmetry expansion shows the extended structure to be a planar offset head-to-head bilayer array (Figure 10b) that is similar to that observed in **2** (Figure 7).

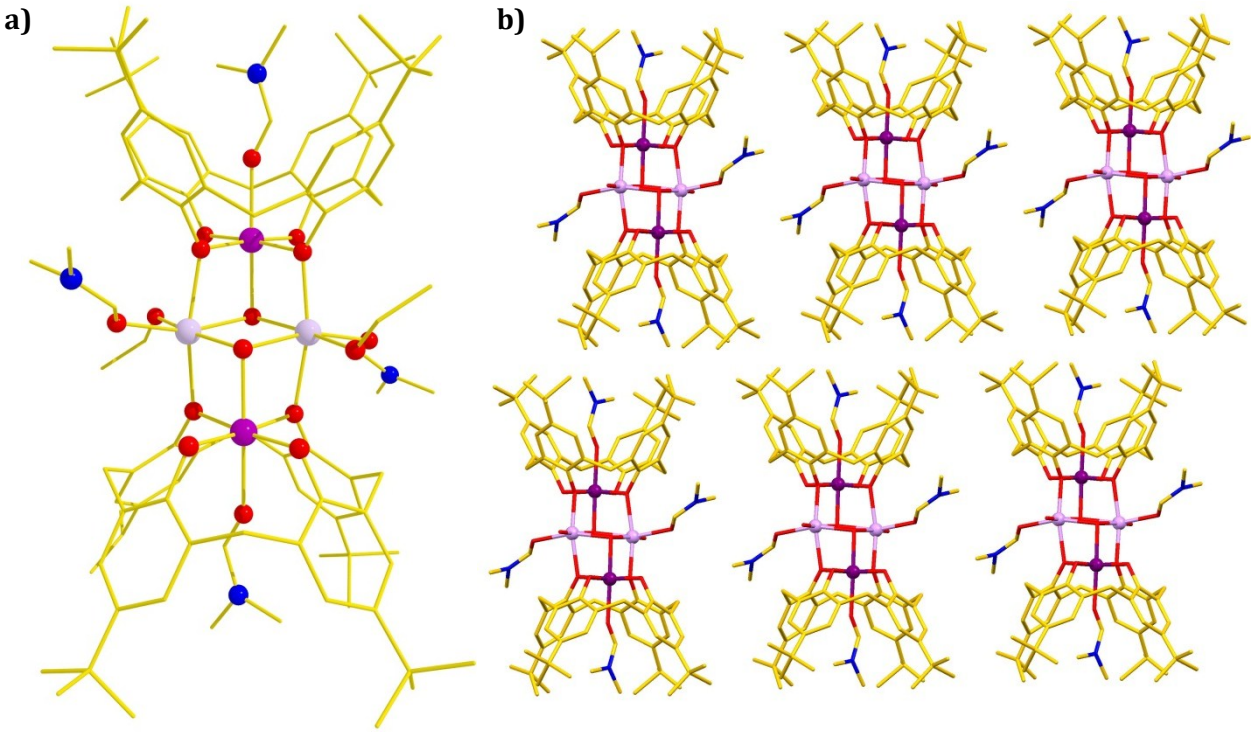

Figure 10. a) Molecular structure of **4**. b) Extended structure of **4** (viewed along the crystallographic *b* axis) showing self-assembly into a planar bilayer and positioning of co-crystallised MeOH molecules. Colour code as in Figure 5.

[$Mn^{III}_2Mn^{II}_2(OH)_2(TBC[4])_2(DMSO)_6$]·2MeOH·2DMSO (5)

Structural analysis of crystals of **5** shows that the reaction conditions employed result in the formation of the {$Mn^{III}_2Mn^{II}_2(OH)_2(TBC[4])_2$} cluster motif, but that the cluster

periphery is composed of six DMSO ligands, four of which are disordered (Figure 11a). In addition to this there are two MeOH and two disordered DMSO molecules of crystallisation. The former of these form hydrogen-bonding interactions with TBC[4] lower-rim O atoms through one crystallographically unique interaction between O10 and O1 with an O···O distance of 2.7151(66) Å. Further symmetry expansion shows the extended structure to be a planar offset head-to-head bilayer array (Figure 12) that is similar to those found in both **2** and **4** despite the disparate nature of the solvent systems used during synthesis.

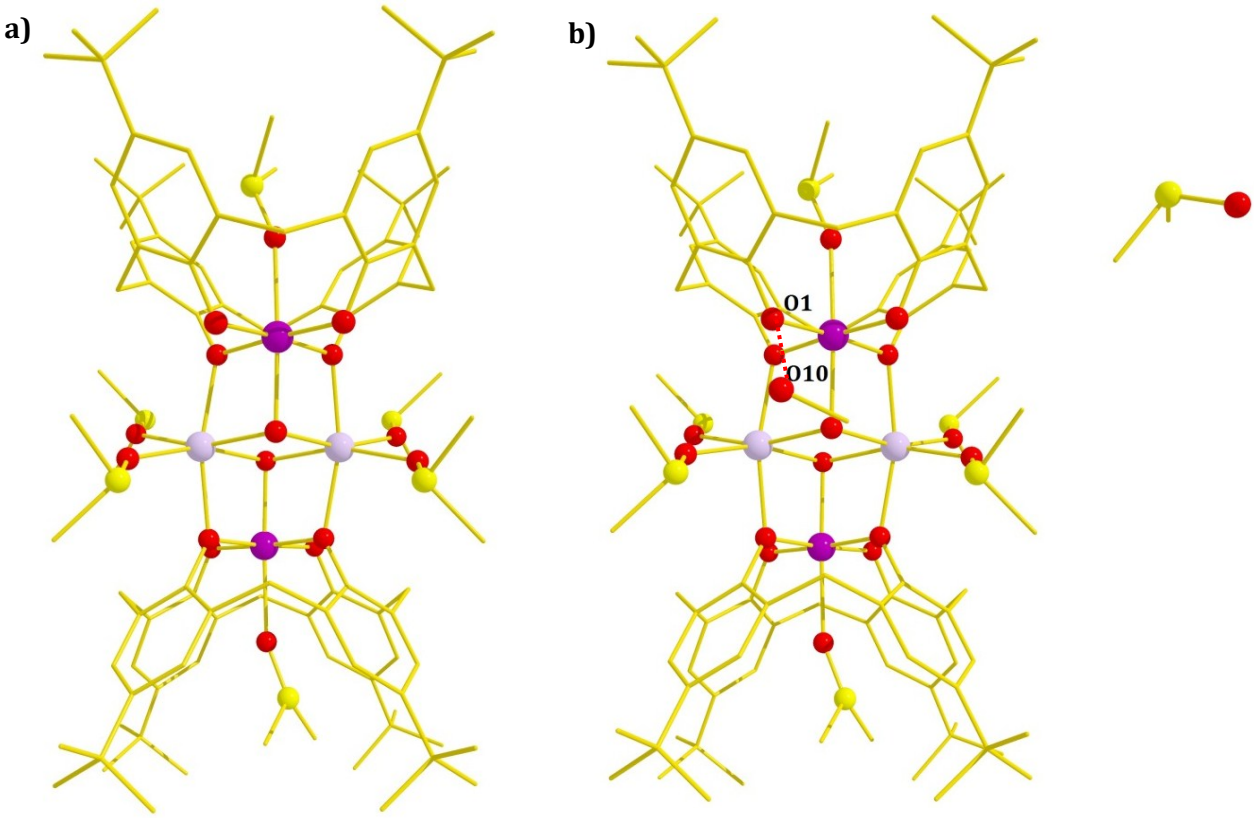

Figure 11. a) Molecular structure of **5**. b) Alternative view of **5** showing co-crystallised MeOH and DMSO molecules and associated hydrogen bonding interactions (shown as dashed lines). Colour code: Mn^{III} = purple, Mn^{II} = pale purple, O = red, S = yellow, C = gold, H-atoms omitted for clarity.

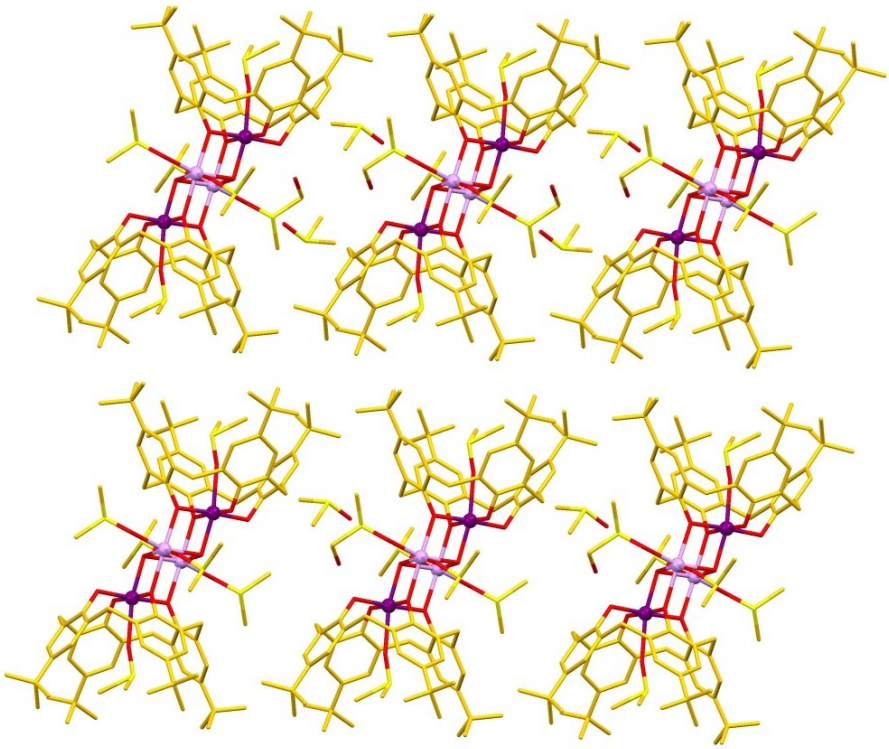

Figure 12. Extended structure of **5** (viewed perpendicular to the crystallographic *bc* plane) showing self-assembly into a planar bilayer array and positioning of co-crystallised MeOH and DMSO molecules. Colour code as in Figure 9.

[$Mn^{III}_2Mn^{II}_2(OH)_2$(TBC[4])$_2$(DMSO)$_6$] (6)

Structural analysis of crystals of **6** shows that the reaction conditions employed result in the formation of the {$Mn^{III}_2Mn^{II}_2(OH)_2$(TBC[4])$_2$} cluster motif, but that the cluster periphery is now composed of six DMSO ligands (Figure 13), four of which are badly disordered. The quality of the single crystal X-ray diffraction data collected for **6** was limited, despite the use of synchrotron data, and co-crystallised solvent present in the crystal lattice showed extreme disorder. It was not possible to model this effectively and, given this, the routine SQUEEZE was applied to the data.[50] This had the effect of dramatically improving the agreement indices, but precludes discussion of the intermolecular interactions between the clusters and co-crystallised solvent species. Although this is the case, symmetry expansion shows the extended structure to deviate from the expected bilayer arrangement. The result of this is that neighbouring clusters pack so as to form isolated pockets that are occupied by the diffuse electron density. Although it is not possible to directly compare the structures of **5** and **6** due to the requirement of the application of SQUEEZE, it should be noted that these two crystal structures were obtained from reactions that differ only in the carboxylate co-ligand employed. We therefore conclude that in this case, the co-ligand exerts influence over

the crystallisation of these building blocks, perhaps by altering the co-crystallised solvent ratios.

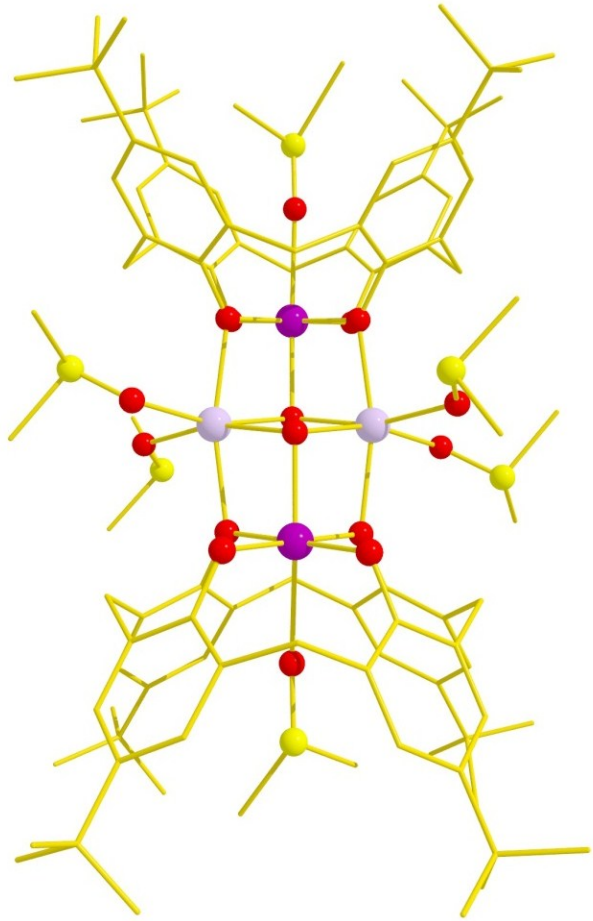

Figure 13. a) Molecular structure of **6**. Colour code: Mn^{III} = purple, Mn^{II} = pale purple, O = red, S = yellow, C = gold, H-atoms omitted for clarity.

[$Mn^{III}_2Mn^{II}_2(OH)_2(C[4])_2(MeOH)_6$]·4MeOH (7)

Structural analysis of crystals of **7** shows that the reaction conditions employed result in the formation of a {$Mn^{III}_2Mn^{II}_2(OH)_2(C[4])_2$} cluster motif with six peripheral MeOH ligands (Figure 14a). In addition to this there are four MeOH molecules of crystallisation that form a hydrogen- bonding network around the capsule periphery (Figure 14b). Within this network there are two sets of crystallographically unique interactions between ligated MeOH ligands, co-crystallised solvent molecules and C4 lower-rim O atoms. In set 1, O7 hydrogen bonds to O9 of a co-crystallised MeOH with an O···O distance of 2.6317(33) Å. O9 subsequently hydrogen bonds to C4 lower-rim O atom O4 with an O···O distance of 2.6108(32) Å. In set 2, O8 hydrogen bonds to O12 of a co-crystallised MeOH with an O···O distance of 2.6333(32) Å. O12 subsequently hydrogen bonds to C4 lower-rim O atom O2 with an O···O distance of 2.6021(31) Å. To

date we have found it significantly harder to isolate single crystals using C[4] as a building block rather than TBC[4], and in our previous report we could only obtain a partial structure of a {$Mn^{III}_2Mn^{II}_2(OH)_2(C[4])_2$} cluster from the solvent system used to form **1**.[40,41] In that case, the molecules assembled in a near-planar bilayer array similar to the TBC[4] analogue, but symmetry expansion of **7** shows the extended structure to be a zigzag bilayer array with additional MeOH molecules sandwiched between [Mn_4] building blocks (Figure 15). A possible reason for this difference may be that in the former case the molecules assemble in an offset head-to-head fashion, and cavity bound/ligated DMF molecules are arranged between C[4] molecules of a neighbouring layer. In the present case the calixarenes are arranged in a more head-to-head fashion, perhaps due to the less sterically demanding nature of the cavity bound/ligated MeOH molecule.

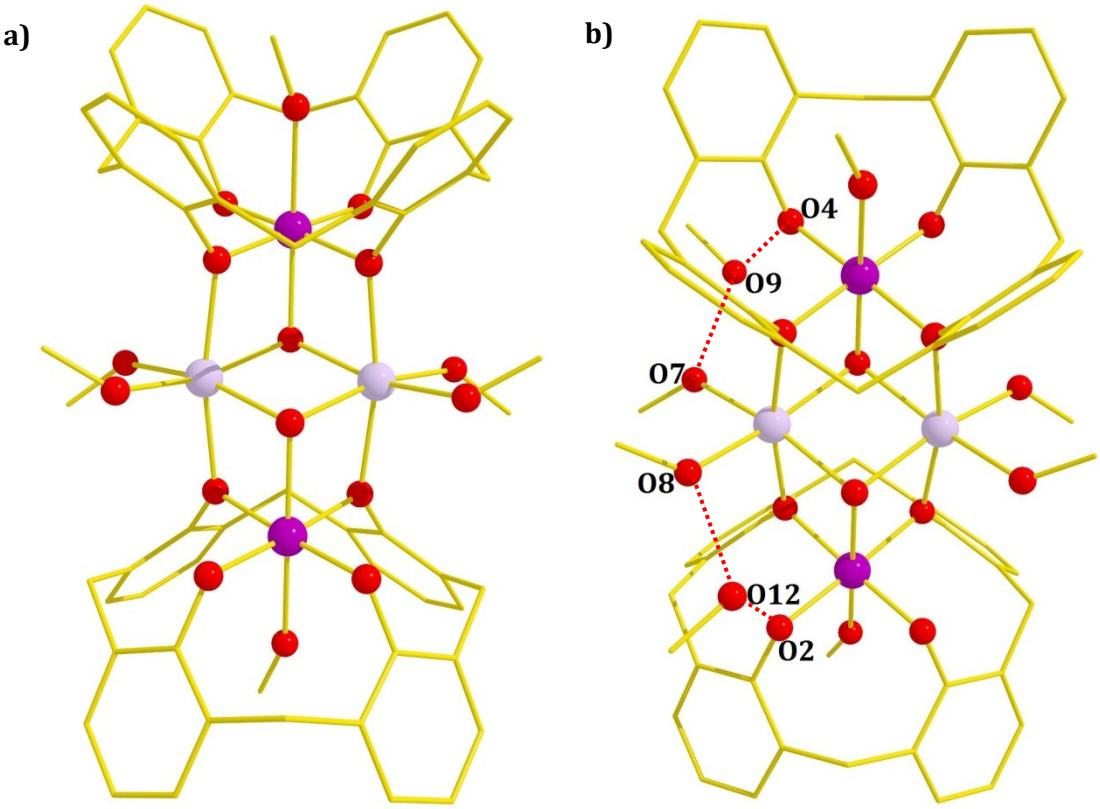

Figure 14. a) Molecular structure of **7**. b) Alternative view of **7** showing co-crystallised MeOH molecules and associated hydrogen bonding interactions (shown as dashed lines). Colour code: Mn^{III} = purple, Mn^{II} = pale purple, O = red, C = gold, H-atoms omitted for clarity.

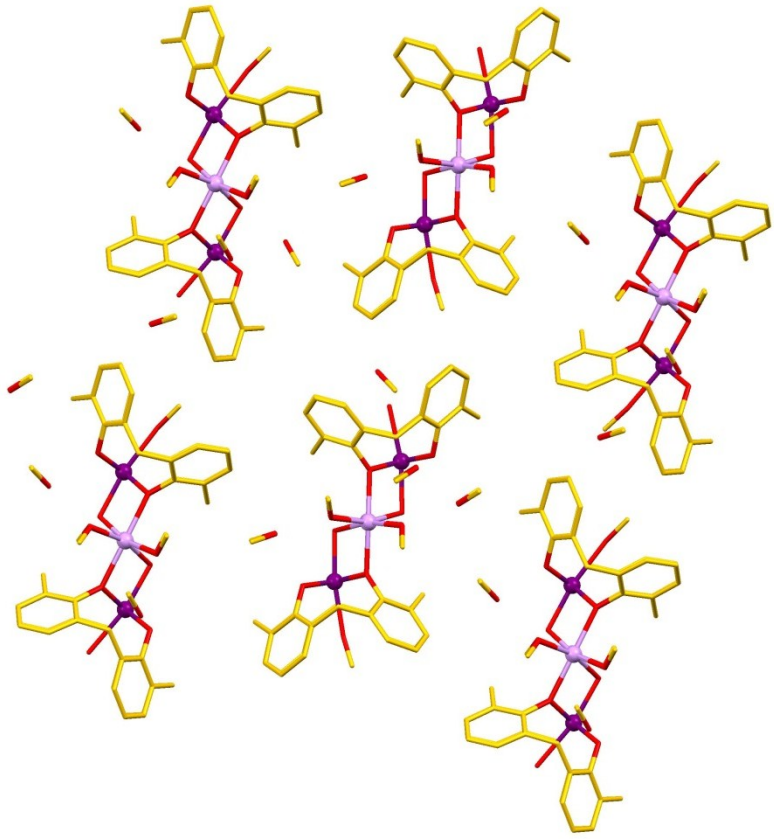

Figure 15. Extended structure of **7** (viewed on the crystallographic *ab* plane) showing self-assembly into zigzag layers and positioning of co-crystallised MeOH molecules. Colour code as in Figure 12.

2.3.2 Magnetic Properties

Solid-state dc magnetic susceptibility measurements were carried out on dried **1**, as a representative example, in the 275–5 K temperature range in an applied field of 0.1 T (Figure 16). The high-temperature $\chi_M T$ value of 15.5 cm^3 K mol^{-1} is close to the spin-only value expected for an uncoupled [$Mn^{III}_2Mn^{II}_2$] unit of 14.75 cm^3 K mol^{-1} with g = 2.0. The $\chi_M T$ value then increases very slowly with decreasing temperature reaching a value of approximately 16.5 cm^3 K mol^{-1} at 100 K, below which it then increases more rapidly reaching a maximum value of ≈ 24.5 cm^3 K mol^{-1} at 5 K. The value expected for a ferromagnetically coupled [$Mn^{III}_2Mn^{II}_2$] unit with an isolated S = 9 ground state (assuming g = 2.0) would be 45 cm^3 K mol^{-1} and thus the experimental data, which are similar to those reported for other $[Mn^{III}_2Mn^{II}_2(OR)_2]^{8+}$ clusters, are suggestive of very weak intra-molecular exchange and the population of numerous S states, even at the lowest temperatures measured.

The experimental data can be fitted using the isotropic 2 *J* model of spin Hamiltonian (1) depicted in Scheme 1 by means of a Levenberg–Marquardt algorithm.[51]

$$\hat{H} = -2J\left(\hat{S}_1\hat{S}_2 + \hat{S}_1\hat{S}_3 + \hat{S}_2\hat{S}_4 + \hat{S}_3\hat{S}_4\right) - 2J'\hat{S}_2\hat{S}_3 \qquad (1)$$

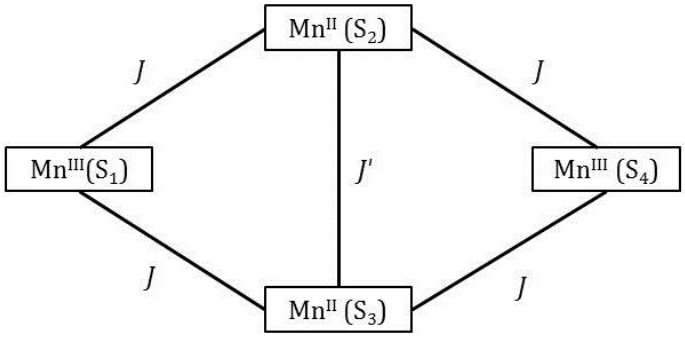

Scheme 1. Cartoon representation of the exchange interactions in **1** and the spin Hamiltonian [Equation (1)] used to fit the experimental data.

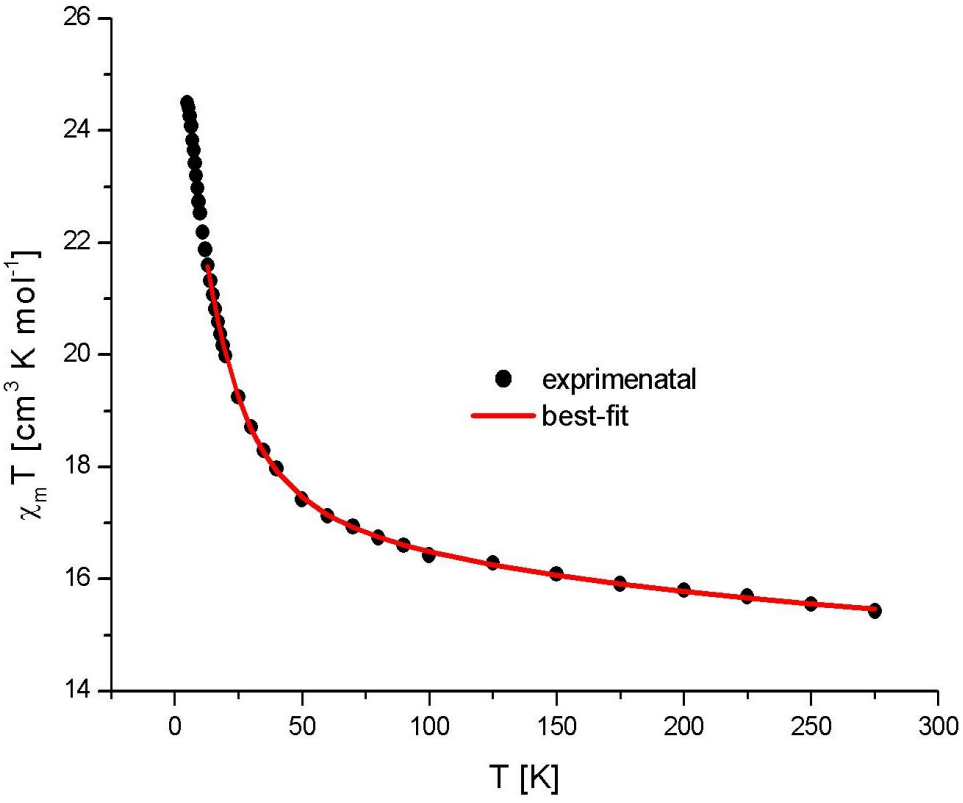

Figure 16. Fit, by use of the Levenberg–Marquardt algorithm, of the $\chi_M T$ product of **1** in the 10 to 275 K temperature range, yielding the best-fit parameters given in the text.

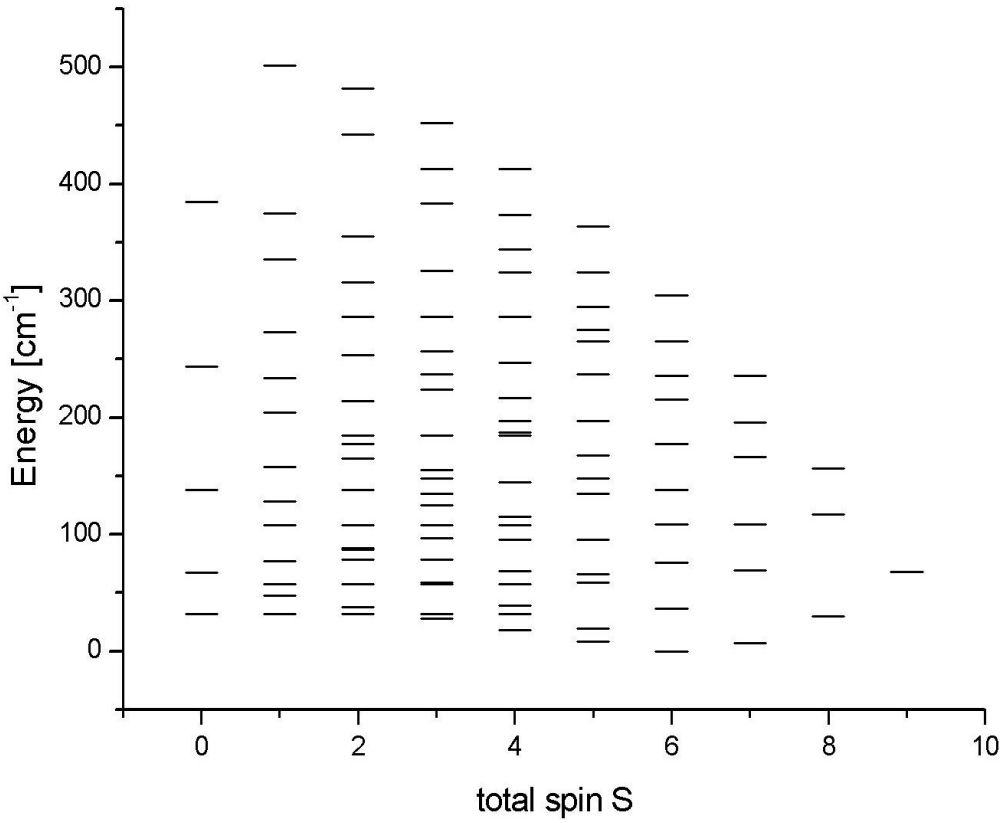

Figure 17. Energy level diagram of the spin-states of **1** determined by diagonalisation of the matrix representation of spin-Hamiltonian (1) with J = 4.93 cm^{-1} and J' = -7.77 cm^{-1}

In Equation (1) indices 1 and 4 correspond to Mn^{III} centres (Mn1 and symmetry equivalent), indices 2 and 3 correspond to Mn^{II} centres (Mn2 and symmetry equivalent), J is the isotropic exchange parameter and $\hat{S}$ the spin operator of a given centre. In addition to the J and J' fitting parameters, the intermolecular interactions were taken into account through the introduction of the Curie–Weiss temperature θ. The best fit parameters obtained (shown as the solid line in Figure 16) in the 10–275 K temperature range are: J= + 4.93 cm^{-1}, J'= -7.77 cm^{-1} and θ = -0.76 K. With these parameters the spin ground state of the system is an S = 6 spin state (Figure 17), with numerous excited states lying just above it. The relative energies of the different spin-states, determined by diagonalisation of the matrix representation of spin Hamiltonian (1) are given Figure 17. The magnitude of the exchange interactions resembles that observed for $[Mn^{III}_2Mn^{II}_2(teaH)_2(acac)_4(MeOH)_2]^{2+}$, although in the latter case distortions of the Mn^{2+}–O–Mn^{2+} central core resulted in all the exchange interactions being very weakly antiferromagnetic.[48] To model the reduced magnetisation of **1** an effective subspace was used instead of the full spin-space of dimension 900, in order to

facilitate computation. This effective subspace, of dimension 83, was constructed by projection of the spin Hamiltonian of the system in the space defined by the eigenvectors of the seven lowest lying spin states (S = 6, 7, 5, 4, 5, 3, 8) obtained from numerical diagonalisation of isotropic spin Hamiltonian (1) in the full spin-space of the system (of dimension 900). Within this subspace and keeping the exchange parameters constant from the fit of the susceptibility data and with a fixed g-value of 2.00, the data from 3 T and above can be fitted (Figure 18) well with $D(Mn^{III})$= −1.375 cm^{-1}.

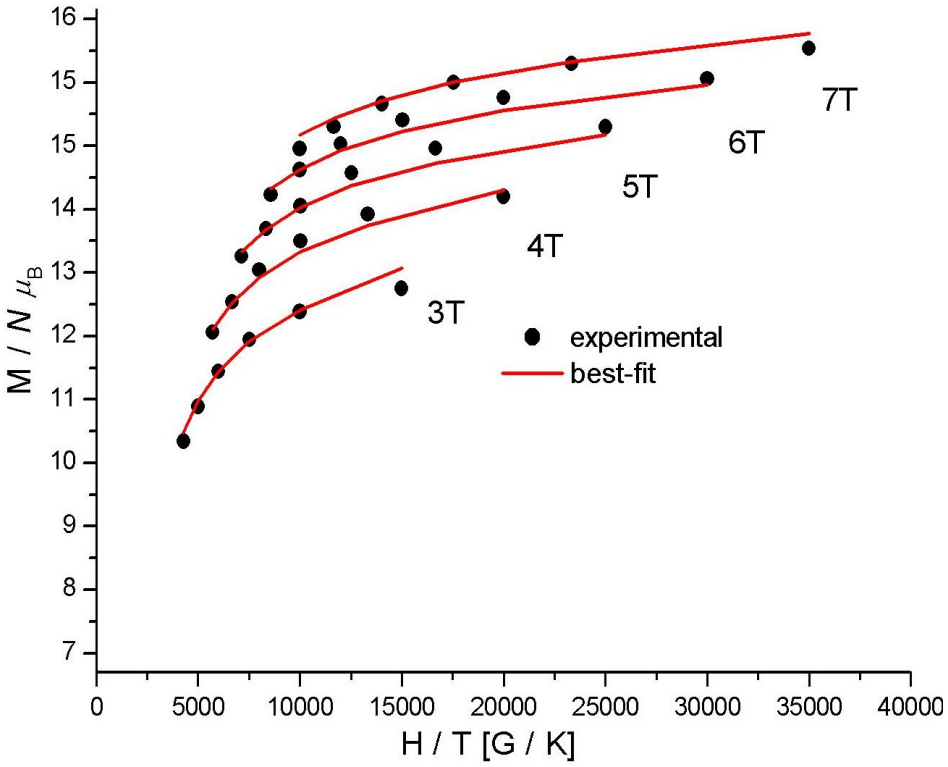

Figure 18. Plot of reduced magnetisation ($M/N\mu_B$) versus H/T for complex **1**. The fit (red lines) is obtained using the parameters obtained from the fit of the susceptibility data to afford $D(Mn^{III})$ = -1.375 cm^{-1}

Ac susceptibility studies carried out on crystalline samples of **1** in the 1.8–10.0 K range in a 3.5 G field oscillating at frequencies up to 1000 Hz (Figure 19) display the tails of frequency-dependent out-of-phase (χ''_M) signals suggestive of SMM behaviour but no peaks. Hysteresis loop measurements were therefore carried out on single crystals using a micro-SQUID assembly with the field applied along the easy axis of magnetisation.[52,53] These show temperature and sweep rate dependent hysteresis loops confirming the SMM behaviour (Figure 20). The loops are indicative of an SMM with no significant intercluster interactions and possessing quantum steps, but one in which many excited states are clearly mixed with the ground state, in agreement with

the powder data. An Arrhenius plot constructed from single crystal dc relaxation data affords U_{eff} = 16.5 K with τ_0 = 6 x 10^{-10} s.

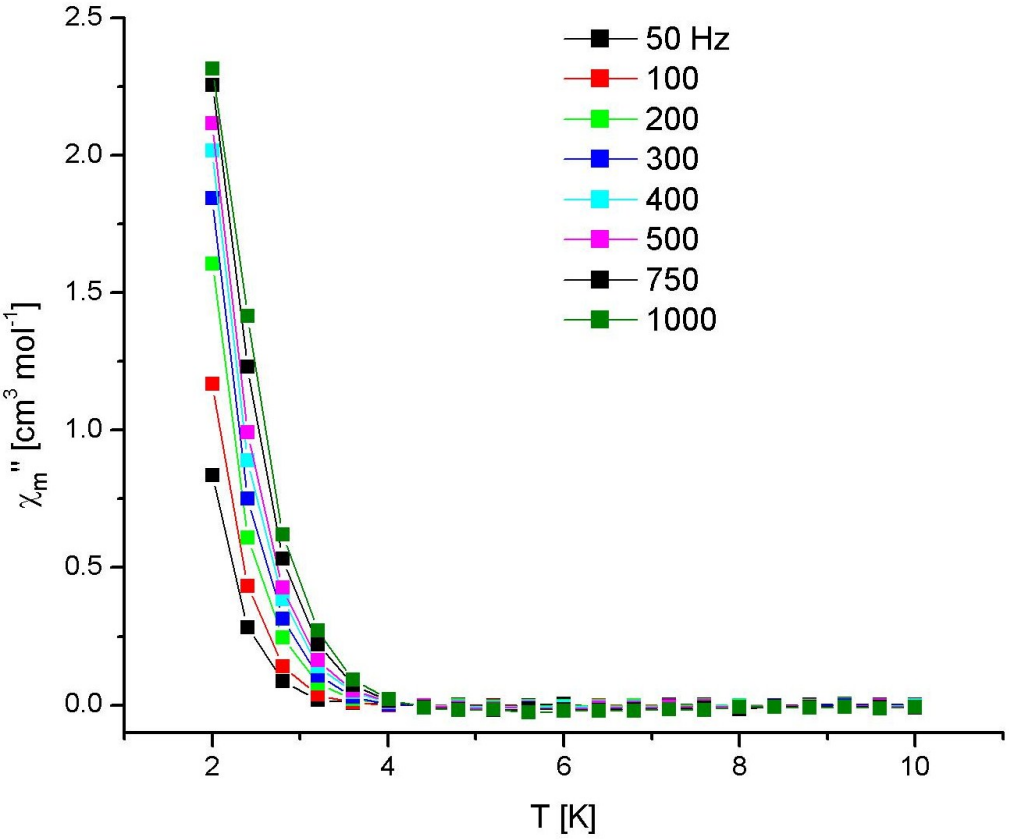

Figure 19. Plot of out-of-phase (χ_M'') ac susceptibility versus temperature in the indicated frequency ranges.

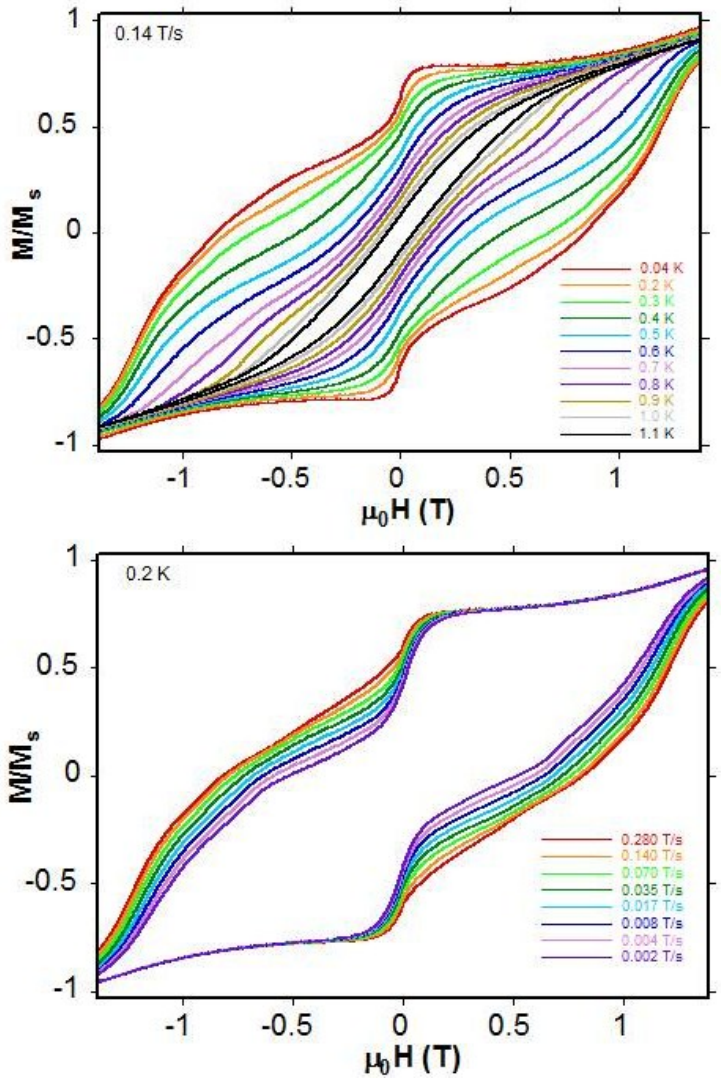

Figure 20. Magnetisation versus field hysteresis loops for a single crystal of **1** at the indicated temperature (top) and field sweep rates (bottom). M is normalised to its saturation value.

2.4 Conclusions

In conclusion we have synthesised and characterised a family of seven calix[4]arene supported [$Mn^{III}_2Mn^{II}_2$] clusters, which behave as single-molecule magnets (SMMs). These clusters can be synthesised from a number of different solvent systems, and disparate solvent composition around the cluster periphery (and also in the crystal lattice as co-crystallised species), affords a number of different self-assembled structures. In all but one case these resemble bilayers found in solvates of TBC[4] and deviation from this typical motif resulted in a structure containing a solvent pocket. These new additions to this series have resulted through our attempted incorporation

of carboxylate ligands, or their inclusion in the reaction mixtures. We have as yet been unable to introduce these co-ligands to the cluster core and have no explanation why this might be so, but the versatility of the cluster periphery suggests that this may eventually be possible under the right conditions. Removal of the upper-rim ^{t}Bu groups on the calixarene starting materials has a marked effect on self-assembly, but the resulting structure still shows bilayer character. Studies with this system continue with a view to introducing such species and further controlling the self-assembly of these SMM building blocks by means of synthetic alteration to the calix[4]arene upper-rim.

2.5 References

1. L. M. C. Beltran and J. R. Long, *Acc. Chem. Res.*, 2005, **38**, 325-334.
2. A. Escuer and G. Aromí, *Eur. J. Inorg. Chem.*, 2006, **2006**, 4721-4736.
3. J. N. Rebilly and T. Mallah, ed. R. Winpenny, Springer, 2006, vol. 122, pp. 103-131.
4. M. Affronte, S. Carretta, G. A. Timco and R. E. P. Winpenny, *Chem. Commun.*, 2007, 1789-1797.
5. A. J. Tasiopoulos and S. P. Perlepes, *Dalton Trans.*, 2008, 5537-5555.
6. R. Bagai and G. Christou, *Chem. Soc. Rev.*, 2009, **38**, 1011-1026.
7. L. N. Dawe, K. V. Shuvaev and L. K. Thompson, *Chem. Soc. Rev.*, 2009, **38**, 2334-2359.
8. K. S. Murray, *Aust. J. Chem.*, 2009, **62**, 1081-1101.
9. M. Shatruk, C. Avendano and K. R. Dunbar, in *Prog. Inorg. Chem.*, Wiley, 2009, pp. 155-334.
10. G. E. Kostakis, I. J. Hewitt, A. M. Ako, V. Mereacre and A. K. Powell, *Phil. Trans. R. Soc. A.*, 2010, **368**, 1509-1536.
11. M. Murrie, *Chem. Soc. Rev.*, 2010, **39**, 1986-1995.
12. L. Bogani, A. Vindigni, R. Sessoli and D. Gatteschi, *J. Mater. Chem.*, 2008, **18**, 4750-4758.
13. L. Bogani and W. Wernsdorfer, *Nat. Mater.*, 2008, **7**, 179-186.
14. D. Gatteschi, A. Cornia, M. Mannini and R. Sessoli, *Inorg. Chem.*, 2009, **48**, 3408-3419.
15. J. Lehmann, A. Gaita-Arino, E. Coronado and D. Loss, *J. Mater. Chem.*, 2009, **19**, 1672-1677.
16. M. I. Khan and J. Zubieta, in *Prog. Inorg. Chem.*, Wiley, 2007, pp. 1-149.
17. M. Moragues-Canovás, C. E. Talbot-Eeckelaers, L. Catala, F. Lloret, W. Wernsdorfer, E. K. Brechin and T. Mallah, *Inorg. Chem.*, 2006, **45**, 7038-7040.
18. E. K. Brechin, *Chem. Commun.*, 2005, 5141-5153.
19. E. S. Barrett, T. J. Dale and J. Rebek, *J. Am. Chem. Soc.*, 2007, **129**, 3818-3819.
20. S. J. Dalgarno, S. A. Tucker, D. B. Bassil and J. L. Atwood, *Science* 2005, **309**, 2037-2039.
21. T. Gerkensmeier, W. Iwanek, C. Agena, R. Fröhlich, S. Kotila, C. Näther and J. Mattay, *Eur. J. Org. Chem.*, 1999, **1999**, 2257-2262.
22. L. R. MacGillivray and J. L. Atwood, *Nature*, 1997, **389**, 469-472.
23. O. Ugono and K. T. Holman, *Chem. Commun.*, 2006, 2144-2146.
24. C. D. Gutsche, *Acc. Chem. Res.*, 1983, **16**, 161-170.
25. C. D. Gutsche, *Calixarenes 2001*, Kluwer Academic Publishers, 2001.

26. D. M. Homden and C. Redshaw, *Chem. Rev.*, 2008, **108**, 5086-5130.
27. A. J. Petrella and C. L. Raston, *J. Organomet. Chem.*, 2004, **689**, 4125-4136.
28. C. Cañada-Vilalta, T. A. O'Brien, M. Pink, E. R. Davidson and G. Christou, *Inorg. Chem.*, 2003, **42**, 7819-7829.
29. D. P. Goldberg, A. Caneschi, C. D. Delfs, R. Sessoli and S. J. Lippard, *J. Am. Chem. Soc.*, 1995, **117**, 5789-5800.
30. R. W. Saalfrank, H. Maid and A. Scheurer, *Angew. Chem.*, 2008, **120**, 8924-8956.
31. R. W. Saalfrank, H. Maid and A. Scheurer, *Angew. Chem. Int. Ed*, 2008, **47**, 8794-8824.
32. Y. Bi, X.-T. Wang, W. Liao, X. Wang, X. Wang, H. Zhang and S. Gao, *J. Am. Chem. Soc.*, 2009, **131**, 11650-11651.
33. C. Desroches, G. Pilet, S. A. Borshch, S. Parola and D. Luneau, *Inorg. Chem.*, 2005, **44**, 9112-9120.
34. C. Desroches, G. Pilet, P. Á. Szilágyi, G. Molnár, S. A. Borshch, A. Bousseksou, S. Parola and D. Luneau, *Eur. J. Inorg. Chem.*, 2006, 357-365.
35. T. Kajiwara, N. Iki and M. Yamashita, *Coord. Chem. Rev.*, 2007, **251**, 1734-1746.
36. C. Aronica, G. Chastanet, E. Zueva, S. A. Borshch, J. M. Clemente-Juan and D. Luneau, *J. Am. Chem. Soc.*, 2008, **130**, 2365-2371.
37. G. Karotsis, M. Evangelisti, S. J. Dalgarno and E. K. Brechin, *Angew. Chem. Int. Ed*, 2009, **121**, 10112-10115.
38. G. Karotsis, S. Kennedy, S. J. Dalgarno and E. K. Brechin, *Chem. Commun.*, 2010, **46**, 3884-3886.
39. G. Karotsis, S. Kennedy, S. J. Teat, C. M. Beavers, D. A. Fowler, J. J. Morales, M. Evangelisti, S. J. Dalgarno and E. K. Brechin, *J. Am. Chem. Soc.*, 2010, **132**, 12983-12990.
40. G. Karotsis, S. J. Teat, W. Wernsdorfer, S. Piligkos, S. J. Dalgarno and E. K. Brechin, *Angew. Chem. Int. Ed*, 2009, **48**, 8285-8288.
41. G. Karotsis, S. J. Teat, W. Wernsdorfer, S. Piligkos, S. J. Dalgarno and E. K. Brechin, *Angew. Chem.*, 2009, **121**, 8435-8438.
42. C. D. Gutsche, M. Iqbal and D. Stewart, *J. Org. Chem.*, 1986, **51**, 742-745.
43. W. Liu and H. H. Thorp, *Inorg. Chem.*, 1993, **32**, 4102-4105.
44. H. H. Thorp, *Inorg. Chem.*, 1992, **31**, 1585-1588.
45. J. B. Vincent, C. Christmas, H. R. Chang, Q. Li, P. D. W. Boyd, J. C. Huffman, D. N. Hendrickson and G. Christou, *J. Am. Chem. Soc.*, 1989, **111**, 2086-2097.
46. E. K. Brechin, J. C. Huffman, G. Christou, J. Yoo, M. Nakano and D. N. Hendrickson, *Chem. Commun.*, 1999, 783-784.
47. J. Yoo, E. K. Brechin, A. Yamaguchi, M. Nakano, J. C. Huffman, A. L. Maniero, L.-C. Brunel, K. Awaga, H. Ishimoto, G. Christou and D. N. Hendrickson, *Inorg. Chem.*, 2000, **39**, 3615-3623.
48. L. M. Wittick, L. F. Jones, P. Jensen, B. Moubaraki, L. Spiccia, K. J. Berry and K. S. Murray, *Dalton Trans.*, 2006, 1534-1543.
49. S. J. Dalgarno, P. K. Thallapally, L. J. Barbour and J. L. Atwood, *Chem. Soc. Rev.*, 2007, **36**, 236-245.
50. A. Spek, *J. Appl. Crystallogr.*, 2003, **36**, 7-13.
51. W. H. Press, S. A. Teukolsky, W. T. Vetterling and B. P. Flannery, *Numerical Recipes In C: The Art of Scientific Computing, 2nd ed.*, Cambridge University Press, 1992.
52. W. Wernsdorfer, *Adv. Chem. Phys.*, 2001, **118**, 99-190.
53. W. Wernsdorfer, *Supercond. Sci. Technol.*, 2009, **22**, 064013.

Chapter 3
Calixarene-Supported Clusters: Employment of Complementary Cluster Ligands

3.1 Introduction

One of the major challenges in the construction of paramagnetic polymetallic cluster compounds is the systematic design and [controlled] assembly of molecules with desirable and/or tuneable magnetic properties.[1-12] This is a non-trivial task since many such species contain high oxidation state metal ions stabilised by a core of bridging oxide and/or hydroxide ions whose presence, number and coordination behaviour is difficult, if not impossible, to control.[1-12] One potential way to circumvent this problem is to take advantage of the known coordination modes of certain ligand types through the self-assembly of complementary cluster ligands, *i.e.* small stable pre-made molecules or metal-organic moieties made *in situ*, that can act as the building blocks from which larger molecules (or indeed coordination polymers) can be made – perhaps even in a logical or step-by-step fashion.[1-12] Of course this approach first requires that a library of complexes, made through (serendipitous) self-assembly, is constructed so that the preferred coordination modes of the ligands with particular metal ions in particular oxidation states, and thus the stable metal building blocks, can be found and exploited.[13] Thereafter one can envision employing different but complementary cluster ligands to build oligomers.

Appealing classes of ligand in this regard are the *p*-tert-butylcalix[*n*]arenes, phosphinates and N,O-chelates such as 2-(hydroxymethyl)pyridine (hmpH), pyridine-2,6-dimethanol ($pdmH_2$) and their many derivatives.[14,15] The *p*-tert-butylcalix[*n*]arenes are versatile cyclic polyphenols that vary in ring size depending on the reaction conditions employed during synthesis.[16-20] They have been used extensively in the formation of supramolecular structures, and in various aspects of coordination chemistry.[21-26] *p*-*t*Bu-calix[4]arene (TBC[4], Figure 1a) is the most readily accessible tetramer of this family of molecules[27] and is a common starting point for the alteration of the general molecular framework.[28]

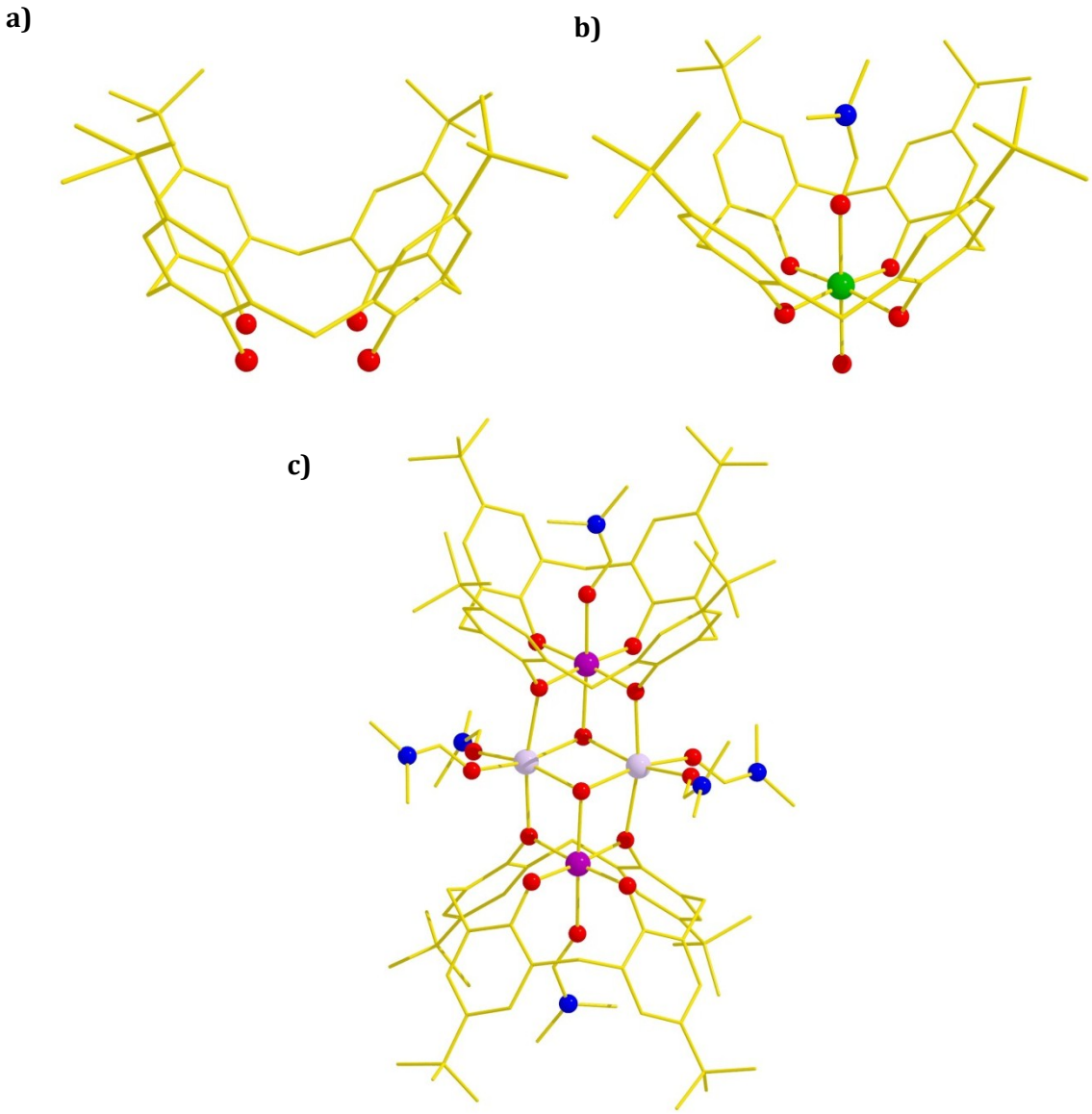

Figure 1. a) *p*-^{t}Bu-calix[4]arene (TBC[4]). b) The $TM^{II/III}$(TBC[4])(OH)(DMF) cluster ligand. c) Molecular structure of $[Mn^{III}_2Mn^{II}_2(OH)_2(TBC[4])_2(DMF)_6]$. Colour code: $TM^{II/III}$ = green, Mn^{III} = purple, Mn^{II} = pale purple, O = red, N = blue, C = gold, H-atoms omitted for clarity.

Their polyphenolic nature should make them ideal pro-ligands for the construction of large polynuclear metal clusters, and despite a surprising paucity of early literature examples, we (amongst others) have recently employed TBC[4] as a cluster support with a view to mapping out associated assembly modes and coordination constraints under a range of conditions.[29-31] Analysis of the common structural features in our TBC[4]-supported clusters shows that whether the calixarene binds a TM^{II} (Cu) or TM^{III} (Mn or Fe) metal centre, the cavity is occupied by a ligated solvent molecule and the O-

atoms of the fully deprotonated lower-rim, in conjunction with a bound hydroxide ligand beneath the complex, act as bridges to other metal centres (Figure 1b). An appropriate example in the context of the current paper (*vide infra*) is the complex $[Mn^{III}_2Mn^{II}_2(OH)_2(TBC[4])_2(solvent)_6]$ shown in Figure 1c.[20]

The pro-ligand 2-(hydroxymethyl)pyridine (hmpH) has a proven track record of success in the construction of Mn clusters.[14,15,32,33] Typically hmp^- acts as a μ-bridge, chelating to one Mn centre through N- and O-atoms and bridging to the second metal *via* the alkoxide group (Figure 2a), though the ligand can also act as a μ_3-bridge. Perhaps this is best illustrated in the complex $[Mn^{III}_2Mn^{II}_2(hmp)_6Br_2(H_2O)_2]^{2+}$ (Figure 2b) and its analogues.[14,15] The metal-oxygen core topology in this family is often referred to as a butterfly (two edge-sharing triangles) with the wingtip (outermost) Mn^{II} ions being ferromagnetically coupled to the body (innermost) Mn^{III} ions. This structure is clearly related to that of $[Mn^{III}_2Mn^{II}_2(OH)_2(TBC[4])_2(dmf)_6]$ shown in Figure 1c and we reasoned that the two cluster ligand moieties / building blocks in Figures 1b and 2a should be complementary and that their simple addition should result in the self-assembly of a structurally related complex.

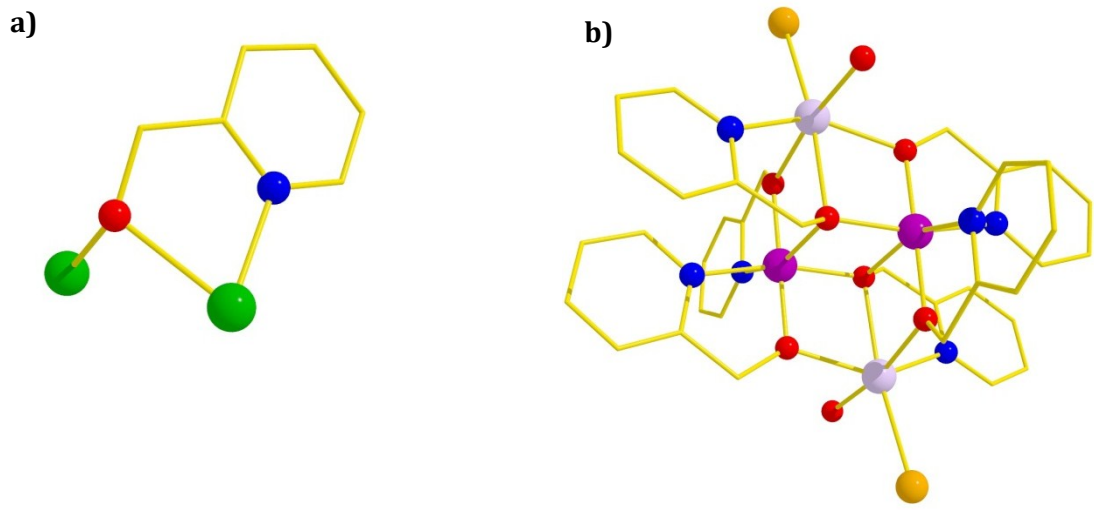

Figure 2. a) The μ-coordination mode commonly found for the hmp^- ligand. b) Molecular structure of $[Mn^{III}_2Mn^{II}_2(hmp)_6Br_2(H_2O)_2]^{2+}$. Colour code: $TM^{II/III}$ = green, Mn^{III} = purple, Mn^{II} = pale purple, O = red, N = blue, Br = orange, C = gold, H-atoms omitted for clarity.

3.2 Experimental

All manipulations were performed under aerobic conditions using materials as received (reagent grade). Elemental analyses (C, H, N) were performed by the EaStCHEM microanalysis service. Variable-temperature, solid-state direct current (dc) magnetic susceptibility data down to 5 K were collected on a Quantum Design MPMS-XL SQUID magnetometer equipped with a 7 T dc magnet. Diamagnetic corrections were applied to the observed paramagnetic susceptibilities using Pascal's constants. TBC[4] was synthesised according to literature procedures.[28,34-36] Full crystallographic details for the structures reported here are listed in Table 2. The oxidation states of the metal and OH^- ions were confirmed by charge balance and bond length considerations, and bond valence sum calculations which compare the sum of the observed bond lengths around an atom against tabulated bond lengths.[37,38]

$[Mn^{III}Mn^{II}(TBC[4])_2(O_2P(H)Ph)(DMF)_2(MeOH)_2]_2$ (8)

$MnCl_2{\cdot}4H_2O$ (0.15 g, 0.75 mmol), TBC[4] (0.1 g, 0.15 mmol), sodium phenylphosphinate ($NaO_2P(H)Ph$) (0.164 g, 1.0 mmol) and NEt_3 (0.1 g, 1.0 mmol) were dissolved in a mixture of DMF (10 mL) and MeOH (15 mL) and stirred for 2.5 h. X-ray quality crystals of **8** were obtained in good yield (~ 40 %) after filtration and diffusion of hexane into the mother liquor. Elemental analysis found (calc. %) for $C_{116}H_{156}Mn_4N_4O_{20}P_2$: C 62.71 (63.09), H 6.83 (7.12), N 2.81 (2.54).

$[Mn^{III}_3Mn^{II}_2(OH)_2(TBC[4])_2(hmp)_2(DMF)_6](TBC[4]\text{-}H){\cdot}xDMF{\cdot}xH_2O$ (9)

$MnCl_2{\cdot}4H_2O$ (0.12 g, 0.6 mmol), Hhmp (0.065 g, 0.6 mmol) and TBC[4] (0.2g, 0.3 mmol) were dissolved in a mixture of MeOH (10 mL and DMF (10 L). After 5 minutes of stirring, NEt_3 (0.182 g, 1.8 mmol) was added, leaving the solution stirring for a further 2 h. X-ray quality crystals were obtained by slow evaporation of the mother liquor over a period of 1 week in ~50 % yield. The complex can also be obtained in similar yield from mixing separate solutions of $MnCl_2{\cdot}4H_2O$, TBC[4] and NEt_3 in MeOH/DMF with $MnCl_2{\cdot}4H_2O$, Hhmp and NEt_3 in MeOH/DMF. Elemental analysis found (calc. %) for $Mn_5C_{162}H_{217}O_{22}N_8$: C 67.34 (67.02), H 7.95 (7.53), N 4.24 (3.86).

Table 2. Crystal structure information for **8** and **9**.

	8[a]	**9**[b]
Chemical formula	$C_{115}H_{162}Mn_4N_4O_{20}P_2$	$C_{169.80}H_{236}Mn_5N_{10.60}O_{26}$
M_r	2202.19	3116.39
Crystal system	Triclinic	Triclinic
Space group	*P*-1	*P*-1
a (Å)	12.5734 (7)	19.5877 (9)
b (Å)	13.2559 (8)	21.2285 (10)
c (Å)	20.3034 (12)	22.6548 (10)
α (°)	74.747 (2)	100.189 (2)
β (°)	73.160 (2)	110.810 (2)
γ (°)	64.054 (2)	102.360 (2)
V (Å^3)	2875.7 (3)	8265.0 (7)
Z	1	2
F(000)	1170	3324
Crystal size (mm)	0.10 × 0.08 × 0.06	0.45 × 0.35 × 0.30
No. of measured, independent and observed [$I > 2\sigma(I)$] reflections	21865, 7023, 4662	129252, 35410, 26610
R_{int}	0.074	0.031
$R_1[I>2\sigma(I)]$	0.076	0.059
$wR_2(F^2)$	0.225	0.151
GOF on F^2	1.04	1.05

[a] Data collected on a Bruker Apex II diffractometer operating with synchrotron radiation (λ= 0.7749 Å) at 100(2) K. [b] Data collected on a Bruker Apex II diffractometer operating with $Mo_{K\alpha}$ radiation (λ = 0.71073 Å) at 100(2) K.

3.3 Results and Discussion

3.3.1 Structural Description

Herein we present two new calixarene supported $[Mn^{III}Mn^{II}]_2$ clusters that employ phosphinate ligands to bridge two ''separate'' $[Mn^{III}Mn^{II}]$ moieties into a dimer of dimers $[Mn^{III}Mn^{II}(TBC[4])_2(O_2P(H)Ph)(DMF)_2(MeOH)_2]_2$ (**8**) and the pro-ligand 2-(hydroxymethyl)pyridine (hmpH) for the construction of a ferromagnetic $[Mn_5]$ cage, $[Mn^{III}_3Mn^{II}_2(OH)_2(TBC[4])_2(hmp)_2(DMF)_6](TBC[4]\text{-}H)\cdot xdmf \cdot xH_2O$ (**9**), whose structure indeed describes the self-assembly of the moieties shown in Figures 1b and 2a.

$[Mn^{III}Mn^{II}(TBC[4])_2(O_2P(H)Ph)(DMF)_2(MeOH)_2]_2$ (8)

We previously presented that the reaction of $MnX_2{\cdot}4H_2O$ (where X = Cl, Br) with TBC[4] and NEt_3 in MeOH/DMF results in the formation of the complex $[Mn^{III}Mn^{II}(OH)(TBC[4])(DMF)_3]_2$ (**1**, Figure 1c).[18] The cluster comprises a planar diamond or butterfly-like core in which the outer (wing-tip, those housed within the TBC[4] polyphenoxide cavity) and inner Mn are III+ and II+ ions respectively. Addition of sodium phenylphosphinate to the reaction mixture used to form complex **1** has an intriguing effect on cluster formation, producing a new complex, $[Mn^{III}Mn^{II}(O_2P(H)Ph)(DMF)_2(MeOH)_2]_2$ (**8**, Figure 3), which is best described as a dimer of dimers consisting of two $[Mn^{III}Mn^{II}]$ moieties held together by two bridging phosphinate ligands. In essence complex **8** is an ''elongated'' version of complex **1** in which two μ_3-bridging OH^- ions have been replaced by two much larger μ_3-bridging phosphinates. The Mn^{3+} ions (Mn1 and symmetry equivalent, s.e.) are located in the cavities of the fully deprotonated TBC[4] molecules and are six-coordinate with the Jahn–Teller axes defined by the O5(DMF)–Mn1–O6(phosphinate) vector. The four equatorial sites are occupied by the O-atoms (O1–O4, 1.897(5)–1.951(5) Å) of a TBC[4] ligand, one of which (O3) bridges in a μ-fashion to one of the two central Mn^{2+} ions (Mn1–O3–Mn2, 106.5(2)°). The phosphinate ligands are μ_3-bridging connecting Mn1 and Mn2 *via* one μ-O atom (Mn1–O6–Mn2, 96.18(18)°), and Mn2 and Mn2' and Mn1 and Mn2' *via* two three atom O–P–O bridges. The core of **8** thus consists of two $[Mn^{III}–(\mu\text{-}O)_2–Mn^{II}]$ dimers linked *via* two three atom O–P–O bridges. The vacant coordination sites on Mn2 are filled by a combination of DMF and MeOH molecules, the latter of which are hydrogen-bonded to two of the monodentate TBC[4] O-atoms (O1–O9, 2.705 Å ; O3–O8, 2.665 Å).

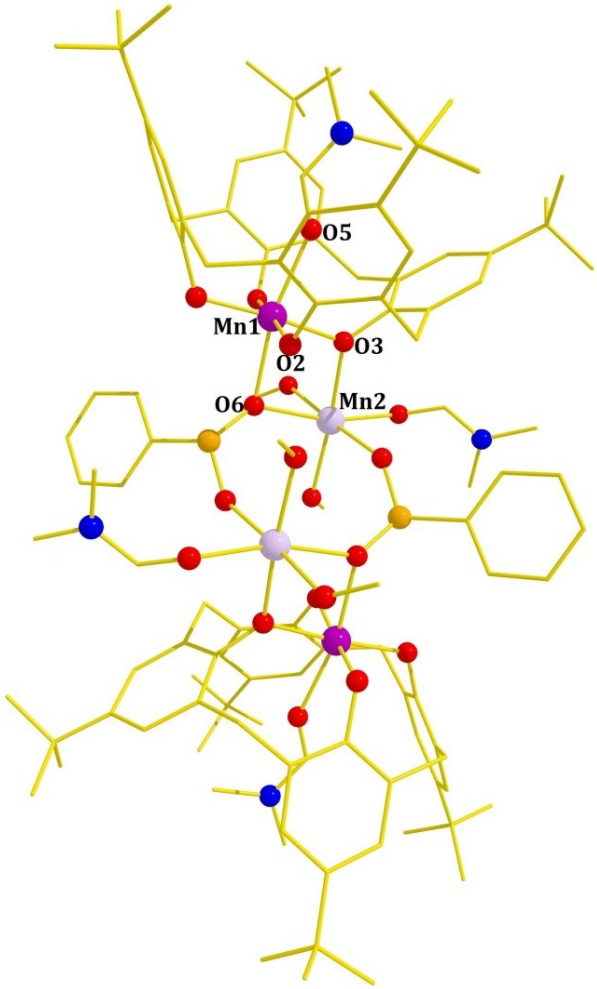

Figure 3. The molecular structure of **8** showing the bridging nature of the phenylphosphinate ligands. Colour code: Mn^{III} = purple, Mn^{II} = pale purple, O = red, N = blue, P = orange, C = gold, H-atoms omitted for clarity.

Examination of the extended structure of **8** reveals that molecules are arranged in a bi-layer arrangement that is similar to the one formed by **1**, in addition to DMF solvates of TBC[4] (Figure 4a).[18,39-41] Within the region of the bi-layer composed of calixarene upper-rim ^{t}Bu groups, the molecules are arranged so as to form a skewed head-to-head arrangement, a feature commonly observed in solvates of TBC[4] (Figure 3b). The closest inter-molecular interactions found within the other region of the bi-layer arrangement are between the C-atoms of the DMF molecules and the methylene C-atoms of the TBC[4] ligands on neighbouring clusters (C···C, ~ 3.6 Å) and between DMF N-atoms (N···N, ~ 3.7 Å). These interactions appear to direct the formation of 1D chains along the *b*-axis as part of the aforementioned bi-layer.

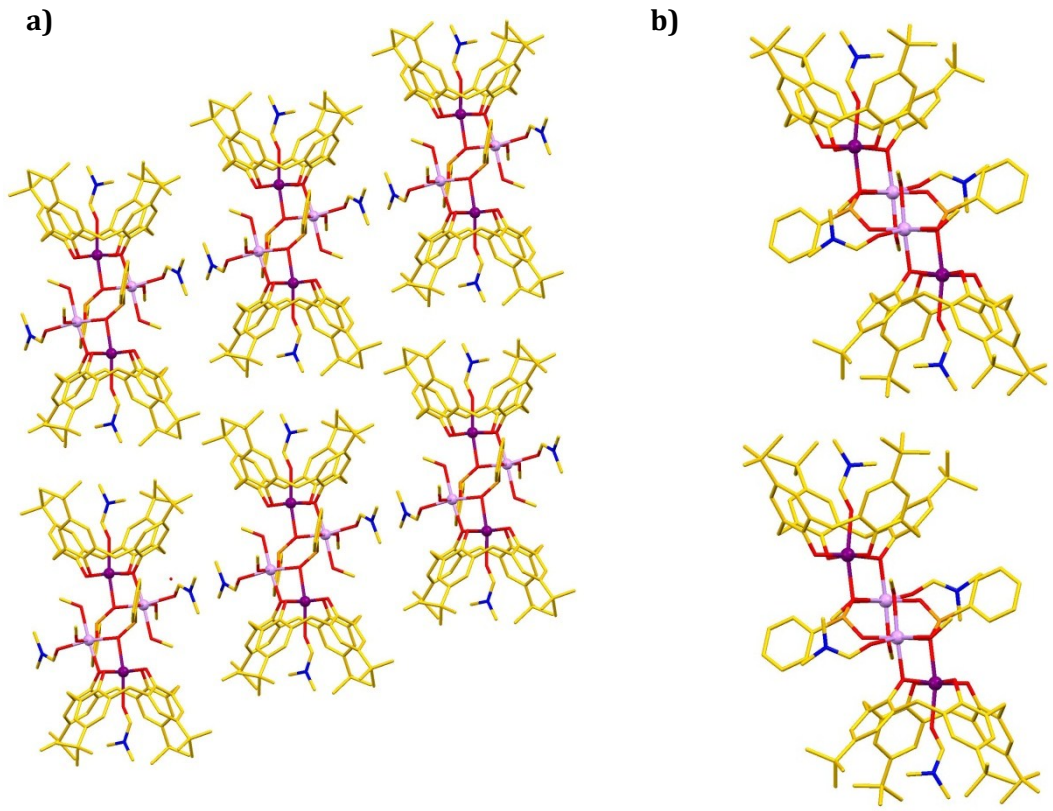

Figure 4. Orthogonal views of a cross section of the extended structure of **8.** a) Self-assembly of complexes into bi-layers reminiscent of the packing of TBC[4] in conventional solvates. b) Skewed head-to-head arrangement of calixarenes within the bi-layer. Colour code as in Figure 3.

Literature searches show that [$Mn^{III}Mn^{II}$] dimers are surprisingly uncommon,[42-44] and the formation of **8** with respect to **1** raises many interesting synthetic questions and identifies opportunities for future exploitation: (a) the [Mn^{III}(TBC[4])] moiety is clearly a stable unit—appearing in all Mn–calix[4]arene clusters isolated to date.[17,18] As such this ''metalloligand'' promises to be an excellent building block for the formation of a plethora of polymetallic Mn^{III}-based cluster compounds whose self-assembly is governed by small changes in reaction conditions. For example, in the absence of any other co-ligands self-assembly affords a hydroxide bridged [$Mn^{III}Mn^{II}$]$_2$ tetramer, **1** (Figure **1**). Addition of phenylphosphinate transforms the tetramer into a dimer of dimers via hydroxide replacement. The isolation of complex **8** suggests that replacement of phenylphosphinate with either bulkier analogues or simply with carboxylates may potentially allow for the isolation of the dimeric [$Mn^{III}Mn^{II}$] unit itself,

whilst the introduction of alternative polynucleating ligands may aid formation of larger oligomers.

$[Mn^{III}_3Mn^{II}_2(OH)_2(TBC[4])_2(hmp)_2(DMF)_6](TBC[4]\text{-}H)\cdot xDMF \cdot xH_2O$ (9)

The reaction of $MnCl_2\cdot 4H_2O$, TBC[4], Hhmp and NEt_3 in a solvent mixture of DMF and EtOH followed by slow evaporation of the mother liquor produces black crystals of **9** in ~50 % yield over 7 days. Crystals of **9** have a triclinic unit cell and structure solution was performed in the space group *P*-1, with the asymmetric unit comprising the entire formula listed above. The metallic skeleton of **9** (Figure 5) describes two vertex-sharing $[Mn^{III}_2Mn^{II}]$ triangles, with Mn1 and Mn5 being in the II+ oxidation state and Mn2-4 being in the III+ oxidation state. Mn3 is the shared vertex. The two μ_3-OH^- ions (O11, O12) lie at the centres of these triangles, but not in the same plane and thus perhaps a more accurate description of the $[Mn^{III}_2Mn^{II}(OH)]$ moiety is that of a partial cubane. The TBC[4] ligands are fully deprotonated and each house a Mn^{III} ion in the centre of their phenolic pocket (Mn2, Mn4); two O-atoms (O1, O2 and O5, O8) are terminally coordinating, but the remaining two (O3, O4 and O6, O7) bridge to the other Mn ions (Mn1, Mn3 and Mn3, Mn5) in the partial cubane. The hmp^- ions chelate to the Mn^{II} ions (Mn1, Mn5) and use their alkoxide arm (O15, O16) to bridge to Mn3. All the Mn ions are six-coordinate, with the remaining sites filled with terminally coordinated DMF molecules: the Mn^{II} ions completing the $\{MnO_5N\}$ coordination sphere, and one on Mn2 and Mn4, both of which reside in the hydrophobic calixarene cavities. The coordination spheres of the III+ ions are thus all $\{MnO_6\}$. The Jahn-Teller axes of the Mn^{III} ions are defined by the OH-Mn-DMF vector for Mn2 and Mn4, and by O4(TBC4)-Mn-O7(TBC4) for Mn3, and are thus approximately co-parallel. The μ_3-OH^- ions are H-bonded to the terminally bonded O-atoms of the TBC[4] ligands (O…O, ~2.8 Å), with the latter also H-bonded to H_2O molecules of crystallisation (O…O, ~2.8 – 2.9 Å).

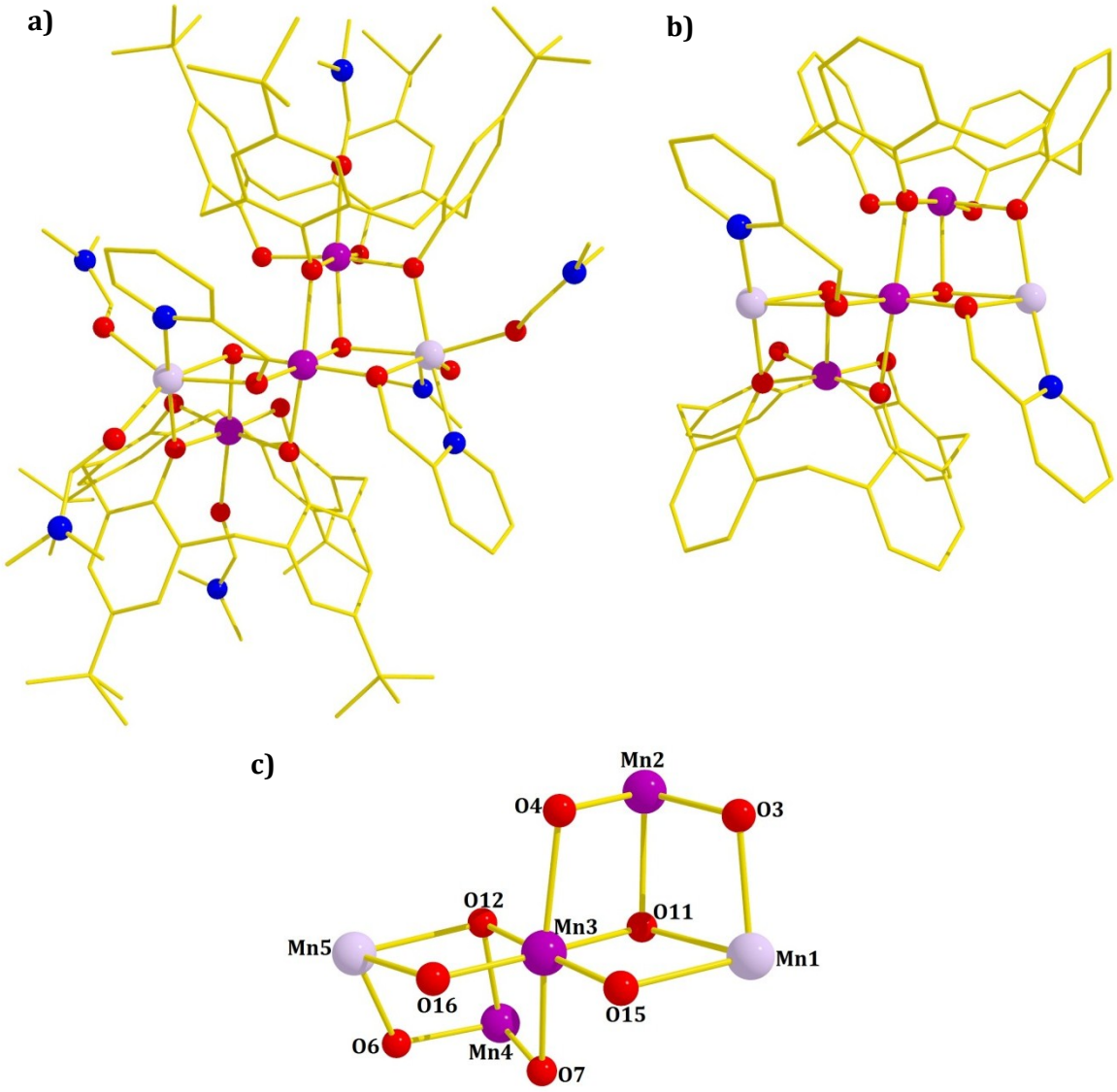

Figure 5. a) Molecular structure of the cation in **9**. b) Molecular structure of the cation in **9** with TBC[4] ^{t}Bu groups and DMF molecules removed. c) Metal-oxygen magnetic core of the cation in **9**. Colour code as in Figure 3.

Charge balance is maintained through the presence of one $(TBC[4]\text{-}H)^-$ anion per Mn_5 cluster. In our previous studies using TBC[4] as a cluster support[17-20] we have observed a propensity for these systems to assemble in a manner akin to the solvates of the calixarene (in anti-parallel bi-layer arrays).[29-31] The extended structure in **9** is unusual in that it contains an additional TBC[4] that is present as a mono-anion. This [TBC4-H] anion co-crystallises orthogonal to the cation, with a DMF of crystallisation occupying the calixarene cavity (Figure 6). An inevitable result of this packing is that the components are unable to form the expected bi-layer array. Despite this feature,

symmetry equivalent cations are still arranged in a manner which is reminiscent to the DMF solvate of TBC[4] in so far as the upper-rim tert-butyl groups are still arranged head-to-head in layers (Figure 7).[18]

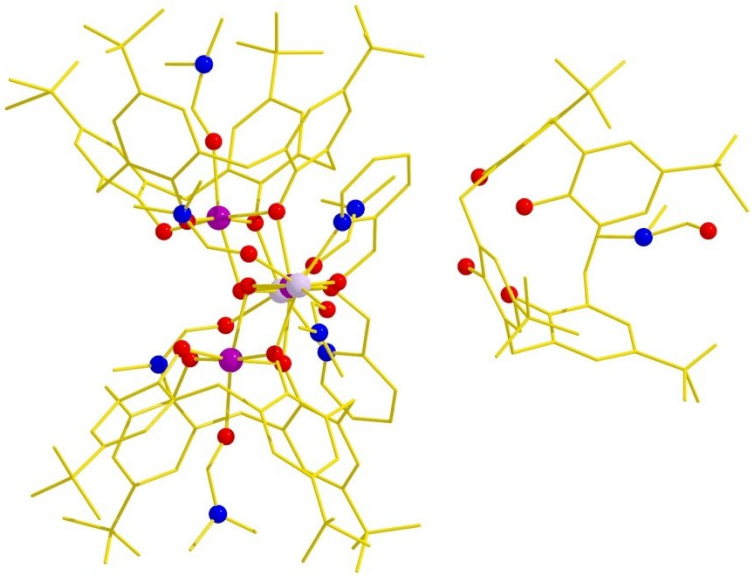

Figure 6. Orthogonal arrangement of the (TBC[4]-H) anion relative to the cation in the asymmetric unit of **9**. Hydrogen atoms and (disordered) ligated / co-crystallised solvent molecules omitted for clarity. Colour code as in Figure 3.

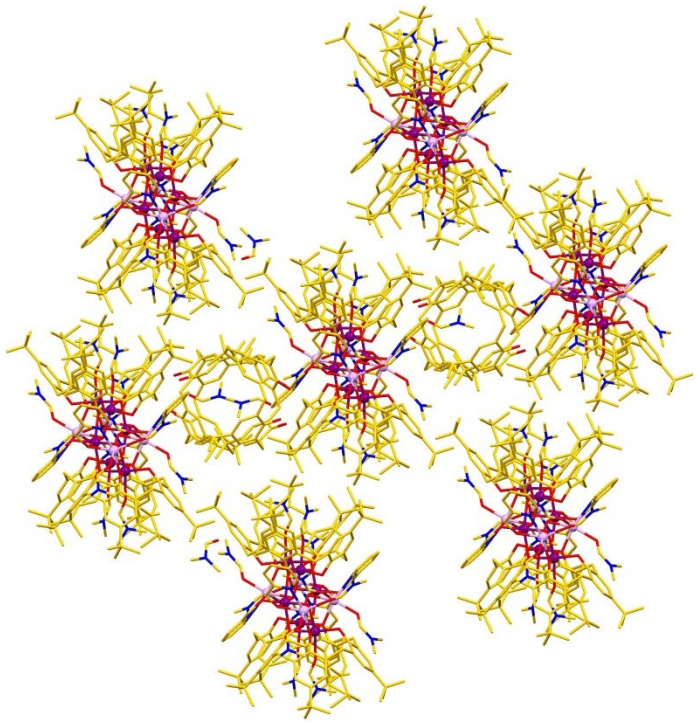

Figure 7. Extended structure of **9** showing the layer-like structure formed by cations. Hydrogen atoms and (disordered) ligated / co-crystallised solvent molecules omitted for clarity. Colour code as in Figure 3.

3.3.2 Magnetic Properties

Solid state dc magnetic susceptibility (χ_M) data on dried **8** were collected in a 0.1 T magnetic field in the 5.0–275 K temperature range (Figure 8). The $\chi_M T$ product at 275 K is approximately 14.67 cm^3 K mol^{-1}, close to that expected for two non-interacting Mn^{III} and Mn^{II} ions with g = 2.0 (14.75 cm^3 K mol^{-1}). As the temperature is decreased the $\chi_M T$ product remains constant to approximately 50 K, below which the value increases slowly reaching a maximum of 17.7 cm^3 K mol^{-1} at 17 K. Below this temperature $\chi_M T$ drops to a value of ~ 11.0 cm^3 K mol^{-1} at 5 K. This behaviour is indicative of the presence of competing ferromagnetic and antiferromagnetic interactions, with the low temperature (T < 17 K) decline in the $\chi_M T$ product assigned to zero-field splitting and/or antiferromagnetic inter-molecular interactions. The experimental data were fitted to isotropic spin Hamiltonian (1) (Scheme 1) using a Levenberg–Marquardt algorithm.[45]

$$\hat{H} = -2J\left(\hat{S}_1\hat{S}_2 + \hat{S}_1\hat{S}_3 + \hat{S}_2\hat{S}_4 + \hat{S}_3\hat{S}_4\right) - 2J'\hat{S}_2\hat{S}_3 + \mu_B B_g S \qquad (1)$$

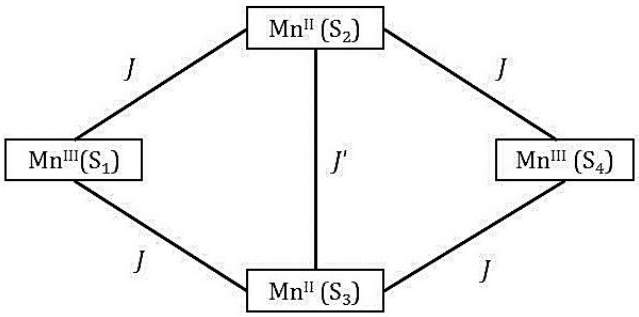

Scheme 1. Cartoon representation of the exchange interactions in **8** and spin Hamiltonian (1).

In spin-Hamiltonian (1) indices 1 and 4 correspond to Mn^{III} centres (Mn1 and symmetry equivalent), indices 2 and 3 correspond to Mn^{II} centres (Mn2 and symmetry equivalent), J is the isotropic exchange parameter, $\hat{S}$ the spin operator of a given centre, μ_B the Bohr magneton, g the isotropic g-factor (fixed to g = 2.0) and B the magnetic field. In addition to the J and J' fitting parameters, the intermolecular interactions were taken into account through the introduction of the Curie–Weiss temperature θ. The best fit parameters obtained (shown as the solid lines in Figure 8) in the 6.5–275 K temperature range are: J = 5.14 cm^{-1}, J' = -8.47 cm^{-1} and θ =-3.0 K. When the fit

temperature range is restricted to between 20 and 300 K, the obtained best fit parameters are: J = 5.07 cm^{-1}, J' = -8.44 cm^{-1} and θ = -3.0 K. Thus, the obtained best-fit parameters are not sensitive to the temperature range of the fit at temperatures higher than 6.5 K and can be considered to describe the system well. However, when the fit temperature range is extended to between 5.0 and 275 K, the best fit parameters are: J = 3.38 cm^{-1}, J' = -4.89 cm^{-1} and θ = -3.6 K. The decrease in the quality of the fit at the lowest temperatures suggests that spin-Hamiltonian (1) is no longer a good model and that anisotropy effects should be taken into account. With J = 5.14 cm^{-1} and J' = -8.47 cm^{-1}, the ground spin-state of complex **8** is an S = 6 spin state. The relative energies of the 110 different spin states, determined by diagonalisation of the matrix representation of spin-Hamiltonian (1), are given in Figure 9.

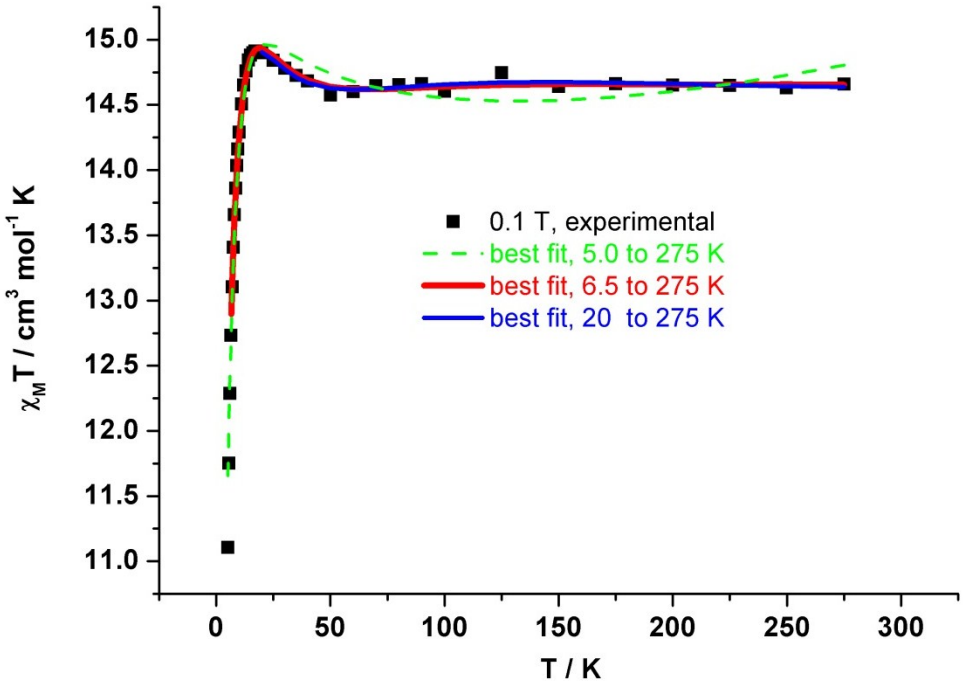

Figure 8. Fit, by use of the Levenberg-Marquardt algorithm, of the $\chi_M T$ product of **8** measured at 0.1 T and in three different temperature ranges, namely 5 to 275 K (green), 6,5 to 275 K (red) and 20 to 275 K (blue), yielding the best fit parameters given in the text.

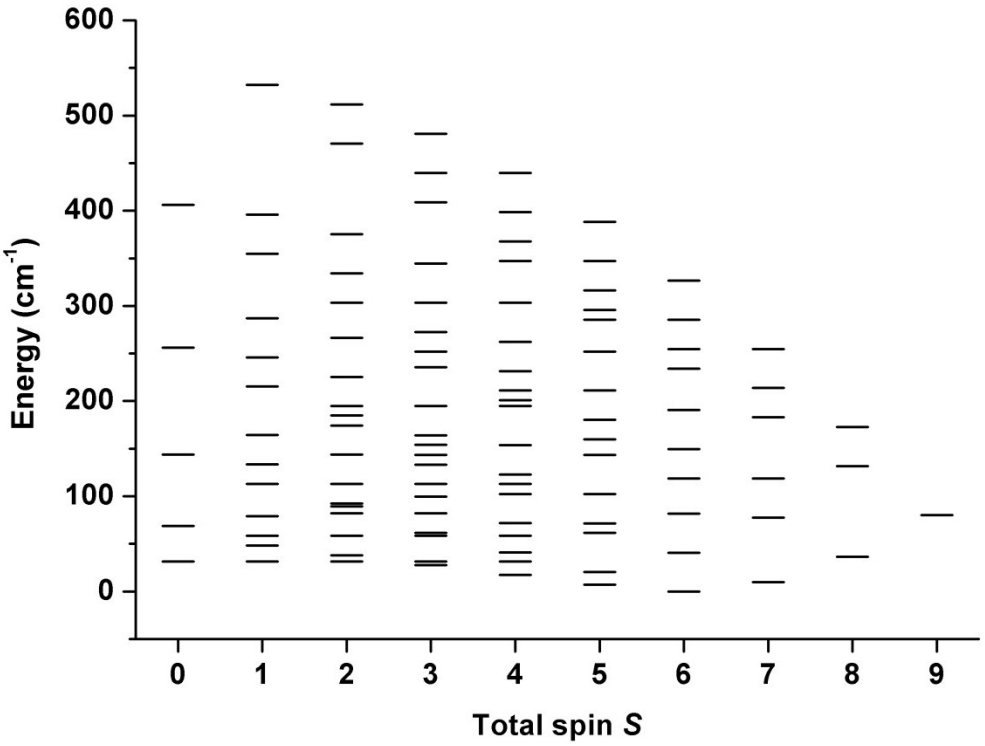

Figure 9. Zero-field energy diagram of the spin-states of **8** determined by diagonalisation of the matrix representation of spin Hamiltonian (1) with J = 5.14 cm^{-1} and J' = -8.47 cm^{-1}.

$[Mn^{III}_3Mn^{II}_2(OH)_2(TBC[4])_2(hmp)_2(DMF)_6](TBC[4]\text{-}H)\cdot xDMF\cdot xH_2O$ (9

Solid state dc magnetic susceptibility measurements were carried out on polycrystalline samples of **9** in the 275-5 K temperature range in an applied field of 0.1 T (Figure 10). The high temperature $\chi_M T$ value of 18.6 cm^3 K mol^{-1} is close to the spin-only value expected for an uncoupled $[Mn^{III}_3Mn^{II}_2]$ unit of 17.75 cm^3 K mol^{-1} with g = 2.0. The $\chi_M T$ value then increases slowly with decreasing temperature reaching a value of approximately 20.3 cm^3 K mol^{-1} at 100 K, below which it then increases more rapidly reaching a maximum value of ~40.3 cm^3 K mol^{-1} at 5.5 K. This behavior is suggestive of weak intramolecular ferromagnetic exchange.

$$\hat{H} = -2\left[J_1\left(\hat{S}_1 \cdot \hat{S}_2 + \hat{S}_1 \cdot \hat{S}_3 + \hat{S}_3 \cdot \hat{S}_5 + \hat{S}_4 \cdot \hat{S}_5\right) + J_2\left(\hat{S}_2 \cdot \hat{S}_3 + \hat{S}_3 \cdot \hat{S}_4\right)\right] + D_{Mn} \sum_{i=2,3,4} \{\hat{S}_{z,i}^2 - S(S+1)/3\} + \mu_B g\vec{B} \cdot \sum_{i=1}^{5} \{\hat{S}_i\} \quad (2)$$

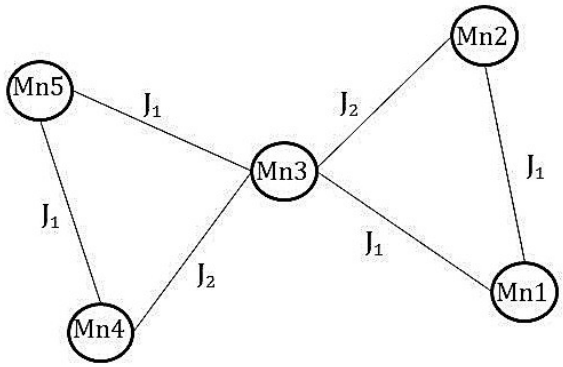

Scheme 2. Cartoon representation of the exchange interactions in **9** and spin Hamiltonian (2).

The experimental $\chi_M T$ data of **9** can only be fitted by use of the anisotropic spin-Hamiltonian model (2), depicted in Scheme 2;[45] where J_1 and J_2 are the Mn^{III}-Mn^{II} and Mn^{III}-Mn^{III} isotropic exchange parameters, respectively, $\hat{S}$ is a spin-operator, i runs from 1 to 5, D is the single-ion axial anisotropy parameter of Mn^{III}, μ_B is the Bohr magneton, $\vec{B}$ is the applied magnetic field vector, and g = 2.00 is the g-factor of the Mn ions. In addition, intermolecular interactions were taken into account through the introduction of the Curie- Weiss temperature, θ. The resulting best-fit curve, obtained by full matrix diagonalisation of the full spin-Hamiltonian matrix of dimension 4500, is shown as the solid red line in Figure 10. The best fit parameters obtained from fitting the $\chi_M T$ data are J_1 = 0.348 cm^{-1}, J_2 = 2.553 cm^{-1} and D = -2.267 cm^{-1} and θ = -1.64 K. Taking into account the zero-field isotropic part of spin Hamiltonian (2) and with these parameters, the ground spin-state of the system is an S = 11 state.

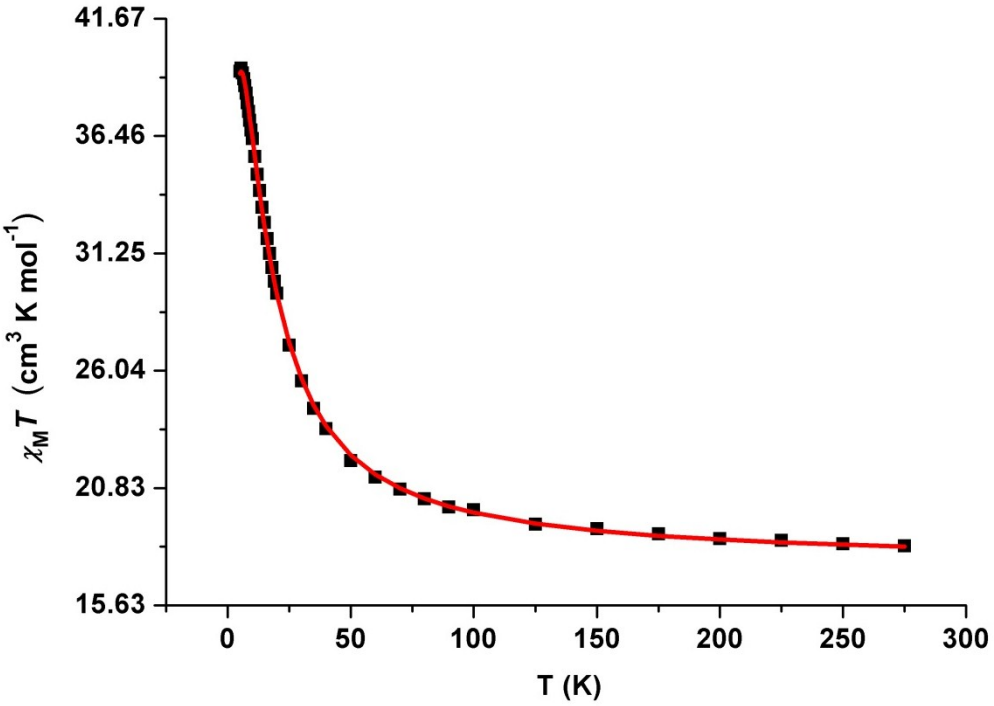

Figure 10. Plot of the χ_MT product of **9** vs. T in the 275 -5 K temperature range in an applied field of 0.1 T. The solid red line is the best-fit of the data.

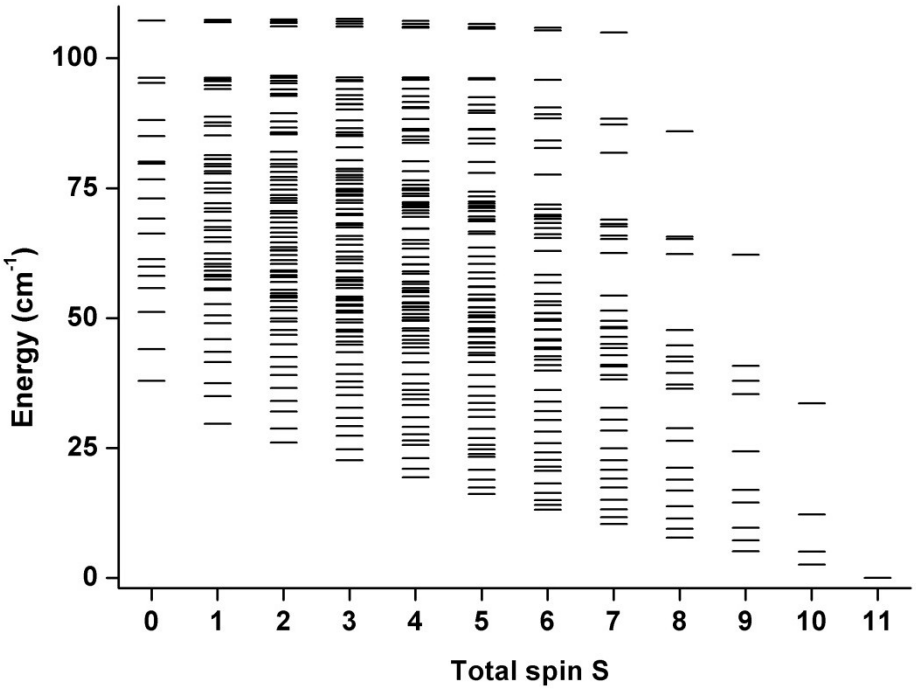

Figure 11. Zero-field energy spectrum of **9**, obtained by diagonalisation of the isotropic part of spin Hamiltonian (2) with J_1 = +0.348 cm^{-1} and J_2 = +2.553 cm^{-1}.

The full zero-field, isotropic, energy spectrum of **9** is given in Figure 11. The magnitude of the exchange interactions resembles that observed for both $[Mn^{III}_2Mn^{II}_2(OH)_2(TBC[4])_2(solvent)_6]$ and $[Mn^{III}_2Mn^{II}_2(hmp)_6Br_2(H_2O)_2]^{2+}$. To better estimate *D*, we modeled the variable-field and variable-temperature magnetisation data of **9** in the temperature range 2 to 7 K and in applied fields from 0.5 to 7.0 T (Figure 12). We again used spin Hamiltonian (2) and the Levenberg-Marquardt algorithm,[45] with J_1 and J_2 fixed and only fitted *D* and θ. The resulting best-fit parameters were D = -2.111 cm^{-1} and θ = -0.080 K, reflecting that the intermolecular interactions are quenched by high magnetic fields. Ac susceptibility studies carried out on crystalline samples of **9** in the 1.8-10.0 K range in a 3.5 G field oscillating at frequencies up to 1000 Hz (Figure 13) display frequency-dependent out-of-phase (χ_M'') signals suggestive of SMM behavior. An Arrhenius plot constructed from these data afford U_{eff} = 42 K with $\tau_0 = 1.125 \times 10^{-10}$ s.

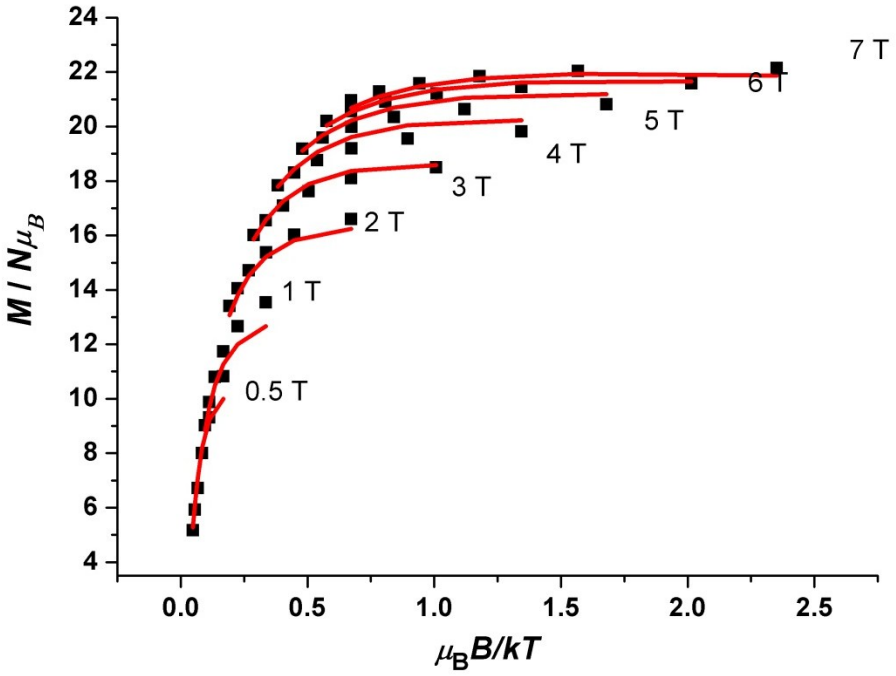

Figure 12. Plot of reduced magnetisation of **9** in the 2.0 – 7.0 K temperature range at the indicated field strengths. The solid red lines are the best fit of the data. See text for details.

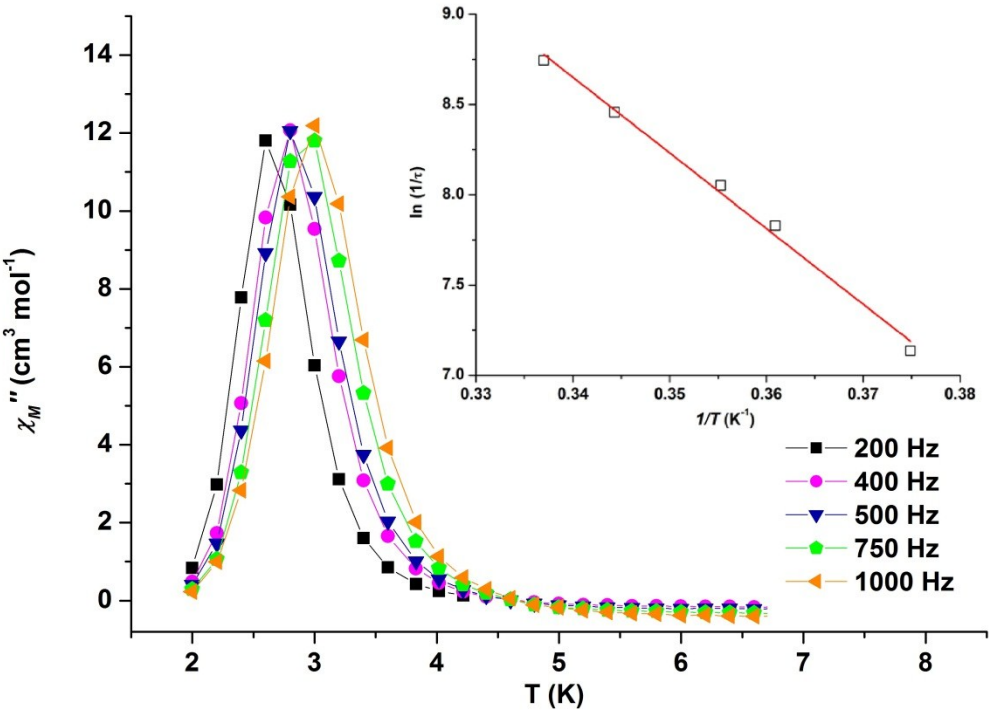

Figure 13. Ac susceptibility studies carried out on crystalline samples of **9** in the 1.8-10.0 K range in a 3.5 G field oscillating at frequencies up to 1000 Hz. Insert: Arrhenius plot constructed from these data afford U_{eff} = 42 K with τ_0 = 1.125 x 10^{-10} s.

3.4 Conclusions

In summary we have formed new calixarene-supported manganese cluster motifs by the introduction of phosphinate and the N,O-chelating 2-(hydroxymethyl)pyridine co-ligands to the magnetic core of a known assembly. Further studies are underway with a view to introducing features that may allow for the expression of control over self-assembly from the periphery of these complexes, as well as via alteration of groups at the upper-rim of the constituent calixarenes. Magnetic studies reveal the presence of both ferro- and antiferromagnetic exchange interactions, resulting in an S = 6 ground state for **8**. The combination of *p*-tert-butylcalix[4]arene and 2-(hydroxymethyl)pyridine produces a ferromagnetic [Mn_5] cage that displays the characteristic bonding modes of each support. This would suggest that an in-depth search of the CCDC database may reveal other hitherto untried ligand combinations that would result in molecules with interesting structural and/or magnetic characteristics.

3.5 References

1. M. Andruh, *Chem. Commun.*, 2011, **47**, 3025-3042.
2. G. Aromí, D. Aguila, P. Gamez, F. Luis and O. Roubeau, *Chem. Soc. Rev.*, 2012, **41**, 537-546.
3. M. Clemente-León, E. Coronado, C. Martí-Gastaldo and F. M. Romero, *Chem. Soc. Rev.*, 2011, **40**, 473-497.
4. E. Colacio, J. Ruiz-Sanchez, F. J. White and E. K. Brechin, *Inorg. Chem.*, 2011, **50**, 7268-7273.
5. L. N. Dawe, K. V. Shuvaev and L. K. Thompson, *Chem. Soc. Rev.*, 2009, **38**, 2334-2359.
6. T. Glaser, *Coord. Chem. Rev.*, 2012, **10.1016/j.ccr.2012.05.005**.
7. F. Habib, J. Long, P.-H. Lin, I. Korobkov, L. Ungur, W. Wernsdorfer, L. F. Chibotaru and M. Murugesu, *Chem. Sci.*, 2012, **3**, 2158-2164.
8. V. Marvaud, C. Decroix, A. Scuiller, C. Guyard-Duhayon, J. Vaissermann, F. Gonnet and M. Verdaguer, *Chem. Eur. J.*, 2003, **9**, 1677-1691.
9. H. Miyasaka and M. Yamashita, *Dalton Trans.*, 2007, 399-406.
10. M. Nihei, Y. Sekine, N. Suganami, K. Nakazawa, A. Nakao, H. Nakao, Y. Murakami and H. Oshio, *J. Am. Chem. Soc.*, 2011, **133**, 3592-3600.
11. T. D. Pasatoiu, M. Etienne, A. M. Madalan, M. Andruh and R. Sessoli, *Dalton Trans.*, 2010, **39**, 4802-4808.
12. G. A. Timco, T. B. Faust, F. Tuna and R. E. P. Winpenny, *Chem. Soc. Rev.*, 2011, **40**, 3067-3075.
13. R. E. P. Winpenny, *J. Chem. Soc., Dalton. Trans.*, 2002, 1-10.
14. E. K. Brechin, J. C. Huffman, G. Christou, J. Yoo, M. Nakano and D. N. Hendrickson, *Chem. Commun.*, 1999, 783-784.
15. J. Yoo, A. Yamaguchi, M. Nakano, J. Krzystek, W. E. Streib, L. C. Brunel, H. Ishimoto, G. Christou and D. N. Hendrickson, *Inorg. Chem.*, 2001, **40**, 4604-4616.
16. C. Aronica, G. Chastanet, E. Zueva, S. A. Borshch, J. M. Clemente-Juan and D. Luneau, *J. Am. Chem. Soc.*, 2008, **130**, 2365-2371.
17. G. Karotsis, S. Kennedy, S. J. Teat, C. M. Beavers, D. A. Fowler, J. J. Morales, M. Evangelisti, S. J. Dalgarno and E. K. Brechin, *J. Am. Chem. Soc.*, 2010, **132**, 12983-12990.
18. G. Karotsis, S. J. Teat, W. Wernsdorfer, S. Piligkos, S. J. Dalgarno and E. K. Brechin, *Angew. Chem. Int. Ed*, 2009, **48**, 8285-8288.
19. S. Sanz, K. Ferreira, R. D. McIntosh, S. J. Dalgarno and E. K. Brechin, *Chem. Commun.*, 2011, **47**, 9042-9044.
20. S. M. Taylor, G. Karotsis, R. D. McIntosh, S. Kennedy, S. J. Teat, C. M. Beavers, W. Wernsdorfer, S. Piligkos, S. J. Dalgarno and E. K. Brechin, *Chem. Eur. J.*, 2011, **17**, 7521-7530.
21. J. L. Atwood, L. J. Barbour, M. J. Hardie and C. L. Raston, *Coord. Chem. Rev.*, 2001, **222**, 3-32.
22. E. S. Barrett, T. J. Dale and J. Rebek, *J. Am. Chem. Soc.*, 2007, **129**, 3818-3819.
23. S. J. Dalgarno, S. A. Tucker, D. B. Bassil and J. L. Atwood, *Science* 2005, **309**, 2037-2039.
24. T. Gerkensmeier, W. Iwanek, C. Agena, R. Fröhlich, S. Kotila, C. Näther and J. Mattay, *Eur. J. Org. Chem.*, 1999, **1999**, 2257-2262.
25. L. R. MacGillivray and J. L. Atwood, *Nature*, 1997, **389**, 469-472.
26. O. Ugono and K. T. Holman, *Chem. Commun.*, 2006, 2144-2146.

27. C. D. Gutsche, *Acc. Chem. Res.*, 1983, **16**, 161-170.
28. C. D. Gutsche, *Calixarenes 2001*, Kluwer Academic Publishers, 2001.
29. S. J. Dalgarno, P. K. Thallapally, L. J. Barbour and J. L. Atwood, *Chem. Soc. Rev.*, 2007, **36**, 236-245.
30. B. M. Furphy, J. M. Harrowfield, M. I. Ogden, B. W. Skelton, A. H. White and F. R. Wilner, *J. Chem. Soc., Dalton. Trans.*, 1989, 2217-2221.
31. J. A. Ripmeester, G. D. Enright, C. I. Ratcliffe, K. A. Udachin and I. L. Moudrakovski, *Chem. Commun.*, 2006, 4986-4996.
32. M. A. Bolcar, S. M. J. Aubin, K. Folting, D. N. Hendrickson and G. Christou, *Chem. Commun.*, 1997, 1485-1486.
33. C. Boskovic, E. K. Brechin, W. E. Streib, K. Folting, D. N. Hendrickson and G. Christou, *Chem. Commun.*, 2001, 467-468.
34. C. D. Gutsche, in *Calixarenes: An Introduction*, RSC, 2008, pp. 27-60.
35. C. D. Gutsche and M. Iqbal, *Org. Synth.*, 1990, **68**, 234.
36. C. D. Gutsche, M. Iqbal and D. Stewart, *J. Org. Chem.*, 1986, **51**, 742-745.
37. W. Liu and H. H. Thorp, *Inorg. Chem.*, 1993, **32**, 4102-4105.
38. H. H. Thorp, *Inorg. Chem.*, 1992, **31**, 1585-1588.
39. G. D. Andreetti, R. Ungaro and A. Pochini, *J. Chem. Soc., Chem. Commun.*, 1979, 1005-1007.
40. E. B. Brouwer, G. D. Enright and J. A. Ripmeester, *J. Am. Chem. Soc.*, 1997, **119**, 5404-5412.
41. J. L. Atwood, L. J. Barbour, A. Jerga and B. L. Schottel, *Science*, 2002, **298**, 1000-1002.
42. D. A. Bardwell, J. C. Jeffery and M. D. Ward, *J. Chem. Soc., Dalton. Trans.*, 1995, 3071-3080.
43. H. R. Chang, S. K. Larsen, P. D. W. Boyd, C. G. Pierpont and D. N. Hendrickson, *J. Am. Chem. Soc.*, 1988, **110**, 4565-4576.
44. H. Diril, H. R. Chang, X. Zhang, S. K. Larsen, J. A. Potenza, C. G. Pierpont, H. J. Schugar, S. S. Isied and D. N. Hendrickson, *J. Am. Chem. Soc.*, 1987, **109**, 6207-6208.
45. W. H. Press, S. A. Teukolsky, W. T. Vetterling and B. P. Flannery, *Numerical Recipes In C: The Art of Scientific Computing, 2nd ed.*, Cambridge University Press, 1992.

Chapter 4
Oxacalix[3]arene-supported supertetrahedron

4.1 Introduction

Methylene-bridged calix[4]arenes have recently emerged as versatile bowl-shaped ligands for the construction of polynuclear metal cluster compounds.[1-5] Upon deprotonation, the polyphenolic lower-rim can be used as a scaffold to bind either transition or lanthanide metal centres (TM and Ln, respectively) which self-assemble to form elaborate molecules exhibiting fascinating structural and magnetic characteristics. The coordination chemistry of the thia-, sulfonyl- and sulfinylcalix[4]arenes has received significant attention;[6-10] these display markedly different metal binding properties to their methylene-bridged analogues due to the presence of additional donor atoms in the ligand framework. In stark contrast the coordination chemistry of the family of oxacalixarenes has been largely ignored; a search of the CCDC database for metal complexes of the oxacalixarene subunit (two phenols linked by an ethereal bridge) reveals 59 hits for a total of 8 ring sizes. This is rather surprising when one considers the potential to subtly tune the nature of the metal binding site by controlled introduction of ≥ 1 ethereal bridge. For example, introduction of one bridge to the calix[4]arene framework produces a trapezoidal rather than square binding site as shown in Figure 1. Furthermore, introduction of multiple ethereal bridges greatly expands the square binding site and may thus invoke coordination chemistry motifs akin to those of the thia-calix[4]arenes.

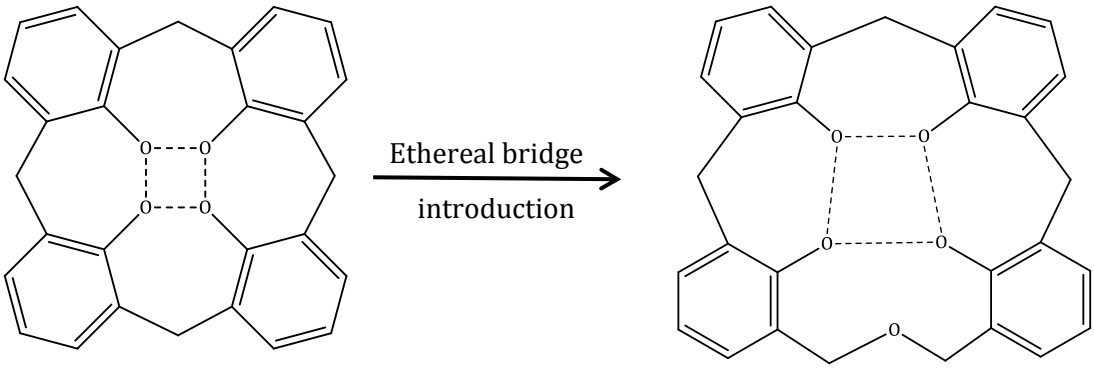

Figure 1. Schematic showing the change in the calix[4]arene metal binding site by introduction of one ethereal bridging group.

p-*t*Bu-Homooxacalix[3]arene (TBOC[3], Figure 2) is a shallow bowl-shaped ligand that accounts for 23 of 59 hits in the abovementioned CCDC search. The majority of these hits are mononuclear complexes containing 4f or 5f elements,[11-16] with only nine

containing TM ions (Sc, Ti, Fe, V, Y, Nb and Ta).[11,17-21] Only two of the latter motifs (a Nb_3(TBOC[3])$_3$ complex and its Ta analogue and a vanadium dimer [{V^V(N-*p*-tolyl)(TBOC[3])}$_2$]) contains more than two metal centres[20,21] and none have been constructed for the investigation of their magnetic properties. Aside from structural properties it is noteworthy to mention that TM oxacalixarene systems (in particular V complexes), investigated chiefly by Redshaw, have significantly greater activity towards olefin polymerization than their methylene-bridged analogues. Structure analysis of the aforementioned complexes reveals that TBOC[3] displays high degrees of versatility in metal binding when in the bowl conformation, in so far as up to all three ethereal oxygens can also coordinate to ions bound at the lower-rim. Bridging group coordination is a common feature in the presence of 4f and 5f ions,[12,13,15,16] but is observed in just two cases for the TMs listed above.[20] Conformational distortion is observed in the binding of Fe[17] and Nb[20] but the cone conformation is preserved in the formation of Sc and V complexes.[18,21]

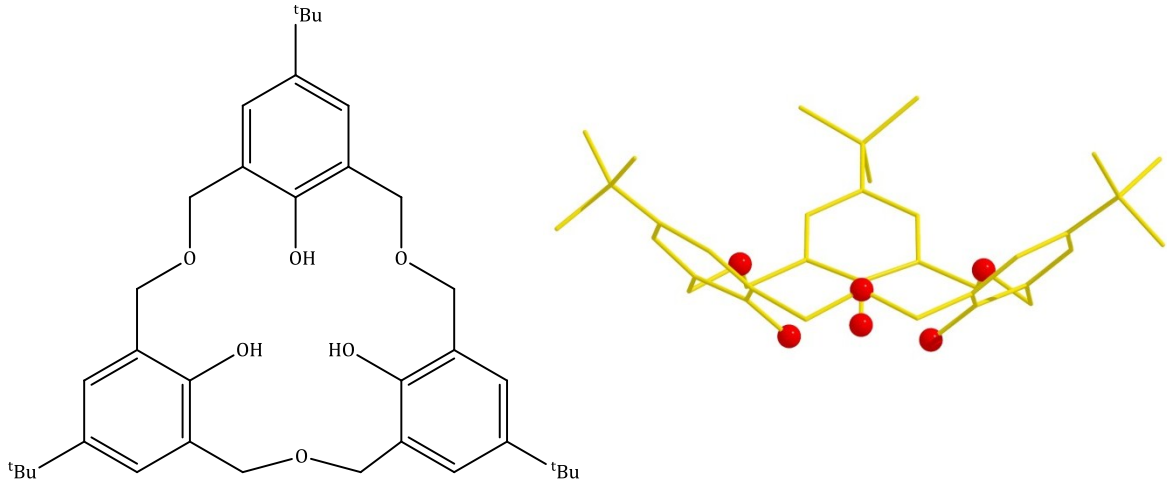

Figure 2. Schematic (left) and single crystal X-ray (right) structure of *p*-^{t}Bu-Homooxacalix[3]arene (TBOC[3]) showing the shallow bowl conformation and position of ethereal O atoms. Colour code: C = gold, O = red, H- atoms and solvent molecules omitted for clarity.

We have observed preferential binding of TM(III) rather than TM(II) ions in our study of manganese and iron coordination chemistry with calix[4]arene.[2-5] Given that TBOC[3] presents a versatile binding cavity, and that it differs markedly from calix[4]arene in terms of size and charge upon full deprotonation, we have begun to investigate the effect this will have on the prevailing coordination chemistry with

manganese performed under bench top conditions. Here we show that TBOC[3] is indeed capable of acting as a suitable support for cluster formation with manganese, that Mn(II) rather than Mn(III) is bound by the tris-phenolic pocket, and that these components self-assemble with additional Mn(II) and Mn(III) ions to form a [Mn_{10}] supertetrahedron with unusual oxidation state distribution.

4.2 Experimental

4.2.1 Syntheses

All manipulations were performed under aerobic conditions using materials as received (reagent grade). Elemental analyses (C, H, N) were performed by MEDAC LTD microanalysis service. Variable-temperature, solid-state direct current (dc) magnetic susceptibility data down to 5 K were collected on a Quantum Design MPMS-XL SQUID magnetometer equipped with a 7 T dc magnet. Diamagnetic corrections were applied to the observed paramagnetic susceptibilities using Pascal's constants. TBOC[3] was synthesised according to a literature procedure[22] and was checked for purity by ^{1}H NMR and mass spectrometry prior to use in cluster synthesis. Full crystallographic details for the structures reported here are listed in Table 3. Selected bond lengths are given in the appendix. The oxidation states of the metal ions were confirmed by charge balance, bond length considerations and bond valence sum calculations which compare the sum of the observed bond lengths around an atom against tabulated bond lengths.[23,24]

$[Mn^{II}_6Mn^{III}_4O_4(TBOC[3])_4(Cl)_4(DMF)_3]\cdot 3.3H_2O \cdot 1.5DMF$ (10)

$MnCl_2\cdot 4H_2O$ (0.1 g, 0.5 mmol), TBOC[3] (0.1 g, 0.17 mmol), NH_4ClO_4 (0.06 g, 0.5 mmol) and NEt_3 (0.02 g, 2 mmol) were added to a solvent mixture of MeCN (10 mL) and DMF (10 mL) and stirred for 2 hours. Filtration of the solution followed by hexane diffusion afforded brown crystals of **10** in ~40% yield after 3 days. Elemental analysis (%), found (calc.) for $C_{160.50}H_{225.10}Cl_4Mn_{10}N_{5.50}O_{36.80}$: C 56.24 (55.91), H 6.43 (6.34), N 2.04 (2.05).

Table 3. Crystal structure information for **10** and **TBOC[3]·DMF**[a]

	10[a]	**TBOC[3]·DMF**[a]
Chemical formula	$C_{160.50}H_{225.10}Cl_4Mn_{10}N_{5.50}O_{36.80}$	$C_{153}H_{213}N_3O_{27}$
M_r	3511.56	2526.26
Crystal system	Monoclinic	Trigonal
Space group	$C2/c$	$P3$
a (Å)	37.8284 (18)	16.5740 (7)
B (Å)	27.8091 (13)	16.5740 (7)
c(Å)	37.6849 (19)	15.5660 (8)
α (°)	90	90
B (°)	114.965 (2)	90
Γ (°)	90	120
V (Å^3)	35939 (3)	3703.1 (3)
Z	8	1
F(000)	14712	1368
Crystal size (mm)	0.40 × 0.30 × 0.25	0.30 × 0.20 × 0.15
No. of measured, independent and observed [$I > 2\sigma(I)$] reflections	133789, 33987, 13217	22249, 8453, 5399
R_{int}	0.141	0.032
$R[I > 2\sigma(I)]$	0.106	0.060,
$wR_2(F^2)$	0.293	0.155
GOF on F^2	1.24	0.90

[a] Data collected on a Bruker Apex II diffractometer operating with $Mo_{K\alpha}$ radiation (λ = 0.71073 Å) at 100(2) K.

4.3 Results and Discussion

4.3.1 Structural Analysis

During the course of our CCDC analysis we noted that the MeCN solvate of TBOC[3] was the only one reported to date.[21] Examination of the extended structure of TBOC[3]·MeCN shows that the calixarenes stack one bowl on top of another to form columns, with MeCN crystallising in interstitial spaces. As we planned to carry out cluster forming reactions in DMF we crystallised TBOC[3] in order to observe related assembly behaviour. Crystals of TBOC[3]·DMF are in a trigonal cell and structure solution was performed in the space group *P*3 To our surprise, structure analysis revealed that four molecules of TBOC[3] arrange at the vertices of a tetrahedron around a central DMF of crystallisation (Figure 3). This assembly behaviour is markedly different to that observed in the acetonitrile solvate, and structure expansion shows that TBOC[3] cavities are occupied by ^{t}Bu groups from symmetry equivalent molecules.

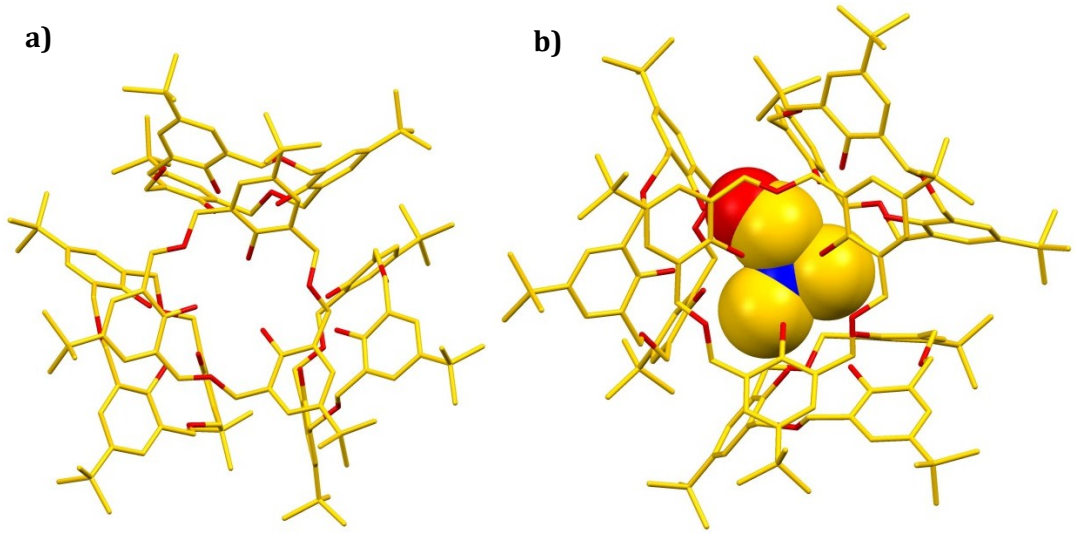

Figure 3. a) Extended structure of TBOC[3]·DMF showing back-to-back calixarene packing. b) Part of the extended structure of the TBOC[3] DMF solvate showing four calixarenes packing around one DMF molecule (shown in space filling mode).Colour code: C = gold, O = red, N = blue, H-atoms and solvent molecules omitted for clarity.

The reaction of $MnCl_2{\cdot}4H_2O$, TBOC[3] and NEt_3 in a solvent mixture of DMF and EtOH followed by vapour diffusion with hexane, produces black crystals of **10** with formula $[Mn^{II}_6Mn^{III}_4O_4(TBOC[3])_4(Cl)_4(DMF)_3]{\cdot}3.3H_2O{\cdot}1.5DMF$. The crystals of **10** crystallise in a monoclinic cell and structure solution was performed in the space group *C*2/*c*. The skeleton of **10** (Figure 4) describes a mixed-valent $[Mn^{II}_6Mn^{III}_4]$ supertetrahedron. The

six Mn(II) ions form two linear, perpendicular arrays: Mn9, Mn10 and Mn5 along the back vertical edge, and Mn1, Mn3 and Mn7 along the front horizontal edge, as drawn in Figure 4b. The cage is held together internally through the presence of four μ_4-O^{2-} ions (O25–O28) to afford a $[Mn_{10}O_4]^{16+}$ core that can also be regarded as four vertex-sharing $\{Mn^{III}_2Mn^{II}_2O\}^{8+}$ tetrahedra. The four μ_3-Cl^- ions (Cl1–Cl4), which themselves define a tetrahedron, each cap one face of the supertetrahedron, occupying the Jahn–Teller coordination sites on the Mn(III) ions (Mn2, Mn4, Mn6, Mn8). The fully deprotonated μ_4-TBOC[3] ligands cap each apex of the tetrahedron, using their three phenolate O-atoms to bond to the centrally housed Mn(II) ion and further bridge to the neighbouring Mn ions on the edges of the supertetrahedron. The Mn(III) ions are all six coordinate and in the axially-elongated octahedral $\{O_4Cl_2\}$ geometries expected for high spin d^4 ions. The Mn(II) ions are five coordinate and in distorted trigonal bipyramidal $\{O_5\}$ geometries, the remaining coordination site on each being occupied by a DMF molecule sitting in the cavity of the TBOC[3] ligand.

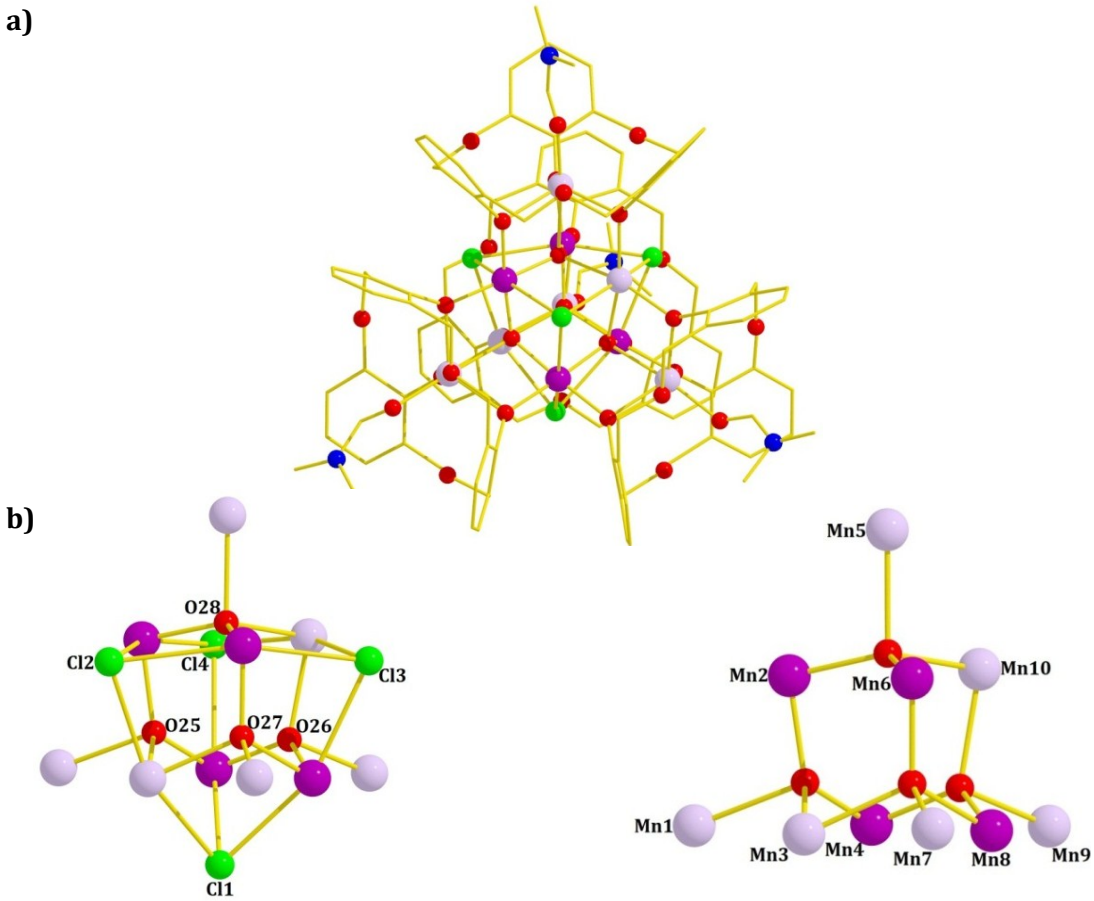

Figure 4. a) Molecular structure of **10**. b) The core of **10** with and without chloride ions (left and right respectively). Colour code: Mn^{III} = purple, Mn^{II} = pale purple, O = red, N = blue, Cl = green, C = gold, H-atoms and ^{t}Bu groups omitted for clarity.

Interestingly the TBOC[3] ligands in complex **10** house Mn(II) ions in their polyphenolic pockets, and these ''cluster ligands'' then further bridge to Mn(III) ions. This is in complete contrast to all known calix[4]arene Mn clusters where the reverse is always true, the Mn(III) ions being housed within the ligand pocket with the Mn(II) ions located ''externally''. The reason for this is somewhat unclear at present and will require the construction of a library of TBOC[3]-based complexes. However, we speculate that the more flexible polyphenolic pocket of TBOC[3] will more happily accommodate a larger ion with flexible geometry, in comparison to the rather rigid requirements of the smaller, Jahn–Teller distorted Mn(III) ion. Indeed the TBC[4] ligand is perfectly set up to provide the four short equatorial bonds demanded by the Mn(III) ion. With only one related example it is only feasible to consider retention of the T_d $(TBOC[3])_4$ unit coincidental, but it is an interesting possibility that such back-to-back calixarene packing may occur in other metal complexes.

Complex **10** is only the sixth example of any polynuclear TM complex built with TBOC[3], the first example to contain more than two paramagnetic TM ions and the first Mn-based cluster of any kind. $[Mn_{10}]$ supertetrahedra are also rather uncommon, a CCDC search revealing only five previous examples.[25-29] Of these, three have a $[Mn^{III}_6Mn^{II}_4]$ oxidation state distribution, one contains only Mn(III) ions, and only the complex $[Mn_{10}O_4(biphen)_4X_{12}]^{4-}$ (biphen = 2, 2'-biphenoxide; X = Cl^-, Br^-) has the $[Mn^{III}_4Mn^{II}_6]$ distribution seen in complex **10**. Figure 5 gives a pictorial comparison of the metallic skeletons of all known $[Mn_{10}]$ supertetrahedra.

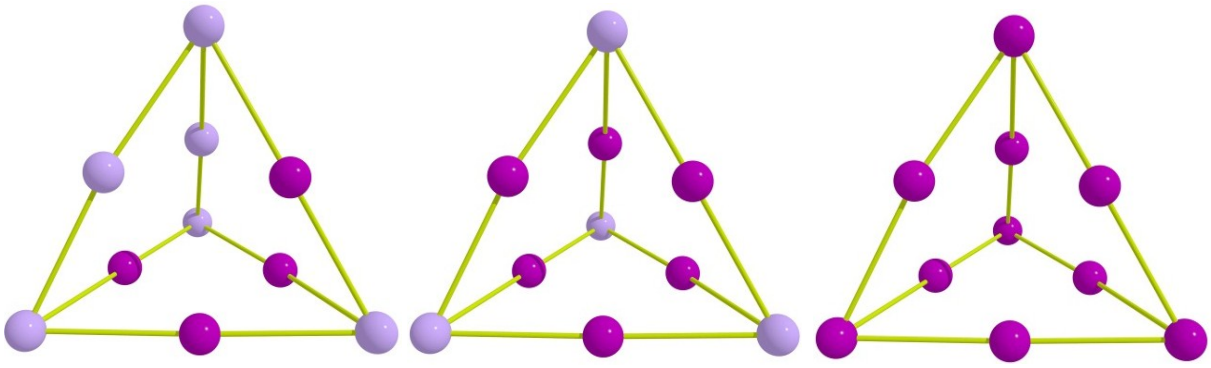

Figure 5. Comparison of the oxidation state distribution in published $[Mn_{10}]$ supertetrahedra. $[Mn^{III}_4Mn^{II}_6]$ (left), $[Mn^{III}_6Mn^{II}_4]$ (middle) and $[Mn^{III}_{10}]$ (right). Colour code: Mn^{III} = purple, Mn^{II} = pale purple.

4.3.2 Magnetic Properties

Solid state dc magnetic susceptibility (χ_M) data on dried, polycrystalline **10** restrained in eicosane were collected in a 0.1 T magnetic field in the 5.0–300 K temperature range (Figure 6). The $\chi_M T$ product at 300 K is approximately 56 cm^3 K mol^{-1}, larger than that expected for a non-interacting [$Mn^{III}_4Mn^{II}_6$] unit with g = 2.0 (38.25 cm^3 K mol^{-1}). As the temperature is decreased the $\chi_M T$ product increases, reaching a maximum value of ~116 cm^3 K mol^{-1} at 30 K. Below this temperature $\chi_M T$ drops to a value of ~101 cm^3 K mol^{-1} at 5 K. This behaviour is indicative of the presence of competing ferromagnetic and antiferromagnetic interactions, with the decrease of the $\chi_M T$ product at lower temperatures assigned to antiferromagnetic intermolecular interactions, zero-field splitting and/or Zeeman effects of the applied field. The presence of multilple Mn(II) ions, which often propagate weak exchange interactions, and the large nuclearity of the cluster likely results in a near continuum of energy levels and no isolated spin ground state. This picture is reflected in the magnetisation versus field data (inset of Figure 6) which shows *M* increasing only slowly with *H*, rather than quickly reaching saturation as one would expect for an isolated spin ground state. Accordingly the data could not be fitted satisfactorily with a simple model assuming only population of the ground spin state. Ac susceptibility studies in the 1.8–10.0 K range in a 3.5 G field oscillating at frequencies up to 1000 Hz (Figure 7) display the tails of frequency-dependent out-of phase (χ_M'') signals (suggestive of SMM behaviour) but no peaks. The behaviour of **10** in general is thus very similar to that observed for $[Mn_{10}O_4(biphen)_4X_{12}]^{4-}$.[25]

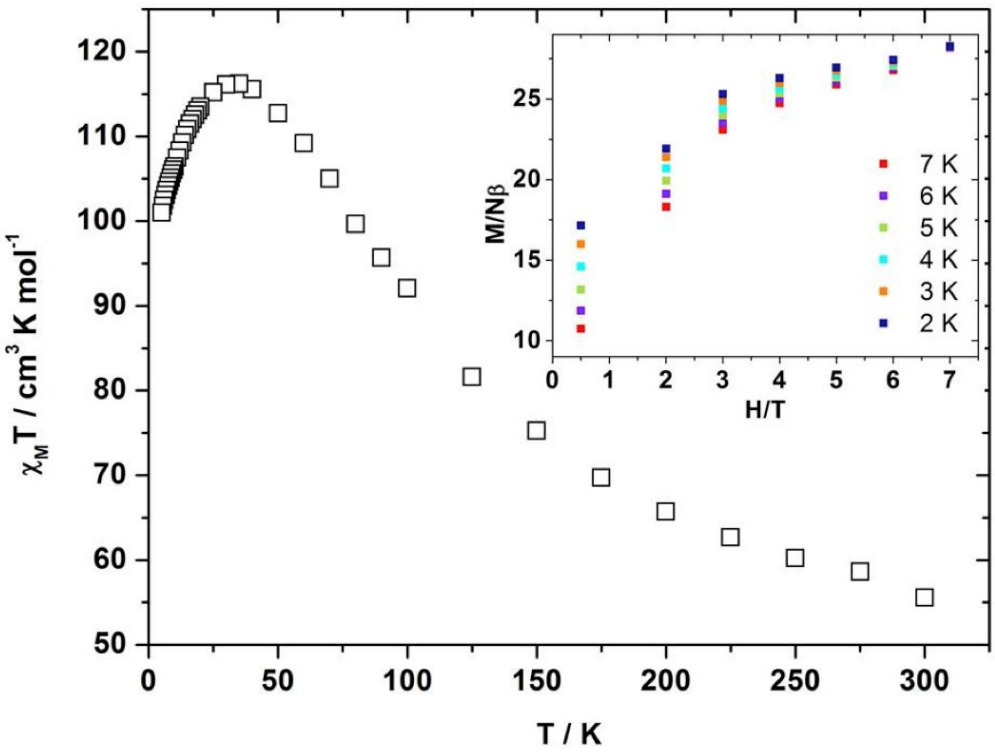

Figure 6. Plot of $\chi_M T$ vs T for complex **10** in an applied field of 0.1 T. Inset: Plot of magnetisation *versus* field at the indicated temperatures and fields.

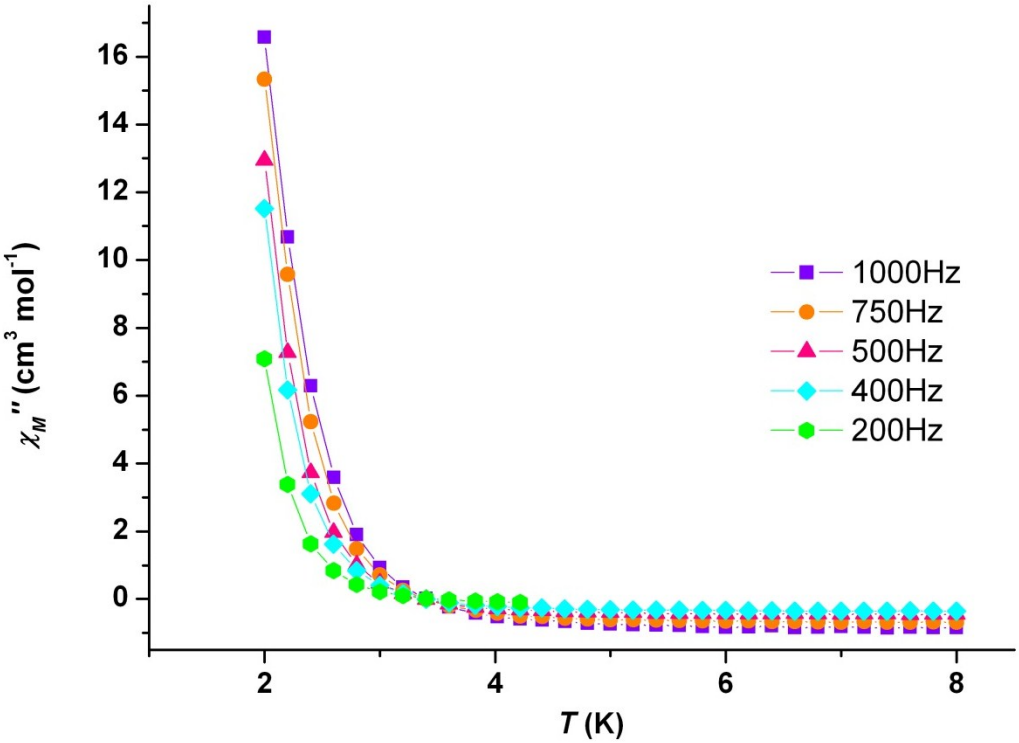

Figure 7. Plot of the out-of-phase (χ_M'') ac susceptibility versus temperature for **10** at the indicated frequencies.

For all reported $[Mn_{10}]$ supertetrahedra possessing the $[Mn^{III}_6Mn^{II}_4]$ oxidation state distribution (Figure 4a) – in which each neighbouring metal is in a different oxidation state – the pairwise magnetic exchange has been found to be ferromagnetic, with the molecules displaying isolated S = 22 ground states.[25-29] For the sole $[Mn^{III}_{10}]$ cluster the ground state is likely S = 0.[26] Complex **10** and $[Mn_{10}O_4(biphen)_4X_{12}]^{4-}$, which contain both Mn(II)–Mn(III) and Mn(II)–Mn(II) nearest neighbours along the edges of their tetrahedra, perhaps not surprisingly, appear to have ground state spin values intermediate between the two.

4.4 Conclusions

TBOC[3] is a promising ligand for the assembly of coordination clusters that have unusual magnetic properties. Exploratory manganese chemistry has afforded a supertetrahedron with unusual oxidation state distribution, suggesting that other clusters with unusual properties may be isolated with different TMs. Versatility in the calixarene conformation may also prove useful in the isolation of new polynuclear lanthanide species. These goals will be the focus of future work, as will be the exploitation of the supertetrahedron motif as a structural building unit.

4.5 References

1. C. Aronica, G. Chastanet, E. Zueva, S. A. Borshch, J. M. Clemente-Juan and D. Luneau, *J. Am. Chem. Soc.*, 2008, **130**, 2365-2371.
2. G. Karotsis, S. Kennedy, S. J. Teat, C. M. Beavers, D. A. Fowler, J. J. Morales, M. Evangelisti, S. J. Dalgarno and E. K. Brechin, *J. Am. Chem. Soc.*, 2010, **132**, 12983-12990.
3. G. Karotsis, S. J. Teat, W. Wernsdorfer, S. Piligkos, S. J. Dalgarno and E. K. Brechin, *Angew. Chem. Int. Ed*, 2009, **48**, 8285-8288.
4. S. Sanz, K. Ferreira, R. D. McIntosh, S. J. Dalgarno and E. K. Brechin, *Chem. Commun.*, 2011, **47**, 9042-9044.
5. S. M. Taylor, G. Karotsis, R. D. McIntosh, S. Kennedy, S. J. Teat, C. M. Beavers, W. Wernsdorfer, S. Piligkos, S. J. Dalgarno and E. K. Brechin, *Chem. Eur. J.*, 2011, **17**, 7521-7530.
6. Y. Bi, X.-T. Wang, W. Liao, X. Wang, X. Wang, H. Zhang and S. Gao, *J. Am. Chem. Soc.*, 2009, **131**, 11650-11651.
7. C. Desroches, G. Pilet, S. A. Borshch, S. Parola and D. Luneau, *Inorg. Chem.*, 2005, **44**, 9112-9120.
8. C. Desroches, G. Pilet, P. Á. Szilágyi, G. Molnár, S. A. Borshch, A. Bousseksou, S. Parola and D. Luneau, *Eur. J. Inorg. Chem.*, 2006, 357-365.
9. T. Kajiwara, N. Iki and M. Yamashita, *Coord. Chem. Rev.*, 2007, **251**, 1734-1746.
10. M. Liu, W. Liao, C. Hu, S. Du and H. Zhang, *Angew. Chem. Int. Ed*, 2012, **51**, 1585-1588.

11. C. E. Daitch, P. D. Hampton, E. N. Duesler and T. M. Alam, *J. Am. Chem. Soc.*, 1996, **118**, 7769-7773.
12. B. Masci, M. Nierlich and P. Thuery, *New J. Chem.*, 2002, **26**, 120-128.
13. B. Masci, M. Nierlich and P. Thuery, *New J. Chem.*, 2002, **26**, 766-774.
14. B. Masci and P. Thuery, *Acta. Crys.,*, 2005, **61**, m2278-m2280.
15. P. Thuéry, M. Nierlich, B. Masci, Z. Asfari and J. Vicens, *J. Chem. Soc., Dalton. Trans.*, 1999, 3151-3152.
16. B. Masci and P. Thuery, *CrystEngComm*, 2007, **9**, 582-590.
17. A. Arbaoui, C. Redshaw, M. R. J. Elsegood, V. E. Wright, A. Yoshizawa and T. Yamato, *Chem.Asian J.*, 2010, **5**, 621-633.
18. C. E. Daitch, P. D. Hampton and E. N. Duesler, *Inorg. Chem.*, 1995, **34**, 5641-5645.
19. P. D. Hampton, C. E. Daitch, T. M. Alam, Z. Bencze and M. Rosay, *Inorg. Chem.*, 1994, **33**, 4750-4758.
20. C. Redshaw, M. Rowan, D. M. Homden, M. R. J. Elsegood, T. Yamato and C. Pérez-Casas, *Chem. Eur. J.*, 2007, **13**, 10129-10139.
21. C. Redshaw, M. A. Rowan, L. Warford, D. M. Homden, A. Arbaoui, M. R. J. Elsegood, S. H. Dale, T. Yamato, C. P. Casas, S. Matsui and S. Matsuura, *Chem. Eur. J.*, 2007, **13**, 1090-1107.
22. M. Miah, N. N. Romanov and P. J. Cragg, *J. Org. Chem.*, 2002, **67**, 3124-3126.
23. W. Liu and H. H. Thorp, *Inorg. Chem.*, 1993, **32**, 4102-4105.
24. H. H. Thorp, *Inorg. Chem.*, 1992, **31**, 1585-1588.
25. D. P. Goldberg, A. Caneschi and S. J. Lippard, *J. Am. Chem. Soc.*, 1993, **115**, 9299-9300.
26. L. F. Jones, G. Rajaraman, J. Brockman, M. Murugesu, E. C. Sañudo, J. Raftery, S. J. Teat, W. Wernsdorfer, G. Christou, E. K. Brechin and D. Collison, *Chem. Eur. J.*, 2004, **10**, 5180-5194.
27. M. Manoli, R. D. L. Johnstone, S. Parsons, M. Murrie, M. Affronte, M. Evangelisti and E. K. Brechin, *Angew. Chem.*, 2007, **119**, 4540-4544.
28. S. Nayak, M. Evangelisti, A. K. Powell and J. Reedijk, *Chem. Eur. J.*, 2010, **16**, 12865-12872.
29. T. C. Stamatatos, K. M. Poole, K. A. Abboud, W. Wernsdorfer, T. A. O'Brien and G. Christou, *Inorg. Chem.*, 2008, **47**, 5006-5021.

Chapter 5

p-tert-Butylcalix[8]arene: An *extremely* versatile platform for cluster formation

5.1 Introduction

Polymetallic 4*f* and mixed 3*d*-4*f* clusters hold great potential for device application with respect to single-molecule magnetism and molecular cooling.[1-8] One of the major challenges in this area is the systematic design and controlled assembly of clusters with particular coordination modes. The *p*-tert-butylcalix[*n*]arenes (TBC[*n*], where *n* indicates the number of aryl units) are cyclic polyphenols that vary in ring size depending on reaction conditions employed during synthesis.[9] Given their polyphenolic nature it is somewhat surprising that, until recently, these molecules have received little attention with respect to the construction of large polynuclear metal clusters.[10-13] In this regard we (amongst others) have employed TBC[4] as a cluster support with a view to mapping out associated assembly modes and coordination constraints over a range of conditions, as the molecule adopts a bowl-shape both prior to and post complexation of either a transition or lanthanide metal center (TM and Ln, respectively).[14-27] With TMs we have synthesized and characterized a range of magnetically interesting species that are based around three distinct cluster motifs; $Mn^{III}_2Mn^{II}_2$TBC[4]$_2$ Single-Molecule Magnets (SMMs) with a planar diamond or butterfly-like core,[18,21] Cu^{II}_9TBC[4]$_3$ clusters based on tri-capped trigonal prisms that behave as versatile anion receptors,[16] and phosphinate-bridged dimers of $Mn^{III}Mn^{II}$TBC[4] dimers that are structurally related to the aforementioned $Mn^{III}_2Mn^{II}_2$TBC[4]$_2$ SMMs.[22] We have also incorporated lanthanide metals into 3*d* systems to afford "square in a square" $Mn^{III}_4Ln^{III}_4$TBC[4]$_4$ clusters that behave as SMMs or magnetic refrigerants depending simply on the Ln employed,[15,17] and $Fe^{III}_2Ln^{III}_2$TBC[4]$_2$ butterflies that represent an important second entry point into mixed 3*d*-4*f* systems.[19] Finally we have also carried out reactions involving just lanthanide salts, and have reported the formation of Ln^{III}_6TBC[4]$_2$ clusters in which the metal centers are arranged at the vertices of an octahedron.[20]

p-tert-Butylcalix[8]arene (TBC[8]) is significantly more flexible than TBC[4] due to annular inversion, and metal complexes[28-49] (TM and Ln) formed with this ligand most frequently adopt three particular conformations: pleated-loop,[28-31,40,41,45,48,49] double-cone,[32,37-39,44,46] and a third in which the molecule wraps around a small cluster in a manner akin to the shell of a tennis ball.[33-35,42,43,49] With respect to Ln TBC[8] complexes (there are only 10 in total in the Cambridge Structural Database), one mononuclear complex has been reported in which the calixarene adopts a pleated-loop

conformation.[40] In this complex the europium center is bound to oxygen atoms of two deprotonated TBC[8] phenol groups, with its coordination sphere being filled by three ligated DMF molecules and one chelating nitrate anion. The remaining nine structures are all dinuclear and all have the TBC[8] in a near-perfect double-cone conformation, are essentially isostructural, and have the general formula $[Ln^{III}_2(TBC[8]\text{-}6H)(Solv)_5]\cdot xSolv$ (where Solv = DMF or DMSO).[32,37-39] All of these structures have similarity in the arrangement of the ligated solvent molecules; two occupy the cavities presented by the near-perfect double-cone TBC[8], one bridges the two Ln centers beneath the double-cone, and the remaining two are positioned either side of said bridging molecule.

Analysis of the common structural features in our TBC[4]-supported clusters shows that, whether the calixarene binds a TM^{II} (Cu) or TM^{III} (Mn or Fe) metal centre, the calixarene cavity is occupied by a ligated solvent molecule. In conjunction with a bound hydroxide ligand beneath the complex, the phenolic O-atoms act as bridges to other Ln or TM centers forming polymetallic 3*d* or 3*d*-4*f* assemblies (Figure 1); i.e. the metal-calixarene moiety can be regarded as a "cluster ligand" from which much larger molecules can be self-assembled.[15-19,21,22] This is also true for Ln^{III}-TBC[4] clusters, although the increased coordination numbers of the lanthanide ions results in a variation in the number of bridging hydroxides present in the resulting assembly, as shown in Figure 2.[20] Similar analysis of the previously reported (and isostructural) Ln^{III}_2TBC[8] complexes described above suggested to us that the solvent occupied coordination sites below the near-perfect double-cone could be used to form larger clusters (e.g. by replacement of the solvent in Figure 3 with multiply-bridging oxo or hydroxo ligands). Here we show that this is indeed the case, and by varying (a) the lanthanide salts employed, (b) the reactant stoichiometries and (c) the solvent systems, all at ambient temperature, it is possible to readily access a series of Ln_1, Ln_2, Ln_4, Ln_5 and Ln_6 complexes.

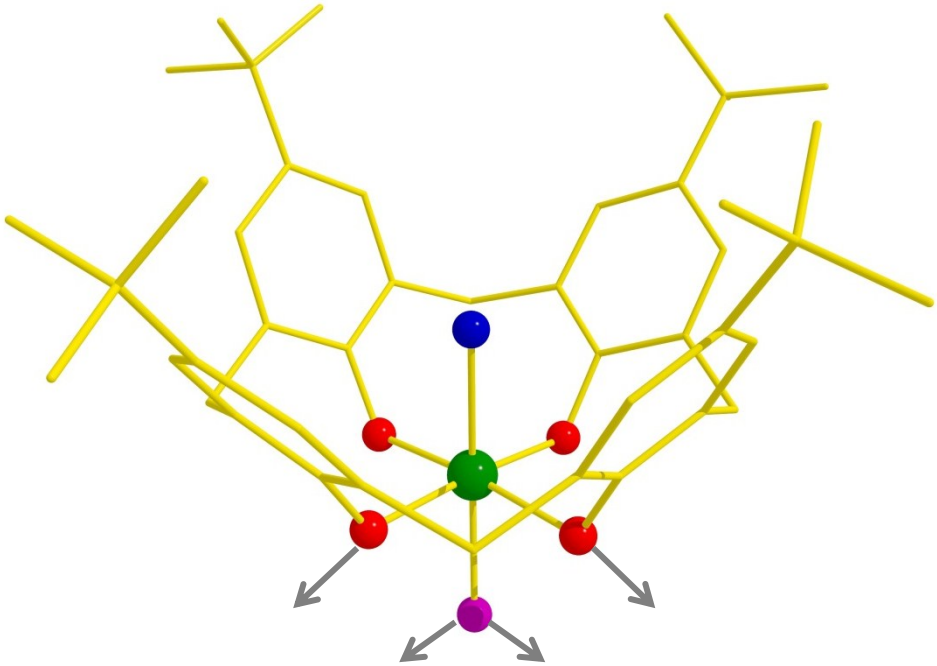

Figure 1. Transition metal (TM^{II} or TM^{III}) TBC[4] fragment with ligated solvent and bridging hydroxide groups shown.[18] Colour code: TM = green, O = red, OH = pink, solvent = blue, C = gold, H- atoms omitted for clarity.

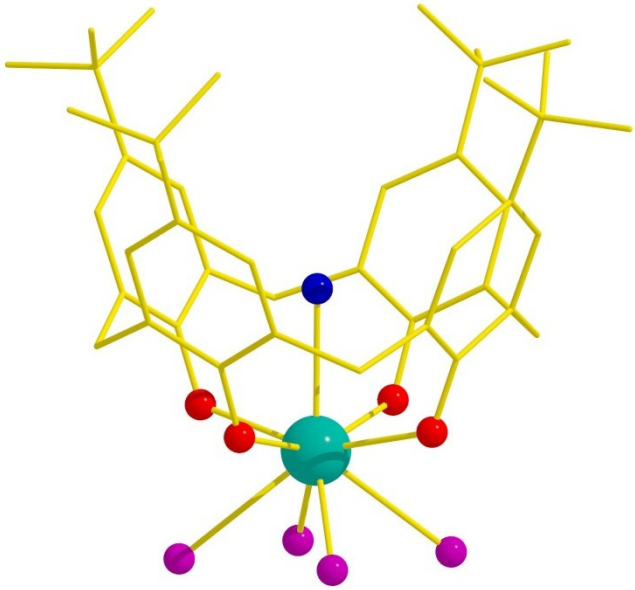

Figure 2. Lanthanide metal TBC[4] fragment with oxygen atoms of ligated solvent and bridging hydroxide groups. Colour code: Ln = teal, O = red, OH = pink, solvent = blue, C = gold, H- atoms omitted for clarity.

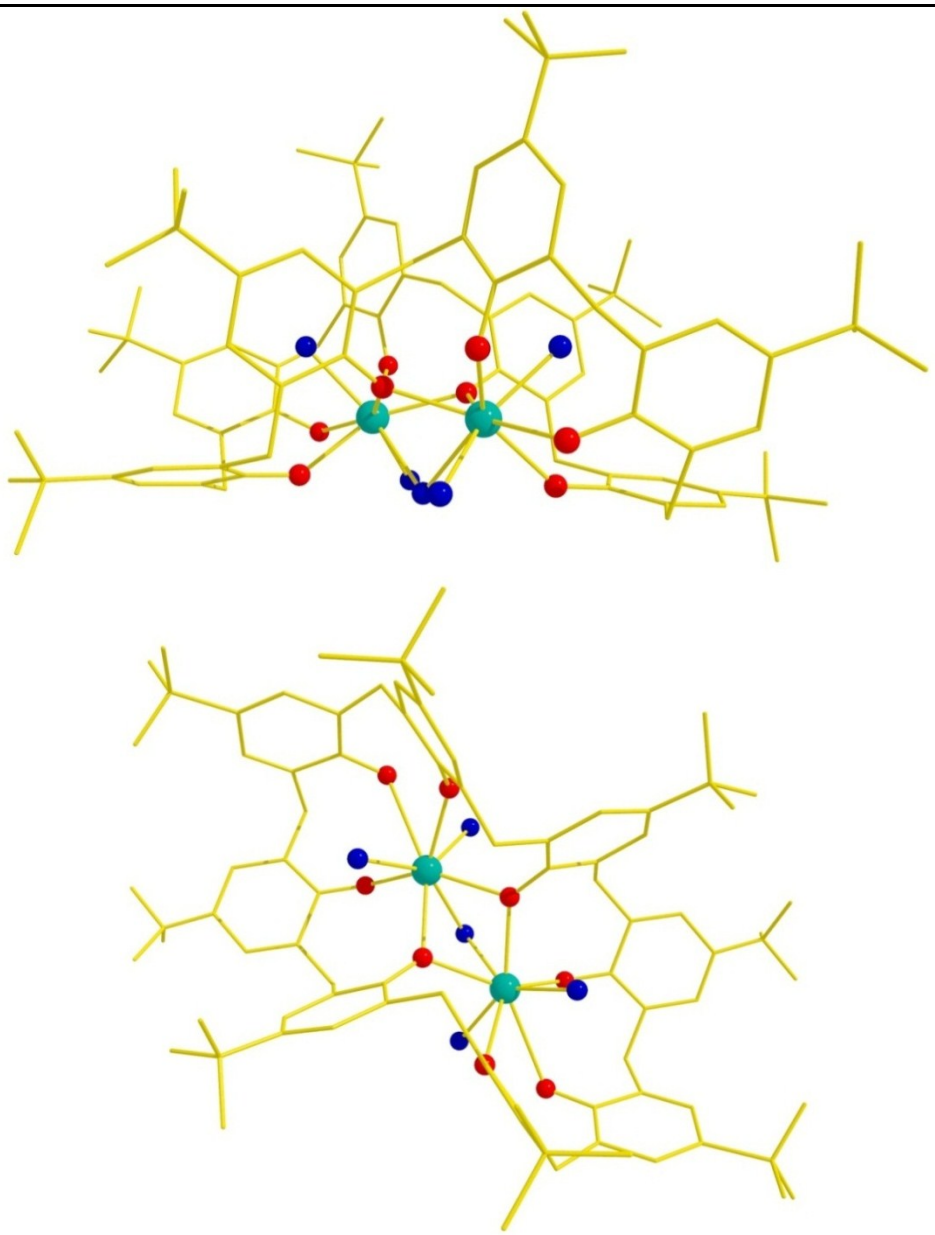

Figure 3. Orthogonal views of the commonly observed Ln_2TBC[8] complex showing oxygen atoms of ligated solvent molecules (terminal and bridging). Colour code: Ln = teal, O = red, solvent = blue, C = gold, H- atoms omitted for clarity.

Furthermore the use of high temperature and pressure results in the formation of larger Ln_7 and Ln_8 complexes, depending on the lanthanide employed. In total six of these complexes are new, with five containing the Ln^{III}_2TBC[8] fragment, despite there being significant changes in degrees of deprotonation of the TBC[8] support. A close inspection of the new, polymetallic (Ln_x, with $x \geq 4$) structures in fact reveals that the metallic skeletons are generally based on octahedra, or the building blocks of octahedra, with complex **12** being a capped triangle, complex **13** a square-based

pyramid, complex **14** an octahedron, complex **15** a capped octahedron and complex **16** a gyrobifastigium (8-vertex 26th Johnson solid, a diagonally bi-capped square plane). Although this report focuses solely on structural aspects of the series, the potential to interchange different Ln centers in some of these cluster types will have marked effects on the resulting magnetic properties. These studies will be reported in due course.

5.2 Experimental

5.2.1 Syntheses

All manipulations were performed under aerobic conditions using materials as received (reagent grade). Elemental analyses (C, H, N) were performed by the EaStCHEM microanalysis service. Full crystallographic details for the structures reported here are listed in Table 4 and selected bond lengths are given in the appendix. The oxidation states of the metal, O^{2-} and OH^{-} ions were confirmed by charge balance, bond length considerations and bond valence sum calculations which compare the sum of the observed bond lengths around an atom against tabulated bond lengths.[50,51]

$[Gd(TBC[8]\text{-}2H)Cl(DMSO)_4]\cdot MeCN\cdot H_2O\cdot(DMSO)_2\cdot hex$ (11)

$GdCl_3\cdot 6H_2O$ (0.19g, 0.5 mmol) and TBC[8] (0.2g, 0.17 mmol) were dissolved in a mixture of acetonitrile (10 mL) and dimethylsulfoxide (10 mL). After 5 minutes of stirring, NEt_3 (0.152 g, 1.5 mmol) was added, leaving the solution stirring for a further 2 h. Colorless single crystals suitable for diffraction studies were obtained by diffusion of hexane (25% yield) over a period of 2 weeks. Elemental analysis found (calc. %) for $GdC_{100}H_{139}O_{13}S_4N$: C 64.95 (61.7), H 7.80 (7.91), N 0.79 (0.67). These values are consistent with solvent loss in this system.

$[Ce^{IV}_4(TBC[8]\text{-}6H)_2(\mu_3\text{-}O)_2(DMF)_4]\cdot(DMF)_5\cdot hex\cdot MeCN$ (12)

$Ce(NO_3)_3\cdot 6H_2O$ (0.217 g, 0.5 mmol) and TBC[8] (0.2g, 0.17 mmol) were dissolved in a mixture of acetonitrile (10 mL) and dimethylformamide (10 mL). After 5 minutes of stirring, NEt_3 (0.152 g, 1.5 mmol) was added, leaving the solution stirring for a further 2 h. Colorless single crystals suitable for diffraction studies were obtained by diffusion of hexane (40 % yield) over a period of 2 weeks. Elemental analysis found (calc. %) for $Ce_4C_{216}H_{292}O_{27}N_{10}$: C 63.68 (63.98), H 7.85 (7.43), N 4.21 (3.74).

$[Tb^{III}_5(TBC[8]\text{-}5H)(\mu_4\text{-}O)(\mu_3\text{-}OH)_4Cl(DMSO)_8(H_2O)_3]Cl_3\cdot(DMSO)_2\cdot(hex)_2$ (13)

$TbCl_3\cdot 6H_2O$ (0.187g, 0.5 mmol) and TBC[8] (0.2g, 0.17 mmol) were dissolved in a mixture of acetonitrile (10 mL) and dimethylsulfoxide (10 mL). After 5 minutes of stirring, NEt_3 (0.152 g, 1.5 mmol) was added, leaving the solution stirring for a further 2 h. Colorless single crystals suitable for diffraction studies were obtained by diffusion of hexane (25 % yield) over a period of 2 weeks. Elemental analysis found (calc. %) for $Tb_5C_{120}H_{205}O_{26}S_{10}Cl_4$: C 43.23 (43.40), H 6.51 (6.22).

$[Ce^{IV}_6(TBC[8]\text{-}6H)_2(\mu_4\text{-}O)_2(\mu_2\text{-}OMe)_4(\mu_3\text{-}O)_2(DMF)_4]\cdot(DMF)_6\cdot hex$ (14)

$Ce(NO_3)_3\cdot 6H_2O$ (0.217 g, 0.5 mmol), TBC[8] (0.2g, 0.17 mmol) and NH_4ClO_4 (0.06 g, 0.5 mmol) were dissolved in a mixture of methanol (10 mL) and dimethylformamide (10 mL). After 5 minutes of stirring, NEt_3 (0.152 g, 1.5 mmol) was added, leaving the solution stirring for a further 2 h. Colorless single crystals suitable for diffraction studies were obtained by diffusion of hexane over a period of 2 weeks. Elemental analysis found (calc. %) for $Ce_6C_{216}H_{308}O_{34}N_{10}$: C 59.18 (58.77), H 7.11 (7.01), N 2.86 (3.16).

$[Dy_7(TBC[8]\text{-}7H)(TBC[8]\text{-}6H)(\mu_4\text{-}O)_2(\mu_3\text{-}OH)_2(\mu_2\text{-}OH)_2(DMF)_9]\cdot(DMF)_3$ (15)

$DyCl_3\cdot 6H_2O$ (0.28 g, 0.75 mmol) and TBC[8] (0.32 g, 0.25 mmol) were dissolved in a mixture of dimethylformamide (10 mL) and MeOH (10 mL). After 5 minutes of stirring, NEt_3 (0.61 g, 6 mmol) was added and the solution stirred for a further 5 minutes. After filtration the solution was placed in Teflon-lined "bomb" and heated to 130 °C for 24 hours. Colorless single crystals suitable for diffraction studies were obtained (20 % yield) after cooling the mixture to room temperature. Elemental analysis found (calc. %) for $C_{212}H_{309}Dy_7N_{12}O_{34}$: C 54.39 (54.09), H 6.43 (6.62), N 3.24 (3.57).

$[Gd_8(TBC[8]\text{-}7H)_2(\mu_4\text{-}CO_3)_2(\mu_5\text{-}CO_3)_2(\mu_2\text{-}HCO_2)_2(DMF)_8)]$ (16)

$GdCl_3\cdot 6H_2O$ (0.28 g, 0.75 mmol) and TBC[8] (0.32 g, 0.25 mmol) were dissolved in a mixture of dimethylformamide (10 mL) and MeOH (10 mL). After 5 minutes of stirring, NEt_3 (0.61 g, 6 mmol) was added and the solution stirred for a further 5 minutes. After filtration the solution was placed in Teflon-lined "bomb" and heated to 130 °C for 24 hours. Colorless single crystals suitable for diffraction studies were obtained (20 % yield). Elemental analysis found (calc. %) for $C_{206}H_{280}Gd_8N_8O_{40}$: C 52.56 (51.91), H 6.13 (5.92), N 2.61 (2.35).

Table 4. Crystal structure information for **11**-**16**.

	11[a]	**12**[a]	**13**[a]	**14**[a]	**15**[b]	**16**[a]
Chemical formula	$C_{108}H_{165}ClGdNO_{15}S_6$	$C_{211}H_{292}Ce_4N_{10}O_{27}$	$C_{120}H_{205}Cl_4O_{26}S_{10}Tb_5$	$C_{216}H_{308}Ce_6N_{10}O_{34}$	$C_{212}H_{299}Dy_7N_{12}O_{34}$	$C_{206}H_{268}Gd_8N_8O_{40}$
M_r	2102.47	3961.03	3320.84	4429.44	4697.13	4754.28
Crystal system	Monoclinic	Orthorhombic	Triclinic	Triclinic	Triclinic	Triclinic
Space group	*C*2/*c*	*Pbca*	*P*-1	*P*-1	*P*-1	*P*1
a (Å)	48.4925 (16)	32.0523 (13)	16.0139 (7)	16.3625 (7)	18.9410 (11)	17.1307 (7)
b (Å)	16.1936 (6)	20.0131 (8)	21.3862 (9)	18.4212 (7)	20.9821 (12)	20.6804 (8)
c (Å)	36.839 (2)	68.846 (3)	23.119 (1)	21.2603 (8)	29.8973 (18)	21.0289 (13)
α (°)	90	90	103.392 (2)	68.652 (2)	81.769 (2)	107.905 (3)
β (°)	126.308 (2)	90	99.438 (2)	68.475 (2)	86.493 (2)	105.883 (3)
γ (°)	90	90	103.357 (2)	87.483 (2)	67.470 (2)	109.705 (2)
V (Å^3)	23311.9 (17)	44162 (3)	7293.5 (5)	5522.5 (4)	10861.7 (11)	6053.0 (5)
Z	8	8	2	1	2	1
F(000)	8936	16608	3372	2294	4778	2390
Crystal size (mm)	0.40 × 0.35 × 0.32	0.30 × 0.25 × 0.20	0.30 × 0.20 × 0.18	0.40 × 0.30 × 0.28	0.35 × 0.30 × 0.25	0.09 × 0.05 × 0.04
No. of measured, independent and observed [$I > 2\sigma(I)$] reflections	124801, 31525, 22746	360636, 45081, 35874	107739, 43735, 35996	82245, 33205, 21735	134390, 30891, 18046	219323, 89956, 69439
R_{int}	0.055	0.087	0.051	0.068	0.114	0.037
$R_1[I > 2\sigma(I)]$	0.067	0.064	0.042	0.050	0.054	0.075
$wR_2(F^2)$	0.187	0.179	0.120	0.122	0.130	0.241
GOF on F^2	1.04	1.19	1.09	0.91	1.00	1.03

[a] Data collected on a Bruker Apex II diffractometer operating with synchrotron radiation (λ= 0.7749 Å) at 100(2) K. [b] Data collected on a Bruker Apex II diffractometer operating with $Mo_{K\alpha}$ radiation (λ = 0.71073 Å) at 100(2) K.

5.3 Results and Discussion

5.3.1 Structural Description

Through a combinatorial approach we have synthesized and characterized six lanthanide complexes of TBC[8]. The first in the series is a variant of the previously reported Ln_1TBC[8] complex[40] in which the chelating nitrate anion is replaced by a chloride. In a number of our experiments we obtained the same general [Ln_2(TBC[8]-6H)(Solv)$_5$]·xSolv complex as that shown in Figure 3, and this will not be discussed further here.[32,37-39] The remaining five new complexes / clusters formed in our experiments all contain a related Ln_2TBC[8] moiety which is in fact a smaller fragment in the construction of frameworks generally based on octahedra, and in which the calixarene adopts either a perfect or near-perfect double-cone conformation. In the case of perfect double-cones this involves a small structural correction to the motif shown in Figure 3. Various additional ligated solvent molecules are present in the different structures described below, and significant changes in the degree of deprotonation of TBC[8] are evident within the series. A description of general cluster composition is also presented.

[Gd(TBC[8]-2H)Cl(DMSO)$_4$]·MeCN·H$_2$O·(DMSO)$_2$·hex (11)

Reaction of TBC[8] with triethylamine and gadolinium(III) chloride hexahydrate in an acetonitrile / dimethylsulfoxide solution, followed by diffusion with hexane, afforded large colorless single crystals that were suitable for X-ray diffraction studies. The crystals are in a monoclinic cell and structure solution was carried out in the space group $C2/c$. Analysis of the asymmetric unit in **11** shows that the complex formed is similar to the Ln_1TBC[8] complex described in the introduction. The TBC[8] in **11** is in a pleated-loop conformation and exists as a di-anion (Figure 4). The Gd^{III} center is seven coordinate and pentagonal bipyramidal, bonding to the two de-protonated TBC[8] phenol groups, a coordinated chloride anion (Gd…Cl, 2.696(1) Å) and four ligated DMSO molecules. The Gd…O bond lengths are in the range 2.316-2.410 Å. Overall the structure is unexceptional, but characterization confirms versatility towards the inclusion of different anions in the complex as a whole.

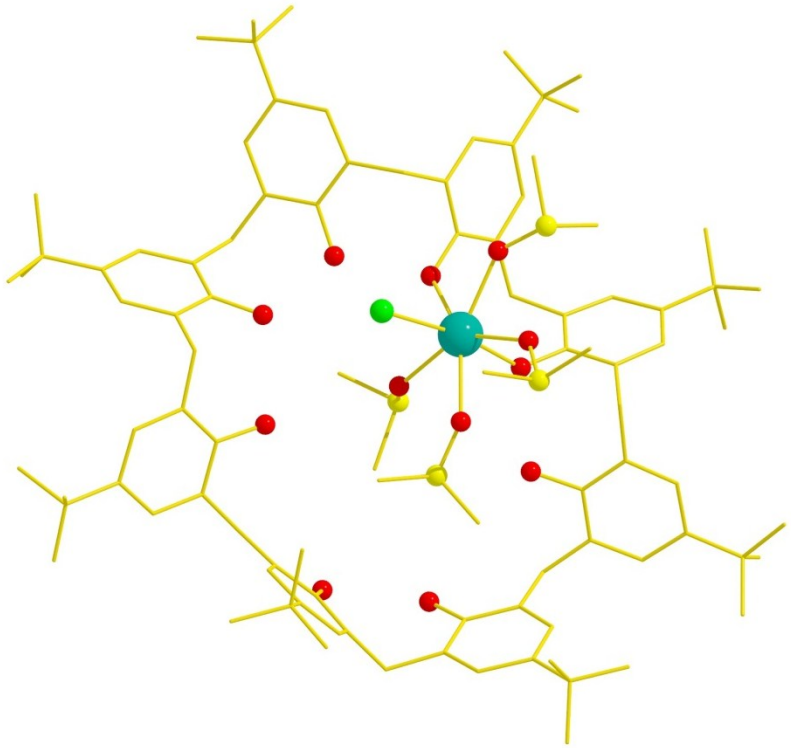

Figure 4. Structure of **11** showing the pleated-loop conformation of TBC[8]. Color code: Gd = teal, O = red, Cl = green, S = yellow, C = gold, non-coordinating solvents and H- atoms omitted for clarity.

$[Ce^{IV}_4(TBC[8]\text{-}6H)_2(\mu_3\text{-}O)_2(DMF)_4]\cdot(DMF)_5\cdot hex\cdot MeCN$ (12)

Reaction of TBC[8] with triethylamine and cerium(III) nitrate hexahydrate in an acetonitrile / dimethylformamide solution, followed by diffusion with hexane, afforded large colorless single crystals that were suitable for X-ray diffraction studies. The crystals are in an orthorhombic cell and structure solution was carried out in the space group *Pbca*. The asymmetric unit in **12** comprises the large TBC[8]-supported Ce^{IV}_4 cluster shown in Figure 5 and three ordered DMF of crystallization. In addition to this there is diffuse electron density associated with badly disordered hexane (one molecule), acetonitrile (one molecule) and DMF (two molecules) of crystallization. The four Ce(IV) ions are connected to each other "internally" by two μ_3-O^{2-} ions (Ce…O, 2.207-2.302 Å), forming a ladder-like $[Ce^{IV}_4O_2]^{12+}$ moiety (Figure 6). This is a commonly observed fragment in TM(III) clusters (*e.g.* in the chemistry of Mn(III) or Fe(III)) and is often referred to as a "butterfly".[52-54] In the context of the present paper and the relationship between complexes **11**-**16**, however, perhaps the most apt description is that of a capped triangle (*vide infra*). The Ce^{IV} centers are all seven-coordinate and pentagonal bipyramidal in geometry. Each TBC[8] exists as a hexa-anion [there are two

intra-molecular H-bonds between neighboring phenolic O-atoms per TBC[8] molecule (*e.g.* O13…O14 and O17…O18 ~2.5 Å)] and bridges three Ce^{IV} ions (Ce1, Ce3, Ce4 or Ce2, Ce3, Ce4) across one complete side of the butterfly. Ligated DMF molecules occupy the cavities generated by each of the TBC[8] molecules in **12**, adopting the double-cone conformation. In this arrangement each TBC[8] is reminiscent of two TBC[4]s and the ligated DMF molecules form intra-molecular interactions with the aromatic rings of the calixarene (symmetry unique CH·····π interactions with CH···aromatic centroid distances of ~3.5 Å).

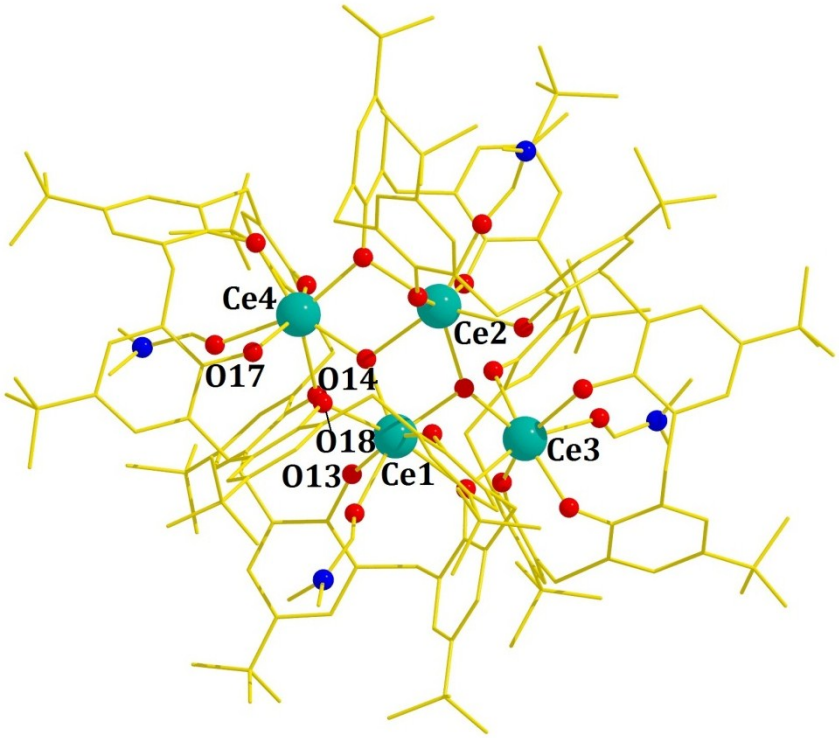

Figure 5. Expanded structure in **12** showing two Ln^{III}_2TBC[8] fragments linked by μ_3-O^{2-} ions. The calixarenes are in the double cone conformation akin to that shown in Figure 3. Color code: Ce = teal, O = red, N = blue, C = gold, H- atoms omitted for clarity.

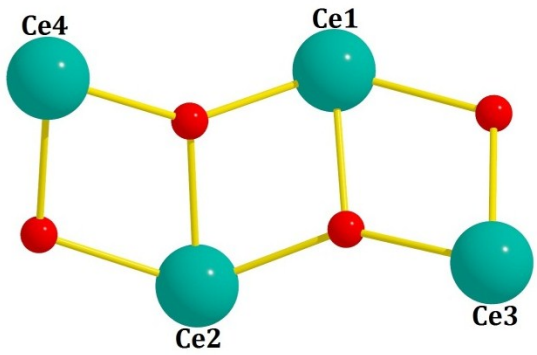

Figure 6. The poly-metallic ladder-like core found in the structure of **12**.

$[Tb^{III}_5(TBC[8]\text{-}5H)(\mu_4\text{-}O)(\mu_3\text{-}OH)_4Cl(DMSO)_8(H_2O)_3]Cl_3\cdot(DMSO)_2\cdot(hex)_2$ (13)

Reaction of TBC[8] with triethylamine and terbium(III) chloride hexahydrate in an acetonitrile / dimethylsulfoxide solution, followed by diffusion with hexane, afforded large colorless single crystals that were suitable for X-ray diffraction studies. The crystals are in a triclinic cell and structure solution was carried out in the space group *P*–1. The asymmetric unit in **13** comprises half of the complex shown in Figure 7, two ordered DMSO of crystallization, and diffuse electron density associated with two hexane molecules of crystallization. The metallic skeleton (Figures 7 and 8) of complex **13** describes a distorted square-based pyramid with Tb1-Tb4 in the square base and Tb5 on the apex. Tb1-Tb4 are connected to each other *via* one μ_4-O^{2-} ion in the basal plane (O11) and to Tb5 *via* four μ_3-OH^- ions, one on each triangular face of the pyramid (O12-O15); the core of the complex is thus $[Tb^{III}_5(\mu_4\text{-}O)(\mu_3\text{-}OH)_4]^{9+}$. The Tb^{III} ions are all eight coordinate and in distorted square antiprismatic geometries, although those in the basal plane are more distorted. All have $[LnO_8]$ coordination spheres with the exception of Tb2 which is bonded to the sole coordinated Cl^- anion. The TBC[8] ligand is penta-ionic with the three protonated arms each H-bonding to one Cl^- counter anion (~3 Å). The latter are also H-bonded to the terminally bonded H_2O molecules. The TBC[8] molecule adopts the double cone conformation (Figure 7), bridging the four Tb ions in the square base of the pyramid. The coordination sites of the metal ions are completed by the presence of several terminally bonded solvent molecules (DMSO and H_2O), with the ligated DMSO molecules occupying the cavities generated by each of the TBC[8] molecules, with CH···aromatic centroid distances of ~3.5 Å. Interestingly Tb5 – the apical metal ion – is not coordinated to the calixarene ligand at all, being connected to the rest of the molecule only through the four μ_3-OH^- ions. Its exterior square face is entirely comprised of terminally ligated solvent, suggesting the possibility of further cluster growth by solvent substitution.

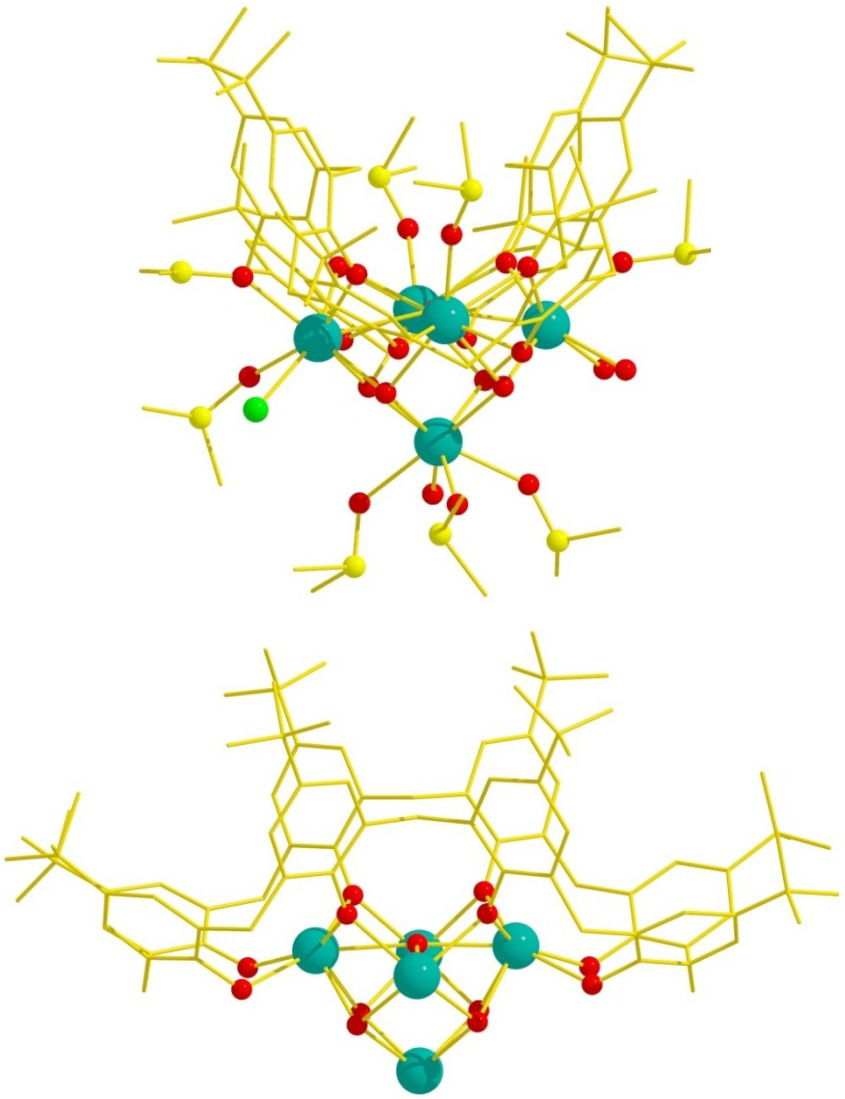

Figure 7. Two views of the structure of **13** showing the double-cone conformation of TBC[8] akin to that shown in Figure 3. Non-coordinating solvents omitted in bottom view for clarity. Color code: Tb = teal, O = red, S = yellow, Cl = green, C = gold, H- atoms omitted for clarity.

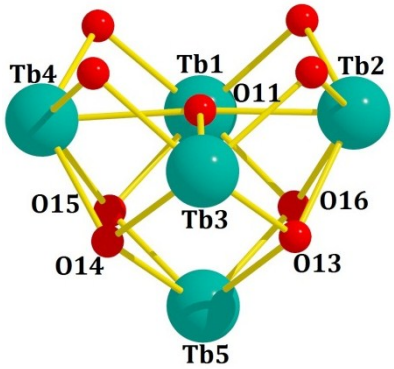

Figure 8. Square pyramidal cluster core found in the structure of **13** showing incorporated μ_4-O^{2-} and μ_3-OH^- ions.

$[Ce^{IV}_6(TBC[8]\text{-}6H)_2(\mu_4\text{-}O)_2(\mu_2\text{-}OMe)_4(\mu_3\text{-}O)_2(DMF)_4]\cdot(DMF)_6\cdot$hex (14)

Reaction of TBC[8] with triethylamine, cerium(III) nitrate hexahydrate and ammonium perchlorate in a methanol / dimethylformamide solution, followed by diffusion with hexane, afforded large colorless single crystals that were suitable for X-ray diffraction studies. The crystals are in a triclinic cell and structure solution was carried out in the space group *P*–1. The asymmetric unit in **14** comprises half of the cluster shown in Figure 9, two ordered DMF of crystallization, and diffuse electron density associated with DMF (1 molecule) and hexane (1 molecule) of crystallization. The metallic skeleton of complex **14** (Figures 9 and 10) is a [Ce^{IV}_6] (squashed) octahedron, with Ce1 and symmetry equivalent (s.e.) sitting on the apical sites and Ce2, Ce3 and s. e. occupying the square plane. The latter is slightly asymmetric and is more rectangular than square with two Ce…Ce distances of the order of 4.7 Å and two being approximately 0.5 Å shorter. The distance between the apical site and the four ions in the rectangular plane is ~ 3.3 Å. All six Ce ions are eight coordinate and in square antiprismatic geometries. The apical sites are connected to the four ions in the square plane (and to each other) *via* two μ_4-O^{2-} ions (O12 and s.e.), four μ-methoxides (O13, O14 and s.e.) and four phenolic μ-O-atoms from the calixarene ligands (O6, O7 and s.e.). The remaining two, near linear, μ-O^{2-} ions (O11 and s.e.) link neighboring Ce(IV) ions across the "short" edges of the rectangle, completing the $[Ce^{IV}_6(\mu_4\text{-}O)_2(\mu\text{-}O)_2(\mu\text{-}OMe)_4]^{12+}$ core. Each TBC[8] exists as a hexa-anion [there is one intra-ligand H-bond between neighboring phenolic O-atoms per TBC[8] molecule (O2…O3, ~2.55 Å) and one inter-ligand H-bond (O13…O14, ~2.45 Å)] and bridges three Ce ions (Ce1-3) across one triangular face of the octahedron. The calixarenes again adopt the double cone conformation with ligated DMF molecules occupying the cavities in a manner identical to that seen for complexes **12** and **13** (Figure 9).

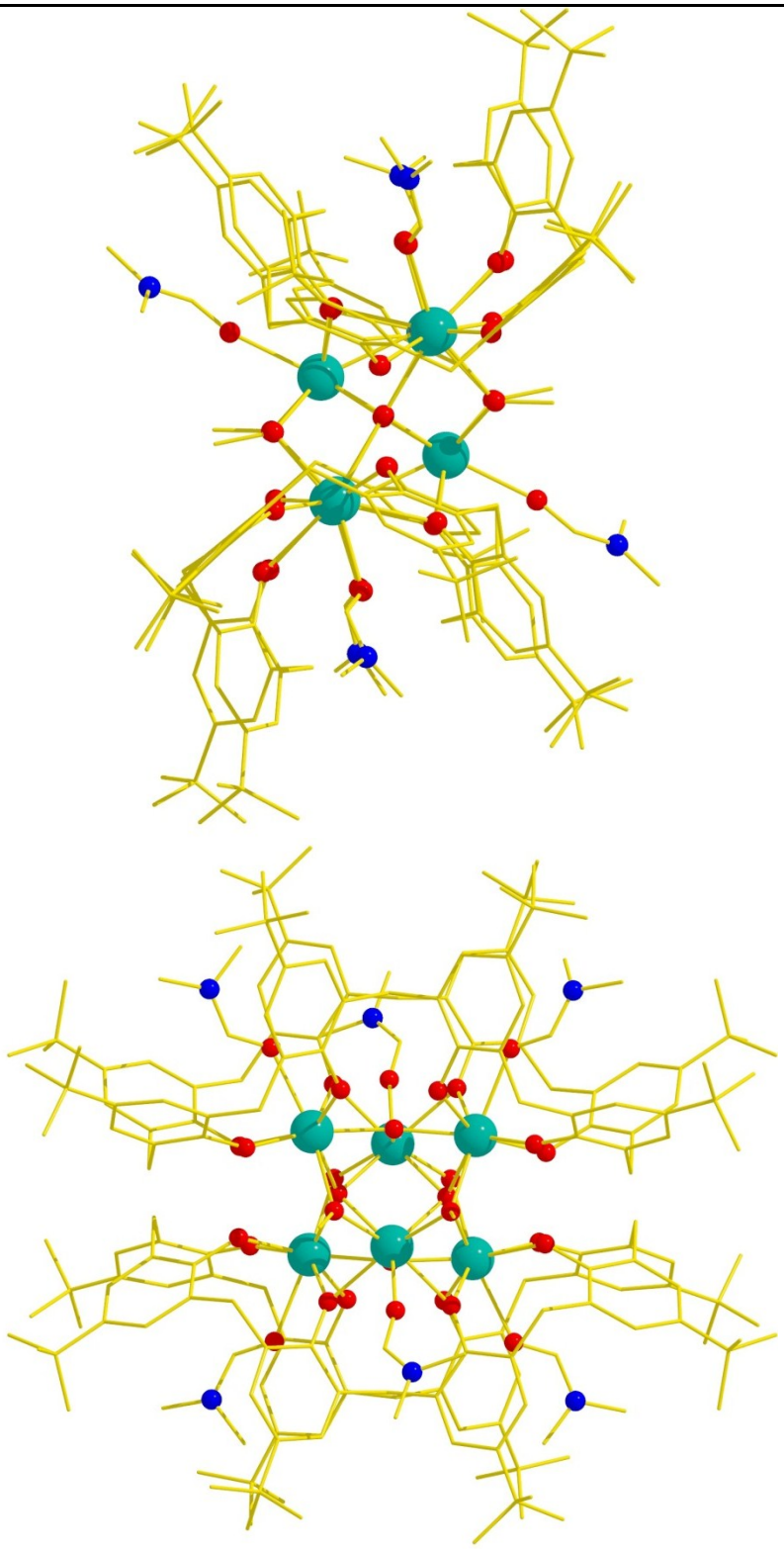

Figure 9. Two views of the structure of **14** showing the double-cone conformation of TBC[8] akin to that in Figure 3 and the metal octahedron. Colour code: Ce = teal, O = red, N = blue, C = gold, H-atoms omitted for clarity.

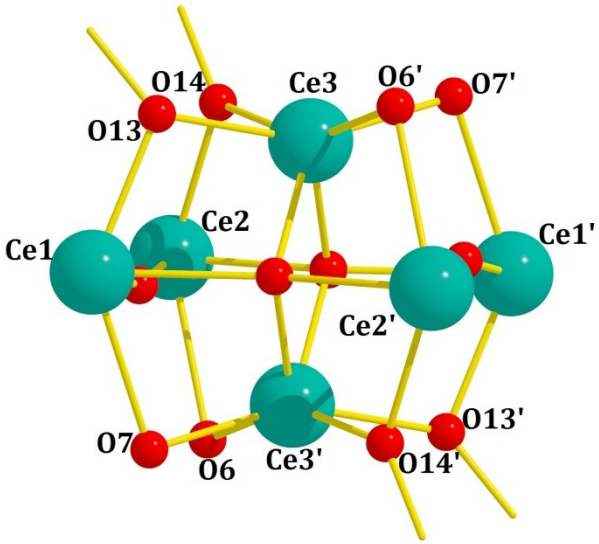

Figure 10. The octahedral cluster core found in the structure of **14** showing incorporated MeO^- and μ_4-O^{2-} ions. Colour code as in Figure 9.

$[Dy_7(TBC[8]\text{-}7H)(TBC[8]\text{-}6H)(\mu_4\text{-}O)_2(\mu_3\text{-}OH)_2(\mu_2\text{-}OH)_2(DMF)_9]\cdot(DMF)_3$ (15)

Solvothermal reaction of TBC[8] with triethylamine and dysprosium(III) chloride hexahydrate in a dimethylformamide / methanol solution, afforded large colorless single crystals that were suitable for X-ray diffraction studies. The crystals are in a triclinic cell and structure solution was carried out in the space group *P*–1. The asymmetric unit in **15** comprises the cluster shown in Figure 11 and three DMF of crystallization. The metallic skeleton of **15** (Figures 11 and 12) is a rather unusual and distorted capped octahedron: Dy4 and Dy5 occupy the apical sites, Dy1, Dy2, Dy6 and Dy7 occupy the square plane and Dy3 caps the triangular Dy5, Dy6, Dy7 face. In fact Dy3 does not sit directly in the center of this face, being skewed closer to the Dy6-Dy7 vector and thus an alternative description is that of Dy3 being edge-capping rather than face-capping. The central cavity of the octahedron is again filled by two μ_4-O^{2-} ions (O31, O32). The edge-capping Dy ion (Dy3) is connected to the octahedron through a combination of two μ_3-OH^- ions (O28, O29) and one μ-OH^- ion (O30). The remaining hydroxide ion (O33) bridges Dy1 and Dy2 in the square plane. The metal-oxygen core is therefore the asymmetric $[Dy^{III}_7(\mu_4\text{-}O)_2(\mu_3\text{-}OH)_2(\mu\text{-}OH)_2]^{13+}$.

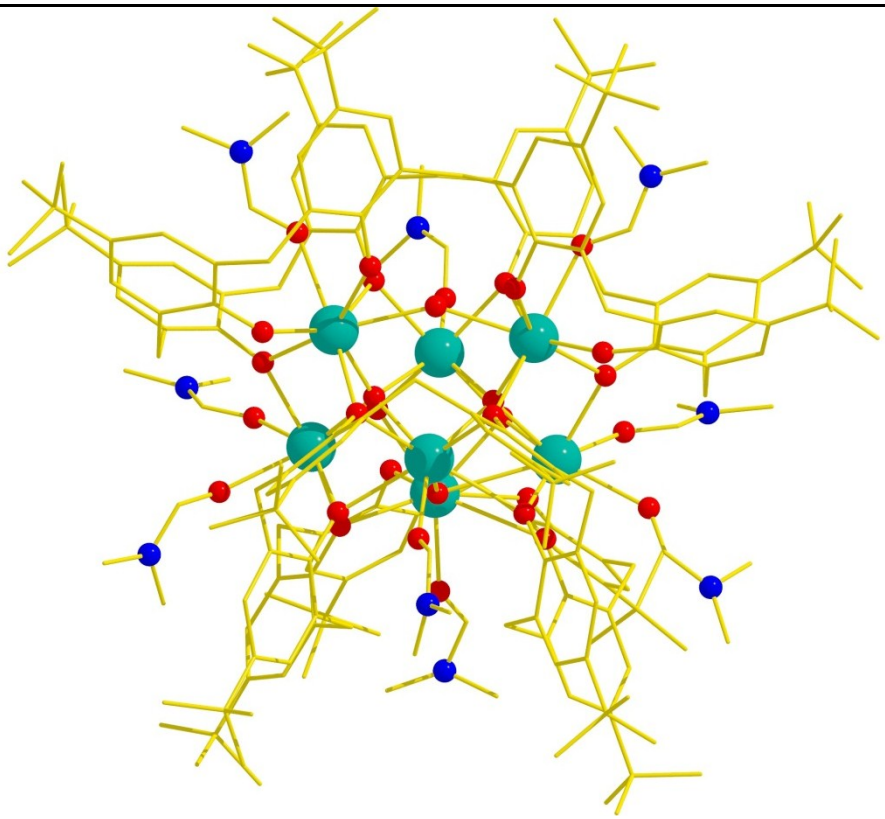

Figure 11. Structure of **15** showing the double-cone conformation of TBC[8]. Colour code: Dy = teal, O = red, N = blue, C = gold, H-atoms omitted for clarity.

The two TBC[8] ligands are present in different levels of protonation, one being TBC[8]-7H and the other TBC[8]-6H. In the 7- ligand the one remaining proton is shared between neighbors O15 and O16 which are both terminally coordinated (Dy3…O16, 2.529(8) Å; Dy7…O15, 2.331(6) Å) and H-bonding to each other (O15…O16, 2.570(4) Å). For the 6- ligand, the protonated arms are O2 and O3, both being bonded terminally with Dy…O distances of 2.745(6) Å and 2.821(7) Å, respectively. Both calixarene ligands adopt the double cone conformation, the 7- ligand bridging a total of six Dy ions and the 6- ligand bridging a total of five Dy ions. The Dy ions are of two types: Dy1, Dy2, Dy4, Dy5, Dy8 are eight coordinate and in square anti-prismatic geometries, whilst Dy3, Dy6 and Dy7 are seven coordinate and pentagonal bipyramidal. The remaining metal coordination sites are again filled with terminally bonded solvent molecules (Figure 11).

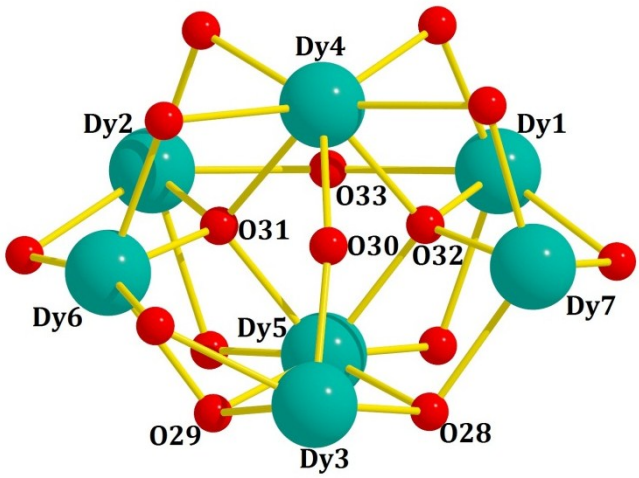

Figure 12. The capped octahedral cluster core found in the structure of **15** showing incorporated μ_4-O^{2-} and μ_3-OH^- ions. Colour code as in Figure 11.

$[Gd_8(TBC[8]\text{-}7H)_2(\mu_4\text{-}CO_3)_2(\mu_5\text{-}CO_3)_2(\mu_2\text{-}HCO_2)_2(DMF)_8]$ (16)

Solvothermal reaction of TBC[8] with triethylamine and gadolinium(III) chloride hexahydrate in a dimethylformamide / methanol solution, afforded large colorless single crystals that were suitable for X-ray diffraction studies. The crystals are in a triclinic cell and structure solution was carried out in the space group *P*1. As the structure was solved in *P*1, the asymmetric unit in **16** comprises the entire cluster shown in Figure 13. The cluster core is disordered over two positions, but for clarity only one will be discussed and shown below. The metallic skeleton of **16** (Figures 13 and 14) is very unusual and conforms to the 26th Johnson solid, the gyrobifastigium. This 8-vertex polyhedron is composed of four squares and four triangles constructed around a central square plane, which in one of the two aforementioned positions is defined by Gd1 – Gd4. On one side the square is bi-capped by Gd5 and Gd6, and on the other Gd7 and Gd8. One μ_4-CO_3^{2-} ion links Gd1 and Gd3 to Gd5 and Gd6, while another on the other side of the cluster links Gd2 and Gd4 to Gd5 and Gd6. One μ_5-CO_3^{2-} ion links Gd7 and Gd8 to Gd1, Gd4 and Gd5, while another on the other side of the cluster links Gd7 and Gd8 to Gd2, Gd3 and Gd6. Gd7 and Gd8 are also doubly linked to one another by two syn, syn μ-formate ligands as shown in Figure 14. The origin of the carbonate ligands is atmospheric CO_2 (in the presence of strong base) and the formate from the breakdown of the DMF solvent under the high temperature, high pressure (solvothermal) reaction conditions. Both are common observed occurrences. Attempts to repeat the synthesis through the deliberate addition of CO_3^{2-} / formate has thus far failed. The metal oxygen core is therefore $[Gd^{III}_8(\mu_4\text{-}CO_3)_2(\mu_5\text{-}CO_3)_2(\mu_2\text{-}HCO_2)_2]^{14+}$. The

two TBC[8] ligands are both present at the same level of deprotonation, that being TBC[8]-7H. The proton is shared between neighbors O5 and O6, and O9 and O16, all of which are terminally coordinated and H-bonding to each other (O5…O6, 2.735 Å; O9…O16, 2,797 Å). Both calixarenes are in the double-cone conformation and both bridge five gadolinium centers. The Gd(III) ions themselves are all 7-coordinate and in pentagonal bipyramidal geometry.

It is interesting to note that complex **16** contains no oxide or hydroxide ions, in contrast to all the other polynuclear Ln cages reported herein. Thus is seems clear, the that CO_3^{2-} ions produced *in situ* have acted as their "replacement" sitting in the centre of the cluster and acting as structure-directing or templating anions. This perhaps suggests an alternative synthetic strategy for the successful construction of large polymetallic Ln cluster compounds – the deliberate use of carbonate as a primary bridging ligand.[55,56]

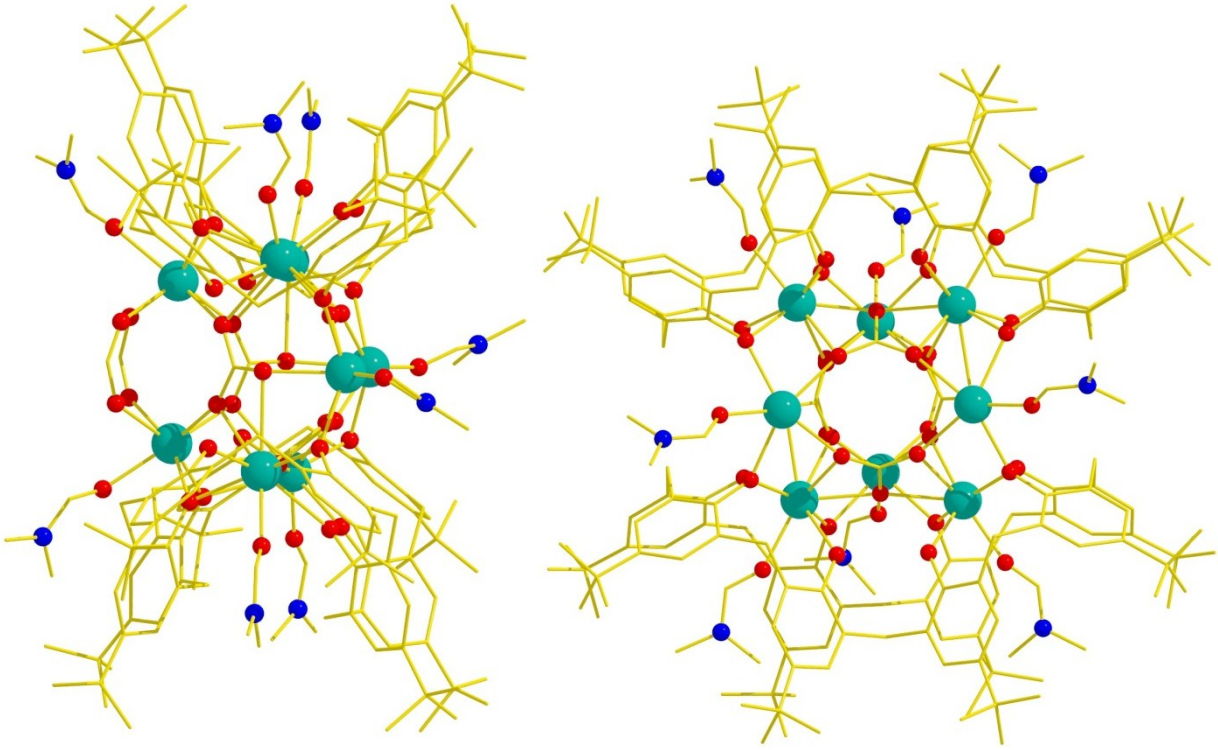

Figure 13. Structure of **16** showing the double-cone conformation of TBC[8] and the asymmetric metal-oxygen core. Colour code: Gd = teal, O = red, N = blue, C = gold, H-atoms omitted for clarity.

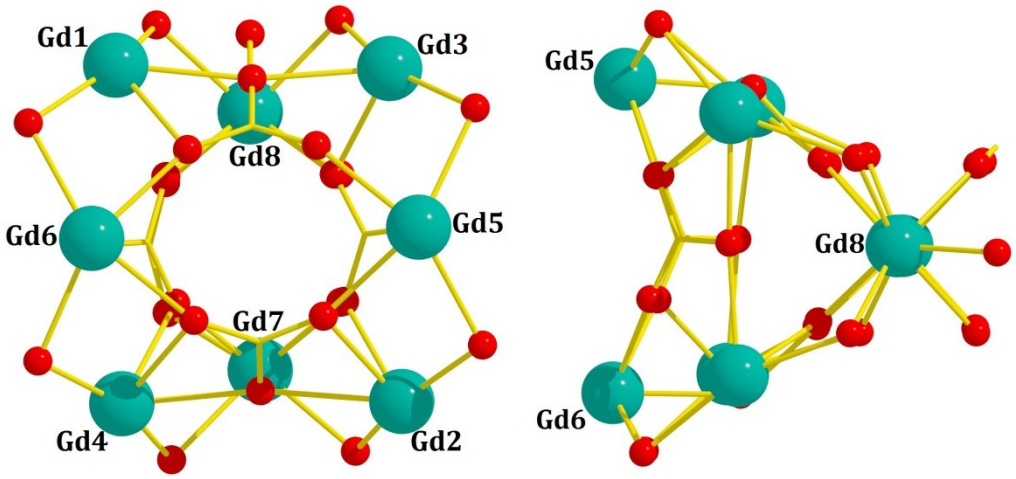

Figure 14. Two views of the gyrobifastigium cluster core found in the structure of **16** showing the incorporated CO_3^{2-} and HCO_2^- ions.

5.3.2 Cluster Construction Analysis

At first, from a quick inspection of Figures 5-14, there appears to be little or no resemblance between complexes **12**-**16**. However, upon closer inspection a clear trend emerges: all the structures are based on octahedra or the building blocks of octahedra. Complex **12** is a capped triangle, complex **13** is a square-based pyramid, complex **14** an octahedron and complex **15** a capped octahedron (Figure 15). The variation in structure type must therefore originate from changes in reaction conditions and in the identity of the metal centre and its oxidation state. The synthetic methodologies are all very similar (see experimental section), and there are some obvious conclusions to be drawn from these experimental details. The reactions that produce complexes **12** and **14** are analogous, the major difference being the change in solvent from MeCN in the former to MeOH in the latter. This introduces MeO^- ions into the reaction mixture and indeed four are incorporated into the crystallized product, each bridging across one vertex of the octahedron. In other words the methoxide ions promote a structural transformation from a capped triangle to an octahedron. In essence this is a simple dimerisation.

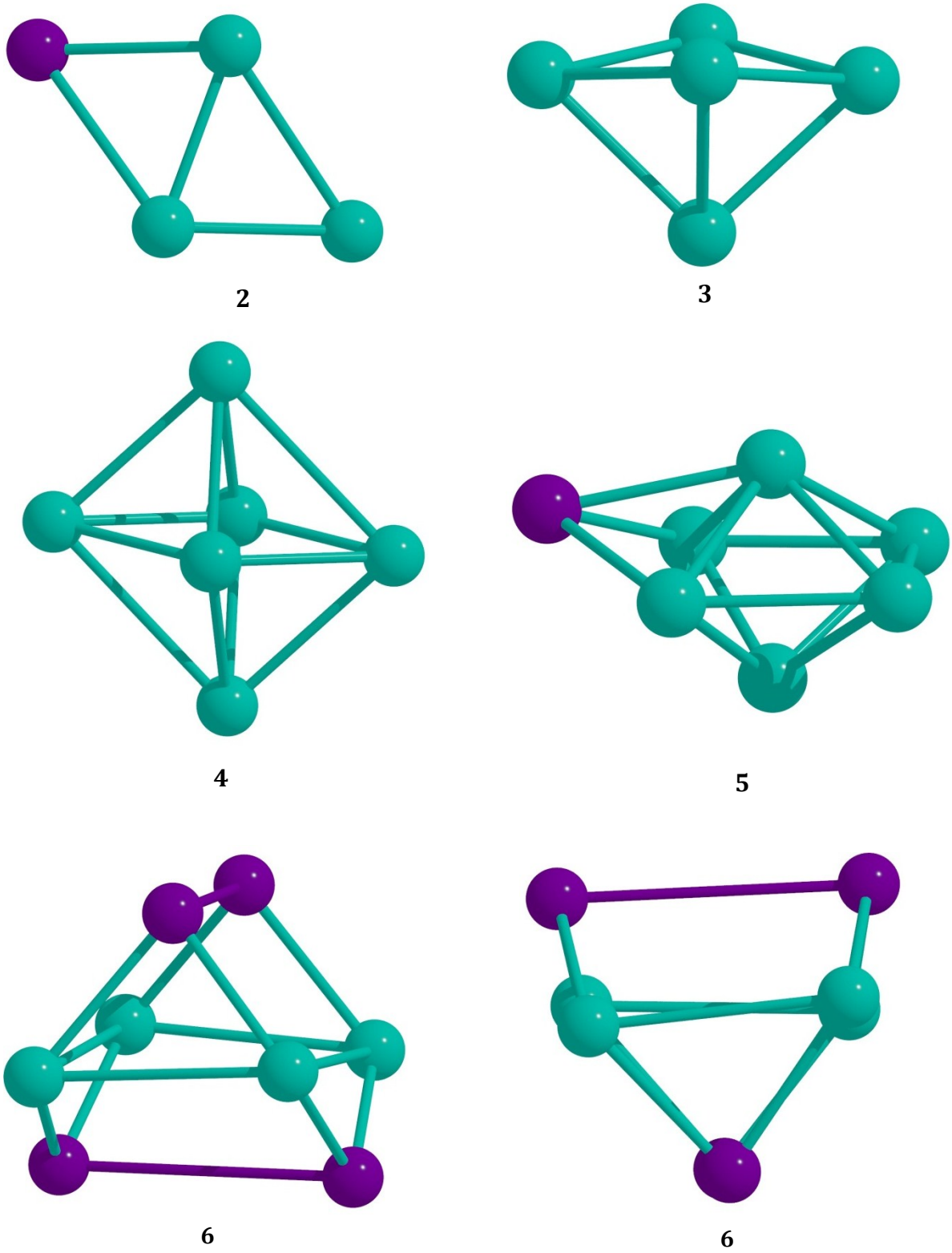

Figure 15. Structure analyses of **12** – **16** showing the common octahedral character associated with each system. Capping lanthanide vertices are shown in purple. Two orthogonal views are shown for **16** to emphasize the diagonal bi-capping found in the gyrobifastigium polyhedron.

The reactions which produce complexes **13** ([Tb^{III}_5]) and **15** ([Dy^{III}_7]) are also analogous and, assuming the small change in size of the Ln has no effect, the major difference here is the ratio of ligand:base used in the reaction [1:9 in the former and 1:24 in the latter] and the use of higher temperature and pressure (solvothermal reaction). In complex **13** both ligands are TBC[8]-6H, while in **15** one ligand is TBC[8]-6H and the other TBC[8]-7H, and it is this additional phenolate arm that bridges to the "extra" capping Dy ion. The octahedron observed in **15** is very similar to that formed with TBC[4], suggesting that this may be a favourable construction core for any calixarene containing multiple equivalents of the bowl-shaped tetramer (e.g. TBC[8], TBC[12] and so on).[20]

Complex **16** is synthesised from an analogous reaction to that used to produce **15**, but with Gd in place of Dy. This is the only structure in the series that deviates markedly from the octahedral construction core shown in Figure 15. Although this is the case the central square plane of the octahedron is evident, with diagonal bi-capping to afford the gyrobifastigium (the 26th Johnson solid). This 8-vertex polyhedron is composed of four squares and four triangles and is persistently formed experimentally with Gd ions. Although further work will be required to fully elucidate why a different structural motif is being formed, we propose that it is likely that the presence of the centrally templating carbonate ions, and/or a threshold in the lanthanide ion size is responsible. The former clearly have a different coordination mode (μ_4 and μ_5) than oxide or hydroxide ions and thus direct the formation of a different metallic skeleton around which the calixarene must wrap. The latter, often referred to as the "Gd-break" simply reflects the larger coordination number often observed for the early, larger lanthanides. Given the coordination number of the Gd(III) ions in **16** however, the effect/presence of the carbonate anions seems a more plausible explanation.

In addition, complex **16** is the only structure in which both cluster supports are TBC[8]-7H. This may therefore suggest that the use of high temperature, high pressure reactions is a route toward achieving full, or nearly full, deprotonation of the calixarene.

In order to conclusively prove this theory we will undertake an expansive combinatorial study of Ln salts, bases (including equivalents used) and solvents employed in cluster formation in a range of temperature pressure conditions. These findings will be reported in due course.

5.4 Conclusions

p-tert-Butylcalix[8]arene has previously been investigated as a support for the formation of small (dinuclear) lanthanide(III) clusters. Our investigations into the use of different experimental conditions and lanthanide metals show that this ligand is in fact extremely versatile in terms of conformation, varying degrees of deprotonation and bridging capacity. This has marked consequences on the resulting ability of the ligand to form a wide range of complexes with cluster motifs containing 2, 4, 5, 6, 7, and 8 lanthanide centers. There are only a small number of reports outlining the use of other large TBC[*n*]s as cluster supports. The results reported here suggest that an enormous range of alternative and possibly larger clusters may be formed with these supports. Future work will therefore focus on exploring analogous chemistry with the entire family of large TBC[*n*]s (where n = 5 – 20). This may show a) that other large TBC[*n*]s display trends in both conformation and level of de-protonation, b) that multiple clusters form simultaneously in solution or c) that particular clusters form selectively under varied experimental conditions. Control over crystallization and experiment will be key in the isolation of specific cluster types with particular lanthanide metals.

With respect to the Ln / TBC[8] clusters reported here, mixed 3*d*-4*f* systems are also under investigation, and the experimental and theoretical investigation of the magnetic properties of **11**, **13**, **15** and **16**, which are non-trivial, will be reported in detail elsewhere.

5.5 References

1. G. Aromí and E. Brechin, in *Structrure and Bonding*, ed. R. E. P. Winpenny, Springer, 2006, vol. 122, pp. 1-67.
2. A. K. Boudalis, Y. Sanakis, C. P. Raptopoulou and V. Psycharis, in *Magnetism and Superconductivity in Low-Dimensional Systems: Utilization in Future Applications*, ed. D. Stamopoulos, Nova Science Publishers Inc., New York, 2008, pp. 1-77.
3. G. Christou, *Polyhedron*, 2005, **24**, 2065-2075.
4. M. Evangelisti and E. K. Brechin, *Dalton Trans.*, 2010, **39**, 4672-4676.
5. M. Evangelisti, F. Luis, L. J. de Jongh and M. Affronte, *J. Mater. Chem.*, 2006, **16**, 2534-2549.
6. D. Gatteschi, R. Sessoli and J. Villain, *Molecular Nanomagnets*, Oxford University Press, 2006.
7. M. Murrie and D. J. Price, *Annu. Rep. Prog. Chem., Sect. A: Inorg. Chem.*, 2007, **103**, 20-38.

8. R. E. P. Winpenny, *Chem. Soc. Rev.*, 1998, **27**, 447-452.
9. C. D. Gutsche, *Calixarenes 2001*, Kluwer Academic Publishers, 2001.
10. Y. Bi, X.-T. Wang, W. Liao, X. Wang, X. Wang, H. Zhang and S. Gao, *J. Am. Chem. Soc.*, 2009, **131**, 11650-11651.
11. C. Desroches, G. Pilet, S. A. Borshch, S. Parola and D. Luneau, *Inorg. Chem.*, 2005, **44**, 9112-9120.
12. C. Desroches, G. Pilet, P. Á. Szilágyi, G. Molnár, S. A. Borshch, A. Bousseksou, S. Parola and D. Luneau, *Eur. J. Inorg. Chem.*, 2006, 357-365.
13. T. Kajiwara, N. Iki and M. Yamashita, *Coord. Chem. Rev.*, 2007, **251**, 1734-1746.
14. C. Aronica, G. Chastanet, E. Zueva, S. A. Borshch, J. M. Clemente-Juan and D. Luneau, *J. Am. Chem. Soc.*, 2008, **130**, 2365-2371.
15. G. Karotsis, M. Evangelisti, S. J. Dalgarno and E. K. Brechin, *Angew. Chem. Int. Ed*, 2009, **121**, 10112-10115.
16. G. Karotsis, S. Kennedy, S. J. Dalgarno and E. K. Brechin, *Chem. Commun.*, 2010, **46**, 3884-3886.
17. G. Karotsis, S. Kennedy, S. J. Teat, C. M. Beavers, D. A. Fowler, J. J. Morales, M. Evangelisti, S. J. Dalgarno and E. K. Brechin, *J. Am. Chem. Soc.*, 2010, **132**, 12983-12990.
18. G. Karotsis, S. J. Teat, W. Wernsdorfer, S. Piligkos, S. J. Dalgarno and E. K. Brechin, *Angew. Chem. Int. Ed*, 2009, **48**, 8285-8288.
19. S. Sanz, K. Ferreira, R. D. McIntosh, S. J. Dalgarno and E. K. Brechin, *Chem. Commun.*, 2011, **47**, 9042-9044.
20. S. Sanz, R. D. McIntosh, C. M. Beavers, S. J. Teat, M. Evangelisti, E. K. Brechin and S. J. Dalgarno, *Chem. Commun.*, 2012, **48**, 1449-1451.
21. S. M. Taylor, G. Karotsis, R. D. McIntosh, S. Kennedy, S. J. Teat, C. M. Beavers, W. Wernsdorfer, S. Piligkos, S. J. Dalgarno and E. K. Brechin, *Chem. Eur. J.*, 2011, **17**, 7521-7530.
22. S. M. Taylor, R. D. McIntosh, C. M. Beavers, S. J. Teat, S. Piligkos, S. J. Dalgarno and E. K. Brechin, *Chem. Commun.*, 2011, **47**, 1440-1442.
23. A. Arbaoui, C. Redshaw, M. R. J. Elsegood, V. E. Wright, A. Yoshizawa and T. Yamato, *Chem.Asian J.*, 2010, **5**, 621-633.
24. V. Esposito, E. Solari, C. Floriani, N. Re, C. Rizzoli and A. Chiesi-Villa, *Inorg. Chem.*, 2000, **39**, 2604-2613.
25. M. Giusti, E. Solari, L. Giannini, C. Floriani, A. Chiesi-Villa and C. Rizzoli, *Organometallics*, 1997, **16**, 5610-5612.
26. M. M. Olmstead, G. Sigel, H. Hope, X. Xu and P. P. Power, *J. Am. Chem. Soc.*, 1985, **107**, 8087-8091.
27. J. Zeller, S. Koenig and U. Radius, *Inorg. Chim. Acta*, 2004, **357**, 1813-1821.
28. R. D. Bergougnant, A. Y. Robin and K. M. Fromm, *Cryst. Growth Des.*, 2005, **5**, 1691-1694.
29. R. D. Bergougnant, A. Y. Robin and K. M. Fromm, *Tetrahedron*, 2007, **63**, 10751-10757.
30. N. P. Clague, J. D. Crane, D. J. Moreton, E. Sinn, S. J. Teat and N. A. Young, *J. Chem. Soc., Dalton. Trans.*, 1999, 3535-3536.
31. N. P. Clague, J. D. Crane, E. Sinn, N. A. Young, W. Clegg, S. J. Coles, S. J. Teat and D. J. Moreton, *Chem. Commun.*, 1999, 379-380.
32. B. M. Furphy, J. M. Harrowfield, D. L. Kepert, B. W. Skelton, A. H. White and F. R. Wilner, *Inorg. Chem.*, 1987, **26**, 4231-4236.
33. V. C. Gibson, C. Redshaw and M. R. J. Elsegood, *J. Chem. Soc., Dalton. Trans.*, 2001, 767-769.

34. V. C. Gibson, C. Redshaw and M. R. J. Elsegood, *New J. Chem.*, 2002, **26**, 16-19.
35. V. C. Gibson, C. Redshaw and M. R. J. Elsegood, *Chem. Commun.*, 2002, 1200-1201.
36. R. A. Green, A. L. Rheingold and C. S. Weinert, *Inorg. Chim. Acta*, 2009, **362**, 3159-3164.
37. J. Harrowfield, M. Ogden and A. White, *Aust. J. Chem.*, 1991, **44**, 1237-1247.
38. J. Harrowfield, M. Ogden and A. White, *Aust. J. Chem.*, 1991, **44**, 1249-1262.
39. J. Harrowfield, M. Ogden, A. White and F. Wilner, *Aust. J. Chem.*, 1989, **42**, 949-958.
40. J. M. Harrowfield, M. I. Ogden, W. R. Richmond and A. H. White, *J. Chem. Soc., Dalton. Trans.*, 1991, 2153-2160.
41. J. M. Harrowfield, M. I. Ogden, B. W. Skelton and A. H. White, *Dalton Trans.*, 2010, **39**, 8313-8318.
42. G. E. Hofmeister, F. E. Hahn and S. F. Pedersen, *J. Am. Chem. Soc.*, 1989, **111**, 2318-2319.
43. E. Hoppe, C. Limberg and B. Ziemer, *Inorg. Chem.*, 2006, **45**, 8308-8317.
44. L. Liu, L. N. Zakharov, J. A. Golen, A. L. Rheingold and T. A. Hanna, *Inorg. Chem.*, 2008, **47**, 11143-11153.
45. R. D. McIntosh, S. M. Taylor, S. Sanz, C. M. Beavers, S. J. Teat, E. K. Brechin and S. J. Dalgarno, *Dalton Trans.*, 2011, **40**, 12265-12270.
46. D. Mendoza-Espinosa, A. L. Rheingold and T. A. Hanna, *Dalton Trans.*, 2009, 5226-5238.
47. S. Petit, G. Pilet, D. Luneau, L. F. Chibotaru and L. Ungur, *Dalton Trans.*, 2007, 4582-4588.
48. P. Thuéry, N. Keller, M. Lance, J.-D. Vigner and M. Nierlich, *Acta Crys.*, 1995, **51**, 1570-1574.
49. C. Redshaw and M. R. J. Elsegood, *Inorg. Chem.*, 2000, **39**, 5164-5168.
50. W. Liu and H. H. Thorp, *Inorg. Chem.*, 1993, **32**, 4102-4105.
51. H. H. Thorp, *Inorg. Chem.*, 1992, **31**, 1585-1588.
52. S. L. Castro, Z. Sun, J. C. Bollinger, D. N. Hendrickson and G. Christou, *J. Chem. Soc., Chem. Commun.*, 1995, 2517-2518.
53. J. K. McCusker, J. B. Vincent, E. A. Schmitt, M. L. Mino, K. Shin, D. K. Coggin, P. M. Hagen, J. C. Huffman, G. Christou and D. N. Hendrickson, *J. Am. Chem. Soc.*, 1991, **113**, 3012-3021.
54. J. B. Vincent, C. Christmas, J. C. Huffman, G. Christou, H.-R. Chang and D. N. Hendrickson, *J. Chem. Soc., Chem. Commun.*, 1987, 236-238.
55. D. L. Bond, D. L. Clark, R. J. Donohoe, J. C. Gordon, P. L. Gordon, D. W. Keogh, B. L. Scott, C. D. Tait and J. G. Watkin, *Inorg. Chem.*, 2000, **39**, 3934-3937.
56. W. Runde, M. P. Neu, C. Van Pelt and B. L. Scott, *Inorg. Chem.*, 2000, **39**, 1050-1051.

Appendix

Table A. Selected bond lengths for complex **2** (Å)

Mn1—O3	1.933 (8)
Mn1—O2	1.944 (7)
Mn1—O1	1.949 (8)
Mn1—O4	2.000 (7)
Mn1—O5	2.153 (7)
Mn1—O8	2.312 (8)
O1—C6	1.375 (11)
N1—C48	1.340 (13)
N1—C49	1.449 (13)
N1—C50	1.477 (13)
C1—C2	1.387 (13)
C1—C6	1.395 (13)
C1—C47	1.532 (13)
Mn2—O7	2.181 (9)
Mn2—O4	2.191 (7)
Mn2—O5	2.197 (8)
Mn2—O6	2.199 (8)
Mn2—O5	2.201 (8)
Mn2—O1	2.271 (8)

Table B. Selected bond lengths for complex **3** (Å).

Mn1—O4	1.9244 (15)
Mn1—O1	1.9249 (15)
Mn1—O2	1.9566 (15)
Mn1—O3	1.9672 (15)
Mn1—O5	2.1446 (14)
Mn1—O8	2.2981 (15)
Mn2—O7	2.037 (15)
Mn2—O6	2.126 (4)
Mn2—O5	2.1624 (15)
Mn2—O3	2.2159 (14)
Mn2—O2	2.2175 (14)
Mn2—O7	2.223 (9)

Table C. Selected bond lengths for complex **4** (Å)

Mn1—O4	1.901 (7)
Mn1—O1	1.915 (7)
Mn1—O3	1.942 (7)
Mn1—O2	1.952 (7)
Mn1—O6	2.160 (6)
Mn1—O5	2.273 (8)
Mn2—O7	2.148 (11)
Mn2—O2	2.167 (6)
Mn2—O6	2.170 (7)
Mn2—O8	2.210 (7)
Mn2—O3	2.258 (6)

Table D. Selected bond lengths for complex **5** (Å)

Mn1—O4	1.899 (4)
Mn1—O1	1.917 (3)
Mn1—O3	1.950 (3)
Mn1—O2	1.952 (3)
Mn1—O5	2.124 (3)
Mn1—O8	2.363 (4)
S1—O6	1.509 (4)
Mn2—O7	2.146 (4)
Mn2—O6	2.149 (4)
Mn2—O5	2.184 (4)
Mn2—O5	2.185 (4)
Mn2—O2	2.201 (3)
Mn2—O3	2.211 (3)
S2—O7	1.361 (6)
S4—O9	1.49 (3)

Table E. Selected bond lengths for complex **6** (Å)

Mn1—O3	1.893 (3)
Mn1—O2	1.904 (3)
Mn1—O4	1.939 (3)
Mn1—O1	1.952 (3)
Mn1—O6	2.111 (3)
Mn1—O7	2.380 (7)
S1—O5	1.521 (4)
Mn2—O8	2.115 (4)
Mn2—O5	2.164 (3)
Mn2—O6	2.177 (3)
Mn2—O1	2.209 (3)
Mn2—O4	2.226 (3)
S3—O7	1.486 (8)
S5—O7	1.525 (13)
S6—O8	1.461 (5)

Table F. Selected bond lengths for complex **7** (Å)

Mn1—O2	1.912 (2)
Mn1—O1	1.9475 (19)
Mn1—O5	2.139 (3)
Mn1—O10	2.345 (3)
O1—Mn3	2.208 (2)
Mn2—O4	1.909 (2)
Mn2—O3	1.943 (2)
Mn2—O6	2.156 (3)
Mn2—O11	2.369 (3)
Mn3—O8	2.145 (2)
Mn3—O7	2.159 (2)
Mn3—O5	2.1708 (19)
Mn3—O6	2.1786 (19)
Mn3—O3	2.214 (2)

Table G. Selected bond lengths for complex **8** (Å)

Mn1—O1	1.897 (5)	Mn2—O8	2.202 (5)
Mn1—O4	1.930 (5)	Mn2—O9	2.223 (5)
Mn1—O2	1.941 (5)	Mn2—O10	2.228 (6)
Mn1—O3	1.951 (5)		
Mn1—O5	2.251 (5)		
Mn1—O6	2.253 (4)		
P1—O7	1.501 (5)		
P1—O6	1.518 (5)		
P1—C48	1.784 (11)		
Mn2—O3	2.162 (4)		
Mn2—O6	2.180 (5)		

Table H. Selected bond lengths for complex **9** (Å)

Mn1—O3	2.136 (2)	Mn4—O12	2.219 (2)
Mn1—O13	2.146 (2)	Mn4—O10	2.250 (2)
Mn1—O14	2.183 (2)	Mn5—O6	2.120 (2)
Mn1—O15	2.229 (2)	Mn5—O17	2.168 (2)
Mn1—N5	2.235 (2)	Mn5—O131	2.190 (4)
Mn1—O11	2.2415 (19)	Mn5—O16	2.192 (2)
O1—Mn2	1.940 (2)	Mn5—O136	2.192 (7)
Mn2—O2	1.898 (2)	Mn5—N6	2.246 (3)
Mn2—O4	1.9553 (19)	Mn5—O12	2.2649 (19)
Mn2—O3	1.972 (2)		
Mn2—O11	2.2231 (19)		
Mn2—O9	2.237 (2)		
Mn3—O15	1.895 (2)		
Mn3—O16	1.902 (2)		
Mn3—O12	1.936 (2)		
Mn3—O11	1.9375 (19)		
Mn3—O4	2.2474 (19)		
Mn3—O7	2.2869 (19)		
Mn4—O5	1.893 (2)		
Mn4—O8	1.929 (2)		
Mn4—O7	1.9557 (19)		
Mn4—O6	1.967 (2)		

Table I. Selected bond lengths for complex **10** (Å)

Mn1—O29	2.046 (9)	Mn5—O32	2.017 (9)
Mn1—O5	2.068 (6)	Mn5—O24	2.098 (6)
Mn1—O6	2.149 (6)	Mn5—O23	2.139 (6)
Mn1—O4	2.152 (6)	Mn5—O22	2.180 (6)
Mn1—O25	2.209 (5)	Mn5—O28	2.188 (6)
Cl1—Mn3	2.602 (3)	Mn6—O28	1.891 (6)
Cl1—Mn8	2.675 (3)	Mn6—O27	1.893 (5)
Cl1—Mn4	2.734 (3)	Mn6—O12	1.951 (6)
Mn2—O25	1.909 (5)	Mn6—O22	1.954 (6)
Mn2—O28	1.915 (6)	Mn7—O31	2.038 (11)
Mn2—O23	1.957 (6)	Mn7—O11	2.101 (7)
Mn2—O4	1.968 (6)	Mn7—O10	2.129 (7)
Mn2—Cl2	2.682 (3)	Mn7—O12	2.131 (6)
Mn2—Cl4	2.696 (3)	Mn7—O27	2.199 (6)
Cl2—Mn3	2.602 (3)	Mn8—O27	1.915 (5)
Cl2—Mn6	2.740 (3)	Mn8—O26	1.914 (5)
Mn3—O5	2.077 (6)	Mn8—O16	1.946 (6)
Mn3—O11	2.098 (7)	Mn8—O10	1.967 (6)
Mn3—O25	2.125 (5)	Mn9—O30	2.021 (11)
Mn3—O27	2.129 (6)	Mn9—O17	2.085 (6)
Cl3—Mn10	2.602 (3)	Mn9—O16	2.146 (6)
Cl3—Mn8	2.686 (3)	Mn9—O18	2.146 (6)
Cl3—Mn6	2.712 (3)	Mn9—O26	2.197 (6)
Mn4—O26	1.886 (6)	Mn10—O17	2.076 (6)
Mn4—O25	1.896 (6)	Mn10—O24	2.079 (6)
Mn4—O6	1.934 (6)	Mn10—O28	2.134 (6)
Mn4—O18	1.951 (6)	Mn10—O26	2.134 (5)
Mn4—Cl4	2.724 (3)		
Cl4—Mn10	2.610 (2)		

Table J. Selected bond lengths for complex **11** (Å)

Gd1—O8	2.240 (3)
Gd1—O12	2.319 (5)
Gd1—O7	2.336 (3)
Gd1—O9	2.364 (3)
Gd1—O10	2.369 (3)
Gd1—O13	2.388 (16)
Gd1—O11	2.408 (3)
Gd1—Cl1	2.6960 (10)
S1—O9	1.515 (3)
S2—O10	1.515 (3)
S3—O11	1.502 (3)
S4—O12	1.501 (6)
S6—O20	1.489 (4)
S7—O22	1.540 (6)
S8—O21	1.41 (2)
S5—O13	1.500 (17)

Table K. Selected bond lengths for complex **12** (Å)

Ce1—O19	2.111 (3)	Ce4—O21	2.426 (3)
Ce1—O22	2.210 (3)	Ce4—O14	2.577 (3)
Ce1—O13	2.266 (3)		
Ce1—O11	2.301 (3)		
Ce1—O12	2.311 (3)		
Ce1—O20	2.413 (3)		
Ce1—O18	2.523 (3)		
Ce1—Ce2	3.5022 (4)		
Ce1—Ce3	3.7676 (4)		
O1—Ce4	2.324 (3)		
O1—Ce2	2.330 (3)		
Ce2—O8	2.121 (3)		
Ce2—O11	2.229 (3)		
Ce2—O2	2.269 (3)		
Ce2—O22	2.302 (3)		
Ce2—O9	2.386 (3)		
Ce2—O7	2.517 (3)		
Ce2—Ce4	3.7705 (4)		
Ce3—O4	2.135 (3)		
Ce3—O5	2.157 (3)		
Ce3—O11	2.227 (3)		
Ce3—O6	2.332 (3)		
Ce3—O12	2.342 (3)		
Ce3—O10	2.412 (3)		
Ce3—O3	2.597 (3)		
Ce4—O15	2.139 (3)		
Ce4—O16	2.145 (3)		
Ce4—O22	2.241 (3)		
Ce4—O17	2.346 (3)		

Table L. Selected bond lengths for complex **13** (Å)

Tb1—O8	2.213 (3)	Tb3—Tb4	3.6144 (3)
Tb1—O9	2.328 (3)	Tb3—Tb5	3.8318 (3)
Tb1—O12	2.396 (2)	Tb4—O6	2.301 (3)
Tb1—O1	2.402 (3)	Tb4—O5	2.320 (2)
Tb1—O15	2.413 (3)	Tb4—O14	2.327 (2)
Tb1—O11	2.465 (2)	Tb4—O22	2.331 (3)
Tb1—O7	2.475 (3)	Tb4—O15	2.353 (2)
Tb1—O6	2.508 (3)	Tb4—O23	2.416 (3)
Tb1—Tb2	3.6779 (3)	Tb4—O24	2.458 (3)
Tb1—Tb4	3.6782 (3)	Tb4—O11	2.646 (2)
Tb1—Tb5	3.8559 (3)	Tb4—Tb5	3.7209 (3)
Cl1—Tb2	2.7433 (9)	Tb5—O18	2.337 (3)
O1—Tb2	2.320 (3)	Tb5—O19	2.356 (3)
Tb2—O16	2.294 (3)	Tb5—O12	2.358 (3)
Tb2—O13	2.335 (2)	Tb5—O14	2.370 (2)
Tb2—O2	2.356 (2)	Tb5—O13	2.385 (2)
Tb2—O12	2.359 (3)	Tb5—O20	2.388 (3)
Tb2—O17	2.365 (3)	Tb5—O15	2.405 (2)
Tb2—O11	2.838 (2)	Tb5—O21	2.489 (3)
Tb2—Tb3	3.6098 (2)		
Tb2—Tb5	3.7512 (3)		
O2—Tb3	2.362 (2)		
Tb3—O10	2.309 (2)		
Tb3—O13	2.374 (2)		
Tb3—O14	2.382 (2)		
Tb3—O5	2.384 (2)		
Tb3—O11	2.390 (2)		
Tb3—O4	2.438 (2)		
Tb3—O3	2.450 (2)		

Table M. Selected bond lengths for complex **14** (Å)

Ce1—O11	2.150 (2)
Ce1—O1	2.188 (3)
Ce1—O13	2.309 (3)
Ce1—O8	2.317 (2)
Ce1—O10	2.440 (3)
Ce1—O12	2.440 (2)
Ce1—O7	2.529 (3)
Ce1—O2	2.670 (3)
Ce2—O11	2.163 (2)
Ce2—O4	2.197 (3)
Ce2—O14	2.339 (3)
Ce2—O3	2.366 (2)
Ce2—O9	2.441 (3)
Ce2—O5	2.460 (2)
Ce2—O6	2.549 (3)
Ce3—O12	2.257 (2)
Ce3—O14	2.316 (2)
Ce3—O13	2.327 (3)

Table N. Selected bond lengths for complex **15** (Å)

Dy1—O32	2.192 (6)	Dy4—O30	2.439 (7)
Dy1—O1	2.307 (7)	Dy4—O14	2.531 (6)
Dy1—O33	2.362 (7)	Dy4—O11	2.563 (7)
Dy1—O8	2.380 (7)	Dy5—O32	2.234 (6)
Dy1—O19	2.381 (7)	Dy5—O31	2.249 (6)
Dy1—O13	2.399 (7)	Dy5—O6	2.314 (6)
Dy1—O7	2.478 (6)	Dy5—O7	2.346 (7)
Dy1—O2	2.745 (7)	Dy5—O29	2.382 (7)
Dy2—O31	2.218 (6)	Dy5—O23	2.404 (7)
Dy2—O4	2.232 (8)	Dy5—O28	2.422 (6)
Dy2—O12	2.357 (6)	Dy6—O31	2.192 (6)
Dy2—O20	2.380 (7)	Dy6—O11	2.285 (6)
Dy2—O5	2.390 (7)	Dy6—O29	2.332 (6)
Dy2—O33	2.417 (7)	Dy6—O22	2.354 (8)
Dy2—O6	2.516 (6)	Dy6—O10	2.374 (7)
Dy2—O3	2.821 (8)	Dy6—O21	2.413 (7)
Dy3—O9	2.208 (7)	Dy7—O32	2.215 (6)
Dy3—O30	2.254 (6)	Dy7—O14	2.272 (6)
Dy3—O17	2.323 (7)	Dy7—O15	2.330 (7)
Dy3—O29	2.387 (6)	Dy7—O28	2.369 (6)
Dy3—O10	2.392 (7)	Dy7—O8	2.384 (7)
Dy3—O28	2.395 (6)	Dy7—O25	2.427 (7)
Dy3—O16	2.528 (7)	Dy7—O24	2.449 (7)
Dy3—O15	2.902 (7)	Dy7—O30	2.832 (6)
Dy4—O32	2.250 (6)		
Dy4—O31	2.265 (6)		
Dy4—O18	2.341 (7)		
Dy4—O12	2.361 (7)		
Dy4—O13	2.376 (7)		

Table O. Selected bond lengths for complex **16** (Å)

Gd1—O9	2.261 (6)	Gd6—O3	2.322 (8)
Gd1—O10	2.311 (6)	Gd6—O4	2.396 (6)
Gd1—O1	2.311 (9)	Gd6—O15	2.401 (6)
Gd1—O2	2.370 (8)	Gd7—O1	2.296 (8)
Gd1—O11	2.492 (6)	Gd7—O2	2.311 (7)
Gd1—O12	2.533 (6)	Gd8—O2	2.318 (7)
Gd1—O3	2.644 (10)	Gd8—O1	2.323 (8)
Gd2—O4	2.219 (6)	Gd8—O13	2.343 (6)
Gd2—O1	2.242 (10)	Gd8—O12	2.345 (5)
Gd2—O5	2.363 (7)	Gd8—O3	2.375 (8)
Gd2—O3	2.370 (7)		
Gd2—O2	2.612 (6)		
Gd3—O14	2.167 (6)		
Gd3—O1	2.351 (6)		
Gd3—O15	2.357 (6)		
Gd3—O13	2.390 (6)		
Gd3—O2	2.479 (9)		
Gd3—O3	2.511 (7)		
Gd3—O16	2.688 (6)		
Gd4—O8	2.204 (6)		
Gd4—O1	2.349 (6)		
Gd4—O7	2.390 (6)		
Gd4—O2	2.465 (10)		
Gd4—O6	2.663 (6)		
Gd5—O1	2.248 (8)		
Gd5—O2	2.380 (6)		
Gd5—O7	2.384 (5)		
Gd5—O10	2.388 (6)		
Gd6—O1	2.134 (8)		